

THE POTASH DEPOSITS AND THEIR ASSOCIATES IN THE AREA
OF THE BOULBY MINE, CLEVELAND

VOLUME 1. TEXT

by

John K. Milne B. Sc.



This thesis is presented for the degree
of Doctor of Philosophy of the University
of Edinburgh in the Faculty of Science

1978

Declaration

I hereby declare that all the work presented in this thesis is my own, except where stated in the text, and that the thesis has been composed by myself.

JOHN K. MILNE

Abstract

Part I of this thesis describes the results of a petrological and geochemical examination of the upper part of the Boulby Halite, Potash and Shale at Boulby aimed at contributing to our knowledge of the geological history of these rocks.

These beds may have been deposited in a basinal/lagoonal (as defined in Chapter 8), supratidal or possibly both of these types of environments. The chemical character of the strata favours the first hypothesis.

Detrital material, of windblown or fluvial origin, was deposited on the halite plain which evolved during the final stages of desiccation of either of the above postulations. A marked dilution of the brines occurred after deposition of the lower beds of the Boulby Shale.

Numerous diagenetic reactions occurred in these beds. In the lower rocks of the Boulby Shale carnallite was replaced by halite, leading to reprecipitation of secondary sylvite; and borate minerals grew and formed a borate nodule bed. In the upper beds of this unit anhydrite has replaced or displaced clays. The sylvite of the Boulby Potash may be secondary.

Fibrous sylvinite veins developed in the rocks from the Boulby Shale to the Upper Anhydrite during burial. The Boulby Potash was overfolded and overthrust (axes N.N.W.-S.S.E.) when it was buried at greatest depth

(2200-3200 metres) towards the end of the Cretaceous and early Tertiary. Subsequently small scale swells (axes at $024^{\circ} \pm 10^{\circ}$) developed in the top of the Boulby Potash and monoclines (E-W axes) formed at its base.

Where relevant, these beds are compared with other evaporite deposits.

Part II describes an experimental study of the system $\text{NaCl-H}_2\text{O}$, at 25°C , and pressures up to 2.5 kilobars. The solubility of NaCl in water increases from 26.42 weight percent at atmospheric pressure to 27.23 weight percent at 2.5 kilobars.

Table of Contents

	<u>page</u>
General introduction to the thesis	1
<u>PART I. Studies in the area of the Boulby Mine</u>	3
<u>CHAPTER 1. Introduction</u>	4
I History of exploration leading to the exploitation of the potassium salts of north-east England	4
II Palaeogeography, tectonic setting and summary of the stratigraphy of the English Zechstein	6
III The Boulby Mine	11
IV The scope and objectives of Part I of the thesis	12
<u>CHAPTER 2. The stratigraphy and structure of the upper part of the Boulby Halite, the Boulby Potash and the Boulby Shale</u>	13
I Introduction	13
II General stratigraphy of the rocks exposed in the Mine	14
III Stratigraphic terminology	17

	<u>page</u>
IV Derivation of the lithostratigraphy of the sequence examined	17
(1) Problems encountered in determining the lithostratigraphy	19
(2) Derivation of the lithostratigraphy	21
(a) The upper part of the Boulby Halite	21
(b) The Boulby Potash	22
(c) The Boulby Shale	23
α) Beds B.S.1 and 2	23
β) Beds B.S.3 and 4	23
γ) Bed B.S.5	24
δ) Bed B.S.6	25
(d) The lowermost rocks of the Rotten Marl (Carnallitic Marl)	25
α) Grey Marl	26
β) Red Marl	26
V Structural geology	27
(1) Sylvinite veins	27
(2) Overfolds and overthrusts	30
(a) Geological observations	31
(b) Interpretation and discussion	35
(3) Swells and depressions in the top of the Boulby Potash	36
(4) Monoclines	38
(5) Summary of the structural history	39

	<u>page</u>
<u>CHAPTER 3. The upper part of the Boulby Halite</u>	41
I Bed B.H.1	41
(1) General features	41
(2) Petrography	43
(3) Residual brines	54
II Bed B.H.2	55
III Summary and conclusions	60
 <u>CHAPTER 4. The Boulby Potash</u>	 61
I General features	61
II Petrography	62
III The origin of the sylvite	67
IV Summary and conclusions	69
 <u>CHAPTER 5. The Boulby Shale</u>	 70
I Beds B.S.1, 4, 5 and 6	70
II Bed B.S.2	78
III Bed B.S.3	82
(1) General	82
(2) Mineralogy of the borates	85
(a) Iron-boracite and ericaite	85
α) General characteristics, lattice parameters and optical properties	86
β) Optical evidence for a relationship between iron-boracite and ericaite	90

	<u>page</u>
γ) Mineral chemistry	91
(i) General	91
(ii) Electron microprobe analyses	91
δ) The nature of the relationship between iron-boracite and ericaite	96
(b) Parahilgardite	99
α) General characteristics	100
β) Optics, lattice parameters and chemical composition	100
γ) The nature and origin of the turbidity in the parahilgardite of the nodules	103
(i) Optical characteristics	103
(ii) Chemical variations	105
(iii) Possible causes of strain	105
(iv) Possible origins of the stress in the parahilgardite	109
(3) The area of iron-boracite nodules	111
(a) The petrography of the host rock	111
(b) Petrography of the nodules	111
(c) Mode of formation of the nodules	124
(4) The area of parahilgardite nodules	128
(a) Petrography of the host rock	128
(b) Petrography of the nodules	135
(c) The mode of formation of the nodules	136
(d) Comparison of the iron-boracite and parahilgardite nodules	137

	<u>page</u>
IV The rocks of the Boulby Shale in the area of the Mine enclosed by roadways 2E, 2S, 5W and 3N and in boreholes S-20, X, Y, D, V, V-D1 and M	138
(1) General	138
(2) Discussion of the economic importance of the secondary halite in the Boulby Shale	140
V Summary and conclusions	141
 <u>CHAPTER 6. Boron geochemistry</u>	 147
I General	147
II Results and discussion	153
 <u>CHAPTER 7. Chemical evolution of the third Zechstein evaporite cycle in the Boulby Mine</u>	 155
I Comparison of this evaporite cycle with experimental data	155
II Origins of MgSO_4 depletion and/or CaCl_2 enrichment in brines	160
III Discussion of the sequence at Boulby	166
 <u>CHAPTER 8. Possible environments of sedimentation</u>	 172
I Basinal origin for the Boulby Halite and Boulby Potash	173
(1) General	173

	<u>page</u>
(2) Proposed hypothesis	175
II Supratidal origin	178
III Discussion	182
(1) Basinal versus supratidal hypothesis	182
(2) The origin of the clays in the Boulby Shale	185
 <u>CHAPTER 9. Estimation of the depth of burial of the beds in the sequence examined</u>	187
I Statement of the problem	187
II Calculations and discussion	192
 <u>CHAPTER 10. Geological history</u>	197
 <u>CHAPTER 11. Comparative studies</u>	206
I Comparison of the geology of the sequence examined at Boulby and other boreholes in north-east England	206
(1) Brief description of the rocks from the upper part of the Boulby Halite to the base of the Rotten Marl in the E and F boreholes	206
(a) The upper part of the Boulby Halite	206
(b) The Boulby Potash	207
(c) The Upper Halite	215
(2) Comparisons and discussion	215

	<u>page</u>
II Comparison of MgSO_4 depleted and/or CaCl_2 enriched evaporite deposits	219
(1) Brief description of the Stassfurt cycle of the German Zechstein	220
(2) Brief description of primary tachyhydrite in Brazil and the Congo	224
(3) Comparison and discussion	225
III Comparison of the principal marine borate deposits of the world	227
(1) General	227
(2) Brief description of marine borate deposits	228
(a) Inder district, Russia	228
(b) The German Zechstein	233
(c) The English Zechstein	234
(d) Texas, New Mexico and Louisiana (U.S.A.)	234
(e) Utah (U.S.A.)	235
(f) Oklahoma (U.S.A.)	236
(g) Nova Scotia and New Brunswick, Canada	236
(h) Congo (Africa)	237
(3) Comparisons and discussion	238

	<u>page</u>
<u>PART II. Experimental studies</u>	247
 <u>CHAPTER 12. An experimental study of the system</u> <u>NaCl-H₂O at 25°C and at pressures up to 2.5</u> <u>kilobars</u>	 248
I Introduction	248
II Experimental equipment	251
(1) Hydrothermal Equipment Review	252
(2) Experimental equipment used in this study	 254
(3) Experimental method and operation of equipment	 257
III Method of chemical analysis	258
IV Results and conclusions	258
 <u>CHAPTER 13. Summary and conclusions</u>	 261
I Part I	261
II Part II	270
 <u>ACKNOWLEDGEMENTS</u>	 272
 <u>APPENDIX 1. Well log data used to compile</u> Plate I	 274
<u>APPENDIX 2. Structural interpretations of the</u> boreholes	 298
<u>APPENDIX 3. Methods of chemical analysis</u>	307

	<u>page</u>
<u>APPENDIX 4.</u> Partial chemical analyses of FeO, MnO and MgO, in apparent concentrations, in iron- boracite and ericaite crystals from nodules in bed B.S.3	308
<u>APPENDIX 5.</u> Aspects of the hilgardite group of minerals and their nomenclature	314
<u>APPENDIX 6.</u> Permutation of stratigraphic data to estimate the depth of burial of the beds of the sequence examined	326
<u>APPENDIX 7.</u> Design of the pressure vessel used to study the system NaCl-H ₂ O	330
<u>APPENDIX 8.</u> Calibration and assessment of the performance of the pressure vessel	332
<u>APPENDIX 9.</u> Determination of the relative standard deviation of an analysis	339
<u>APPENDIX 10.</u> Publication	341
<u>REFERENCES</u>	342

General Introduction to the Thesis

In March, 1975, I visited the Boulby Mine, near Loftus, Cleveland, England. Cleveland Potash Ltd. (hereafter referred to as C.P.L.) opened the Boulby Mine in 1973 to extract the sylvinite (sylvite-halite rock) of the third Zechstein evaporite cycle for the manufacture of KCl for fertilizer production. The Chief Geologist, Mr. P.J.E. Woods, and the Management of C.P.L. indicated that they would be prepared to allow an academic geological study of the rocks exposed in the Mine. This provided a unique opportunity for a three dimensional geological examination of a salt deposit which had previously only been observed in cores from boreholes. In addition it allowed for the exchange of ideas between academic and industrial geologists.

In my initial eight months at the Grant Institute I completed an experimental investigation of the phase equilibria of the system $\text{NaCl-H}_2\text{O}$ at 25°C and at pressures up to 2 kilobars. This system was described by Adams (1931) and my study of it was intended as a precursor to similar experiments in polycomponent systems. It was thought necessary to investigate a simple system to develop and calibrate experimental equipment as well as verify Adams' (1931) result.

At about the time that I visited the Boulby Mine, however, Potter et al. (1975; and personal communication)

indicated that they were pursuing a similar line of study which was more advanced than my own. The news of Potter et al.'s investigation prompted me, with the permission of my supervisors, to change the subject of my farther study and take up the opportunity of examining the evaporite rocks exposed in the Boulby Mine.

Although both of these studies are relevant to evaporite geology, they cannot readily be integrated within this thesis. The dissertation is, therefore, divided into two parts: the first, and major part, describes the rocks examined at the Boulby Mine; Part two presents the experimental study mentioned above.

For clarity the thesis is presented in 2 volumes: Volume 1 comprises the text and tables and Volume 2 presents the figures. The plates are in the back pocket of Volume 2.

PART 1

STUDIES IN THE AREA OF THE BOULBY MINE

CHAPTER 1

INTRODUCTION

The Boulby Mine has come into production as the result of thirty years of exploration and assessment of the Upper Permian potassium salt beds of north-east England. Much of our present knowledge of these Permian rocks results from information gained from boreholes sunk in the search for potash (here defined as a rock containing potassium salts) in this area.

I The History of Exploration leading to the Exploitation of Potassium Salts in North-East England

Potassium salt deposits were first found incidentally by the D'Arcy Petroleum Company in 1939, in the E2 borehole (Figure 1.1), near Aislaby, during their search for hydrocarbons in England. World War II prevented further exploration. In 1952, however, ICI and Fisons drilled a number of boreholes to assess the feasibility of mining potassium salts. They abandoned the effort subsequently because of the depth of the sylvinite (over 1000 m. in the Whitby area) and the difficulties of shaft sinking through the water bearing Bunter Sandstone.

In 1961 Armour Chemical Industries Ltd. in partnership with Pittsburgh Plate Glass Ltd. took out mineral

rights on an area to the south-west of Whitby near Egton Moor and commenced to determine the viability of solution mining the potassium salts using methods developed in North America. On the strength of their results they combined with Shell and formed Whitby Potash Ltd. (W.P.L.) with the intention of removing 450,000 tons of KCl per annum by solution mining. W.P.L. was granted permission to do so in May, 1970, but brining has not, as yet, commenced.

Meanwhile ICI had been assessing the nature of the potassium salt deposit to the north-west of Whitby. They found potassium salts in the S-1 borehole in the vicinity of Staithes. Further boreholes were drilled to assess the potential of the sylvinite. The results of these, and the Canadian experience of sylvinite mining at depth, prompted ICI to invite Charter Consolidated Ltd. (C.C.L.) to join them in a feasibility study for a mining venture, with C.C.L. providing the mining expertise and ICI the industrial processing knowledge. ICI and C.C.L. first formed ICI (Minerals) Ltd. to finish the assessment of the deposit and upon successful completion they established Cleveland Potash Ltd. (C.P.L.). In early 1968 C.P.L. applied for planning permission to set up the Boulby Mine to produce 1.5 million tons of KCl per annum and the pilot borehole for shaft sinking (S-20) commenced in September of that year. The Boulby Mine is now open and has been mining sylvinite since 1973.

In the late 1960's Rio Tinto Zinc, through its subsidiary Yorkshire Potash Ltd. (Y.P.L.), was re-investigating the area south-east of Whitby (Figure 1.1), around Robin Hood's Bay, for potassium salts. In May, 1970, Y.P.L. was granted permission to begin conventional mining within that area. Mining has not yet commenced.

The planning permission for mining in the W.P.L. and Y.P.L. concession areas has recently expired and these companies are having difficulty renewing them due to a local environmentalist lobby. In March, 1977, Shell sold its interest in W.P.L. to Consolidated Goldfields Ltd.

The general character and petrology of the potassium salts of north-east England, found during this exploration period, have been described by various authors, the most important of which are Stewart (1949; 1951a,b; 1956; 1963a), Fleck (1950), Armstrong et al. (1951) and Raymond (1953). Much reference will be made to these authors in the text of this thesis.

II Palaeogeography, Tectonic Setting and Summary of the Stratigraphy of the English Zechstein

In Permian times north-east England lay on the western margins of a subsiding intracratonic basin occupying broadly the area of the present North Sea and parts of continental Europe (Figure 1.2). This depression stretched from Cleveland to the Baltic Sea

and south into Germany and Poland. To the north and west the basin was flanked by the eroded Caledonian landmass whilst to the south it abutted the Variscan mountain chain which stretched from Ireland, through Belgium to the present Bohemian Mountains. The Ferro-Scandian-Russian Shield formed the eastern margin of the depression.

Sedimentary facies distribution suggests that the basin was subject to syn-sedimentary subsidence throughout the Permian and much of the Mesozoic. The areas of relatively slower subsidence (for example the Mid North Sea High, Taylor and Colter, 1974; Billingham Ridge, Smith, 1974) had a profound influence over the course of sedimentation for much of the Permian and they probably acted as minor barriers within the basin itself.

In the Lower Permian the centre of the basin lay in approximately the middle of the present southern North Sea Basin. The rocks comprise breccias, sands, sandstones, siltstones and evaporites and their distribution is closely related to the landsurface of the time. Breccias are found flanking areas of slightly elevated ground, for example in north-east England, whilst aeolian sands occupy much of the lower ground. Towards the centre of the depression red siltstones and mudstones were deposited sometimes in association with lacustrine evaporites (Brunstrom and Walmsley, 1969; Glennie, 1972; Marie, 1974). Glennie (1972) showed that the disposition of the rock types is very similar to that found in present

day deserts, particularly those receiving inland drainage. By the end of the Lower Permian it is probable that much of the basin was below contemporary sea level.

The beginning of the Upper Permian was marked by the flooding of this inland desert depression and the creation of the Zechstein Sea. It is most probable that marine conditions prevailed from the north with the Boreal Sea overlapping part of the low lying Caledonian "bar". There is little evidence to suggest that the Zechstein Sea was connected, via the Carpathians, to the Tethys Sea which lay to the south.

It has been suggested by Smith (1970) that the initial marine incursion was very rapid, as there has only been a small amount of redistribution of the aeolian sands beneath. The Zechstein Sea initially inundated the lower parts of the land surface and then encroached on the higher parts.

Subsequent sedimentation patterns for the Upper Permian were controlled by the configuration of the basin floor, a series of sea level fluctuations of possible glacio-eustatic origin (Smith, 1970) and the arid climate (palaeolatitude 20 - 30N) of the time. The delicate interplay of these factors led to the development of four definite evaporite cycles (The Don, Aislaby, Teesside and Staintondale Groups in north-east England, see Table 1.1) and possibly a fifth (recognized by Stewart (1954) and Smith (1974) in England and Dr. C. Kåding

(pers. comm.) in Germany) in the Zechstein basin. In the English Sector of the North Sea all of the cycles except the fifth have a basal carbonate, which is overlain by sulphate rocks. Halite is developed in the second, third and fourth cycles and carnallite and sylvite are also present in the third and fourth cycles.

The sediments of the first two cycles formed prograding wedges off the neighbouring landmasses (Figure 1.3) but by the end of the second cycle the basin was filled in spite of differential subsidence. In the third and subsequent cycles sediments accumulated more uniformly in the space provided by further subsidence and minor sea level changes. During this time the surrounding landmasses were much reduced, giving rise to negligible depositional slopes. Smith (1974) has suggested that the Zechstein Sea was no more than a few metres deep by the end of the third Zechstein evaporite cycle (Teesside Group). Towards the end of the Upper Permian the Zechstein Sea was reduced to a series of separated or linked lagoons which were infilled and covered by Triassic epicontinental sandstones and mudstones.

Rhys (1974) has correlated the Zechstein evaporites of north-east England (Table 1.1) with those of north Germany; the Don Group in north-east England is equivalent to the Werra Series in Germany; the Aislaby Group is equivalent to the Stassfurt Series; the Teesside Group correlates with the Leine Series and the Staintondale

	CENTRAL YORKSHIRE	MID-EAST YORKSHIRE	YORKSHIRE COAST	CYCLES	
Upper Permian	Lower Mottled Sandstone	Lower Mottled Sandstone	Lower Mottled Sandstone		Sherwood Sandstone Group
	Permian	Permian Upper Marls with evaporite-solution residues at base	Saliferous Marl		Eskdale Group
			Top Anhydrite	EZ5	
			Sleights Siltstone		
			Upper Halite and Upper Potash		
	Upper	Upper Anhydrite	Upper Anhydrite	EZ4	Staintondale Group
	Marls	Upgang Formation	Upgang Formation		
		Carnallitic Marl	Carnallitic Marl		
	Upper Magnesian Limestone	Boulby Halite	Boulby Halite and Boulby Potash	EZ3	Teesside Group
		Billingham Main Anhydrite	Billingham Main Anhydrite		
		Upper Magnesian Limestone	Upper Magnesian Limestone		
	Permian Middle Marls	Middle Marls = Fordon Evaporites	Fordon Evaporites	EZ2	Aislaby Group
		Kirkham Abbey Formation	Kirkham Abbey Formation		
		Hayton Anhydrite	Hayton Anhydrite	EZ1	Don Group
Lower Magnesian Limestone (Upper)					
Hampole Beds	Lower Magnesian Limestone -----	Lower Magnesian Limestone -----			
Permian Lower Marls	Lower Magnesian Limestone (Lower)				
Lower Permian		Marl Slate	Marl Slate		
	Basal Permian (Yellow) Sands and Breccias				

Table 1.1 Correlation of Permian strata in north-east England (after Smith, 1974)

Group is equivalent to the Aller Series.

III The Boulby Mine

The Mine is situated near the east coast a few miles east of Loftus (N.G. 715185; Figures 1.1 and 2.1) to take advantage of the onshore and offshore high grade sylvinite deposit of the third Zechstein evaporite cycle at a depth of 1100 to 1200 metres. The site is also the most suitable for ease of access and local amenities.

The surface installations cover an 80 acre site and include mine shafts and ore treatment plant and a rail loading facility. Conventional room and pillar mining techniques are employed. Currently sylvinite is mined using both explosive and continuous mining techniques, but in the future it is hoped to use only the latter.

The sylvinite is partially crushed underground before being carried to the surface where, after further crushing, in an impact crusher and rod mills, the KCl is separated from the halite and insoluble material (Figure 1.4) by a froth flotation technique. The product is then dried and screened before being graded for industrial use. The waste material is discharged 1770 metres offshore by a sub-marine tunnel.

The finished products are carried by rail to C.P.L.'s port facility on the South Bank of the River Tees where they are dispatched to British and overseas destinations.

IV The Scope and Objectives of Part I of the Thesis

The Boulby Mine has exposed an almost complete section of the third Zechstein evaporite cycle comprising, in ascending order, the upper part of the Upper Magnesian Limestone, the Billingham Main Anhydrite, the Boulby Halite, Boulby Potash and Boulby Shale.

In the Mine there is excellent three dimensional exposure of the upper part of the Boulby Halite, the Boulby Potash and Boulby Shale. These beds have never before been exposed for a three dimensional geological examination in north-east England.

The aim of Part I of this thesis is, therefore, to describe the geology, mineralogy, petrology and boron geochemistry of the rocks of the upper part of the Boulby Halite, the Boulby Potash and Boulby Shale exposed in the Mine and in the boreholes from the C.P.L. concession area. These studies have enabled the writer to contribute to the understanding of the geological history of these rocks which is of considerable importance to the extraction of the potash ore.

It has also been possible to use the geological observations made in the Mine to suggest possible structures to account for the sequences of rocks observed in the boreholes. Where relevant, the rocks examined in this study are compared with other salt deposits throughout the world and interpreted in the light of chemical phase equilibria studies.

CHAPTER 2

THE STRATIGRAPHY AND STRUCTURES OF THE UPPER PART OF THE BOULBY HALITE, THE BOULBY POTASH AND THE BOULBY SHALE

I Introduction

This chapter describes:-

(i) the stratigraphy of the upper 10 metres of the Boulby Halite, the Boulby Potash and the Boulby Shale exposed in the C.P.L. concession area, and

(ii) the structural geology of these rocks in the Mine.

In an area where the rocks are known to have flowed the stratigraphy can only be safely determined in conjunction with a knowledge of the structural geology. The localities and cross-sections of the boreholes are shown in Figure 2.1 and Plate I (back envelope) respectively.

The borehole cross-sections in Plate I have been constructed from logs compiled by the writer whilst making a detailed examination of the rocks. The well-logs are presented in Appendix 1. The structural interpretations of the borehole sequences are given in Appendix 2 as, although they are of considerable commercial importance, they do not add to our knowledge of the geological history of the rocks. All the geological field observations and samples collected in the Mine come from roadways developed by 10th January, 1977.

Figure 2.2 shows a plan of the underground mine workings and explains the method of naming localities. The important underground service areas of the Mine (i.e. control room, work shops, etc.) are marked in the map. No. 1 shaft is used for carrying potash ore to the surface, whilst No. 2 shaft is for lifting men and materials.

Mine datum is 2000 metres below mean sea level (M.S.L.), although the majority of the workings are approximately 1100 metres below this.

II General Stratigraphy of the Rocks Exposed in the Mine

The Mine exposes rocks of the third Zechstein evaporite cycle from the top of the Upper Magnesian Limestone to the base of the Rotten Marl. These rocks have a regional dip of 5° in a south-easterly direction.

The rocks of the upper part of the Boulby Halite, the Boulby Potash and the Boulby Shale are intensely deformed in parts of the Mine and the C.P.L. concession area and this has resulted in much variation in the vertical sequence and thickness of strata. However a complete sequence of strata is exposed, in the correct order, in parts of the Mine and in borehole S-20 which was drilled on the site of No. 2 Shaft (Woods, 1973). Table 2.1 shows the general stratigraphy observed in borehole S-20. A general north-south cross-section of

Table 2.1

The stratigraphic units of the third Zechstein evaporite
cycle of the S-20 borehole and the Boulby Mine

<u>Stratigraphic unit</u>	<u>Depth below O.D. in S-20</u>	<u>Thickness in S-20</u>
	1203.7 m.	
Boulby Shale		1.3 m.
	1205.0 m.	
Boulby Potash		3.3 m.
	1208.3 m.	
Boulby Halite		43.4 m.
	1251.7 m.	
Billingham Main Anhydrite		17.0 m.
	1268.7 m.	
Upper Magnesian Limestone		28.3 m.
	1297.0 m.	

the succession and a plan and description of where these units outcrop in the Mine are shown in Figures 2.3 and 2.4 respectively.

The Upper Magnesian Limestone is a uniform, bedded, grey-brown, argillaceous dolomite containing laminae of organic matter. In the uppermost 1.5 metres it has well developed ripple laminae. It makes a sharp contact with the overlying Billingham Main Anhydrite.

The Billingham Main Anhydrite is predominantly a crystalline, fine grained, grey anhydrite rock with occasional beds of dolomite and halite. A few nodular anhydrite beds occur in the lower part of the sequence.

The Boulby Halite is a coarse grained, clear to grey halite rock with some bands of orange halite and minor quantities of anhydrite and clays. The anhydrite content increases towards the base. In the uppermost metre a grey-green halite-clay rock is sometimes developed which is often veined by halite from below. The contact with the overlying Boulby Potash is usually sharp but may be brecciated.

The Boulby Potash is a banded, medium grained, grey to red sylvinite which contains fragments of anhydritic clay. The contact of the Boulby Potash and the overlying Boulby Shale varies from sharp to intensely brecciated depending upon the amount of movement that has taken place. This will be discussed in greater detail later in the chapter.

The Boulby Shale is composed of shales and siltstones which vary in composition both vertically and laterally. Some of the rocks in this stratigraphic unit are now dominantly composed of halite, although it is probable that this has replaced original shales and siltstones. The contact of the Boulby Shale with the overlying Rotten Marl is almost always brecciated as a result of movement.

III Stratigraphic Terminology

Throughout the text reference will be made to "the rocks (or beds) of the upper part of the Boulby Halite, the Boulby Potash and the Boulby Shale", these being the units which have been studied in this thesis. For brevity these units will be referred to as "the sequence examined". The beds of the upper part of the Boulby Halite and the Boulby Shale have been given the abbreviated symbols shown in Table 2.2 for clarity and ease of reading.

IV Derivation of the lithostratigraphy of the sequence examined

These rocks have been subject to extensive diagenetic and post-burial modification by brines and various forms of tectonic activity. Plate I, to which the reader is referred throughout this section, shows that the strata do not occur in the same order in the different boreholes

Table 2.2

The lithostratigraphy of the sequence examined in the
Boulby Mine and C.P.L. concession area

Cycle	Zone	Subzone	Subzone symbol (where used)	Thickness
EZ4	Rotten Marl	Red Marl	-	up to 31.52 m.
		Grey Marl	-	0.0-0.9 m.
EZ3	Boulby Shale	Grey anhydrite- clay shale	B.S.6	0.0-0.12 m.
		Halite-anhydrite- clay rock	B.S.5	0.0-0.75 m.
		Anhydritic shale/ siltstone	B.S.4	0.0-9.3 m.
		Borate Nodule Bed	B.S.3	0.2-0.8 m.
		Anhydrite-halite band	B.S.2	0.0-0.07 m.
		Black sylvite- halite-clay shale	B.S.1	0.0-0.2 m.
	Boulby Potash	Sylvinite	-	0.0-13.4 m.
	Boulby Halite	Grey-green halite- clay rock	B.H.2	0.0-1.0 m.
		Coarse grey-brown halite rock with pink-white halite bands	B.H.1	4.0 m.

and this is also true of the Mine. Nevertheless it has been possible to derive the original sequence of strata observed in the C.P.L. concession area and this is shown in Table 2.2.

(1) Problems encountered in determining the lithostratigraphy

There have been 3 major problems in determining the lithostratigraphy of these rocks in the Mine and C.P.L. concession area:-

- (i) observational limitations,
- (ii) the modification of the rocks by brines, and
- (iii) problems of tectonic origin.

(i) Observational limitations:- In the Mine the majority of the roadways (average height 3 metres) have been worked in rocks from the upper part of the Boulby Halite to bed B.S.4. Consequently the thickness and nature of the contacts between the strata overlying bed B.S.4 have only been recorded from boreholes.

The boreholes expose a full sequence of strata, but one is unable to observe lateral changes in the rocks which are known to occur over a few metres in the Mine. In the case of some boreholes, therefore, it has not been possible to provide a unique interpretation of the strata.

(ii) The modification of the rocks by brines:- The

rocks of the Boulby Shale have been modified by:-

- (a) KCl-NaCl rich solutions percolating up from the Boulby Potash and forming sylvinite veins, and subsequently by
- (b) solutions of uncertain origin from which halite was precipitated. This halite has frequently replaced and very possibly displaced pre-existing minerals.

In the boreholes it has been difficult, and in some cases impossible, to distinguish between sylvinite of the Boulby Potash and recrystallized vein sylvinite. The previous character and nature of the contacts between some strata have been difficult to establish because of the intensity of halite replacement/displacement. In the boreholes, in particular, detailed microscopic examination of these rocks has often been necessary.

(iii) Problems of tectonic origin:- The rocks of the sequence examined have firstly been subject to plastic deformation which has caused them to flow laterally and secondly the Boulby Potash has been subject to gravity deformation. Lateral flow has resulted in the formation of almost horizontal overfolds and overthrusts. The Boulby Potash has risen up into, and in some cases passed through, the Boulby Shale as a consequence of gravitational uplift.

The thickness of the individual beds varies considerably because of the lateral flowage and

gravitational deformation and in all cases it has only been possible to state the range in thickness of a given bed. The original thicknesses of the beds are unknown.

(2) Derivation of the lithostratigraphy

(a) The upper part of the Boulby Halite

Bed B.H.1 (Table 2.2.) is immediately overlain by Boulby Potash in most of the roadways in the Mine which expose the contact between these two rocks. However at a few localities, for example roadway 1W, 42 metres south of 2S and roadway 1W, 44 metres south of 1S, elongate lenses (7 metres long and 1 metre thick) and breccias of rounded fragments (up to 0.4 metres in diameter) of bed B.H.2 outcrop sandwiched between bed B.H.1 below and the Boulby Potash above. The presence of slickensides and well developed gneissoze textures in the rocks of B.H.1 below the Boulby Potash indicate movement has taken place along this contact in the Mine.

Bed B.H.2 directly overlies bed B.H.1 in boreholes Y, U, V-D1, L and S-20, occurs as inclusions in B.H.1 in borehole A, and as inclusions in the basal rocks of the Boulby Potash in boreholes X, V-D1, L and S-20. Plate I shows that in the boreholes rocks adjacent to the contact between the Boulby Halite and the Boulby Potash are often slickensided.

These observations in the Mine and the boreholes strongly suggest that bed B.H.2 was originally deposited over the whole C.P.L. concession area and that it has subsequently been subject to large scale tectonic deformation which has often resulted in its complete removal from the stratigraphic sequence.

The thickness of bed B.H.2 ranges from 0.00 - 1.00 metre in the Mine and the boreholes. However in borehole Y, where it is 1.00 metre thick, its upper and lower contacts are sharp and show few signs of movement and this may represent the minimum original thickness of the bed in this area.

(b) The Boulby Potash

The unit is recognized in most of the Mine and in all the boreholes. It is only absent in a few areas of Panel No. 1 in the Mine where it is known to have flowed laterally and risen by gravity tectonics. The unit varies in thickness from 0.0 to 10.0 metres in the Mine and 0.0 to 13.4 metres in the boreholes. In the few areas of the Mine where there is little tectonic deformation the bed makes a sharp contact with the overlying rocks of the Boulby Shale.

(c) The Boulby Shale

α) Beds B.S.1 and 2

In the Mine these beds outcrop between the Boulby Potash and bed B.S.3 in roadway K of the South Spearhead and in roadways D and No. 1 cross-cut south off L in the East Spearhead. Bed B.S.2 is also found as inclusions in breccias in Panel No. 1. In much of the remainder of the Mine the Boulby Potash is directly overlain by bed B.S.3; the contact frequently being slickensided. It, therefore, seems likely that beds B.S.1 and 2 have been obliterated by lateral flowage.

The above rocks are also absent from the boreholes except for an inclusion of bed B.S.2 at the base of the sylvinite in borehole M which is situated 2.5 km. south-east of the Mine (Figure 2.1). These beds may originally have been deposited over the whole area and may be absent where the rocks have been subject to tectonic activity, but equally, they may not have been deposited throughout the area.

β) Beds B.S.3 and 4

Bed B.S.3 outcrops in the Mine wherever the Boulby Shale is exposed except in areas of extensive brecciation caused by overfolding and gravity deformation (Panel No. 1). It varies in thickness from 0.2 to 0.8 metres in the Mine and grades upwards into bed B.S.4.

Boreholes A, B, C, V and S-20 expose these beds

directly overlying the Boulby Potash. In boreholes D, M and L bed B.S.4 is observed veined by fibrous sylvinite. Bed B.S.4 is recognized as rounded inclusions in the Boulby Potash in boreholes U, F, V-D1, and M-D2 and is absent from boreholes X and Y. Although bed B.S.3 is only present in 5 boreholes these are sufficiently far apart as to suggest that it is a subsurface feature throughout the C.P.L. concession area. It has probably been eliminated in the other boreholes by tectonic deformation for which there is abundant evidence in the Mine. The presence of bed B.S.4 in all the boreholes except X and Y indicates that it subcrops over the entire C.P.L. concession area.

The nature of the contact between beds B.S.4 and 5 has only been observed twice in the Mine and boreholes. A sharp undulating contact was viewed immediately beneath the roof in No. 1 cross-cut north off 4a in Panel No. 2 of the Mine (Figure 2.2) and in borehole V. The contact has been obliterated by replacive halite in borehole S-20.

8) Bed B.S.5

The fact that this bed overlies bed B.S.4 in areas of relatively undeformed rock in No. 1 cross-cut north off roadway 4a in Panel No. 2 and in the nearby S-20 borehole (No. 2 Shaft) in the Mine strongly suggests that this is the original order of the strata. This is reinforced by the recognition of this sequence in

borehole V which is situated 2 km. south-east of the Mine (Figure 2.1). This bed is brecciated, or out of sequence, most probably because of tectonic activity, in all the other boreholes, but its widespread presence in the boreholes strongly suggests that it subcrops over the entire C.P.L. concession area.

The unit ranges in thickness from 0.00 - 0.75 metres in the boreholes. In many cases this rock type has been almost completely replaced or displaced by clear halite and is only recognized by the presence of remnant deep red halite porphyroblasts.

5) Bed B.S.6

This rock type is only observed in borehole S-20 where it has a gradational contact, over 2 cm., with the underlying unit. It is impossible to tell if this bed was ever deposited over the entire C.P.L. concession area. It has a sharp contact with the overlying grey marl.

(d) The lowermost rocks of the Rotten Marl (Carnallitic Marl)

The stratigraphy and distribution of these rocks are considered here because they are often found as inclusions in the Boulby Potash and Boulby Shale. The base of the Rotten Marl is taken as the lower contact of the Grey Marl (Smith, 1974).

a) Grey Marl

This bed is only observed in the Mine in occasional Rotten Marl downslumps into the Boulby Shale and Boulby Potash. It forms a discrete bed at the base of the Rotten Marl in boreholes X, Y, V and S-20. It is also found as fragments in the rocks of the Boulby Shale in boreholes D, V, V-D1, M and L. The widespread occurrence of this bed strongly suggests that it subcrops over the entire C.P.L. concession area.

Where the unit forms a bed in the boreholes it is usually only a few centimetres thick except in S-20 where it is 0.9 metres thick. Although the original thickness of the bed is unknown the presence of rounded fragments of it, up to 10 cm. in diameter, in the Boulby Shale suggests that the bed was at least 10 cm. thick after deposition.

The bed is observed to make sharp, slickensided, and brecciated contacts with the overlying red marl in the boreholes.

β) Red Marl

This bed is only observed in the Mine, at a distance, in blowholes and downbulges into the Boulby Shale and Boulby Potash. It is, however, found in all the boreholes capping the grey marl or the rocks of the Boulby Shale. It has, therefore, a widespread occurrence in the C.P.L. concession area and varies in thickness from

0.00 to 31.52 metres.

V Structural Geology

The following structural elements have been observed in the sequence examined in the Mine:-

- (i) Red fibrous sylvinite veins in the Boulby Shale and overlying rocks,
- (ii) Overfolds and overthrusts,
- (iii) Small scale swells and depressions along the upper contact of the Boulby Potash, and
- (iv) East-west trending monoclines.

Slickensides are associated with all these structural features and are not considered separately. A map of these structures is shown in Plate II.

(1) Sylvinite Veins

Red fibrous sylvinite veins, which are believed to originate from the Boulby Potash, cross-cut all the rocks from the Boulby Potash to the base of the Upper Anhydrite of the Staintondale Group. These veins are observed in all the areas of the Mine where the Boulby Shale outcrops (Figure 2.4). There is, however, much lateral variation in the intensity of veining in the Boulby Shale with the veins composing over 50% of some rocks. No areal pattern to the intensity of veining was recognized. Figure 2.5 shows typical recrystallized fibrous sylvinite

veins cross-cutting the Boulby Shale in Panel No. 1.

The fibrous sylvinite veins are rarely seen emanating from the Boulby Potash because extensive lateral movement, caused by subsequent overfolding, has brecciated the original contact or completely removed the basal rocks of the Boulby Shale. However the Boulby Potash is a deep red colour where the veins are observed rising out of it (Figure 2.6). The veins rise vertically and the fibres are frequently perpendicular to the walls. When the veins are 10 to 30 cm. above the Boulby Potash they sometimes curve and branch.

The majority of the veins range from 1 to 10 cm. in width although the walls are occasionally up to 60 cm. apart. Most of the veins have recrystallized and exhibit a granular texture because of movement subsequent to their formation. However some sylvinite veins cross-cut slickensides of minor lateral extent (Figure 2.7) whilst others have accumulated beneath these slickensides (Figure 2.8 and Plate III).

There are two types of fibrous sylvinite vein in areas of less deformed rocks:-

- (i) Steeply inclined veins (over 45°) in which the fibres are almost horizontal, and
- (ii) gently inclined veins in which the fibres are frequently almost vertical.

It is not uncommon for a gently inclined vein to bend around and become steeply inclined, or vice versa, with

the consequent change in orientation of the fibres.

The walls of the veins are usually planar or crenulated. However in a few cases the walls grade laterally from planar to crenulated within the same vein. The walls of some veins are also markedly slickensided. The sylvite and halite fibres, which are up to 1.5 mm. in width, are sometimes straight and vary from gently to steeply inclined to the vein walls. In many veins, however, the fibres are curved and oblique to the vein walls (Figure 2.9).

A small number of fibrous sylvinite veins contain inclusions of their host rock. These inclusions are rounded to angular and up to 5 cm. in maximum dimension. In contrast the recrystallized sylvinite veins contain many inclusions of the host rock.

The sylvinite veins do not contain any cavities and the fibrous habit of the sylvite and halite crystals, although uncharacteristic, does not indicate that the minerals grew off the edges of an open fissure or vag. Durney and Ramsey (1973) have observed similar fibrous veins in the rocks of the Helvetic Nappes of Switzerland. They have shown that these fissures become filled with crystalline material by solution and diffusion of matter from the surrounding rocks and that the fibrous habit of the minerals is controlled by the incremental dilation of veins during stress. Durney and Ramsey (1973) further suggested that the direction of growth of the crystals

in the veins, and hence the crystal habit, is controlled by the orientation of the least principal stress at the growth surface. There the least work is done against the external stress system when growth occurs in that direction. Any change in the direction of minimum stress causes the fibres to grow in a different direction and leads to the development of curved fibres. It seems likely, therefore, that the KCl-NaCl solutions from the Boulby Potash percolated or diffused into fissures as they formed in the overlying rock and sylvite and halite crystals grew in the direction of least stress.

(2) Overfolds and Overthrusts

The structures which have been interpreted as almost horizontal overfolds and overthrusts occur in the eastern part of the East Spearhead and in Panel No. 1 (see Plate II). The main problem encountered in observing and interpreting these structures has been the very restricted outcrop afforded by the roadways in this area of the Mine. The majority of the roadways have only been driven in the Boulby Shale because it is highly enriched in sylvinite veins and also because the Boulby Potash is attenuated in this area of the Mine. However a few localities have revealed much of the structures.

(a) Geological observations

The east end of roadway B in the East Spearhead:-

In Figure 2.10A it can be seen that the Boulby Potash and rocks of the Boulby Shale are mirrored about the Boulby Halite at this locality. The Boulby Halite is highly gneissoze and has sharp slickensided upper and lower contacts with the Boulby Potash which also has a gneissoze fabric and contains many small rounded inclusions (up to 3 cm. in diameter) of anhydritic shale /siltstone (bed B.S.4). These inclusions are particularly abundant along the contact between the Boulby Potash and the Boulby Shale. In this area of the Mine the rocks of the Boulby Shale are not brecciated but they are markedly slickensided. Unfortunately the vertical roadway walls have prevented the measurement of the direction of slickensiding in the Boulby Halite and Boulby Shale. All these features suggest that the rocks have been deformed by a process which has led to bed repetition.

Roadway G, east of No. 6 cross-cut in the East Spearhead and the rocks of Panel No. 1:-

Figure 2.11A shows that in roadway G, east of No. 6 cross-cut the Boulby Potash outcrops in the middle of the Boulby Halite and is also present as a bed high above the roof of the roadway. The thickness of the lower

potash bed varies irregularly from 0.3 to 2.0 metres. The tail of the potash is abruptly terminated by the halite although there are a few inclusions (0.1 mm. in maximum dimension) of potash in the halite (Figure 2.11B). The lower contact between the potash and halite is irregular but sharp. However the upper contact between the potash and the pink-white halite band is serrated with each "tooth" being approximately 5 cm. long and inclined at a low angle (Figure 2.11B). In Figure 2.11C the pink-white halite band is sharply truncated by the potash. In places the halite and potash have gneissoze fabrics.

The lower potash bed observed between No. 8 cross-cut north and No. 8 cross-cut south of roadway G (Figure 2.11D) is directly overlain by a breccia of sylvinite veined anhydritic shale /siltstone (Boulby Shale) 0.5 metres thick. The shale fragments (50% of the rock) of the breccia are rounded to angular (maximum dimension 5 cm.) and are set in a matrix of partially recrystallized fibrous sylvinite veins. The lower contact of the breccia with the potash is sharp and highly slickensided whilst the upper contact with the halite is gradational over 5 cm. It is not possible to tell if the brecciated anhydritic shale/siltstone overlies the lower potash bed in the roof of the roadway because the high proportion of sylvite in the rock would cause it to be recorded on

the gamma ray probe* as "Boulby Potash". The anhydritic shale/siltstone is completely absent, however, in the tail regions of the lower potash bed.

The lower bed of the potash in roadway G can be traced laterally into roadway H. However the roadways further south and east in the East Spearhead and Panel No. 1 have all been driven further up the succession in the upper beds of the potash and Boulby Shale which are high above the roofs of roadways G and H (Figure 2.11A).

The potash in Panel No. 1 varies in thickness from 0.0 to 1.0 metres except at the junction of roadway L and No. 7 cross-cut south where it is 5 metres thick. In Panel No. 1 the contact between the potash and Boulby Shale is often slickensided. The Boulby Shale is extensively brecciated and frequently composed of rounded to angular blocks (up to 2 metres in maximum dimension) set in a matrix of recrystallized sylvinite veins. The majority of these fragments, however, range from 0.5 metres in width downwards as shown in Figure 2.12.

* The gamma ray probe is an instrument used to measure the percentage of KCl in the rock. It measures the amount of gamma radiation emitted from the rock as the K^{40} isotope breaks down to Ar^{40} . The amount of gamma radiation is approximately proportional to the percentage of K in the rock.

The vertical roadway walls have often precluded measurement of the direction of slickensiding along the contact between the potash and the Boulby Shale in Panel No. 1. In areas where these rocks are unaffected by the development of swells in the top of the potash the slickensides have a north-east to easterly trend. However in the majority of cases several generations of slickensides override each other, possibly indicating many phases of movement.

No boreholes were drilled in the floors of the roadways in the eastern part of the East Spearhead and Panel No. 1 to determine the lateral extent of the lower Boulby Potash bed observed in roadways G and H.

No. 5 cross-cut between roadways R and T in the East Spearhead:-

Figure 2.13 shows a cross-section of the rocks observed at the locality in which the Boulby Potash and Boulby Shale fold around a nose of Boulby Halite. The halite is a coarse grey-white partially gneissoze halite rock which has sharp unslickensided contacts with the potash above and below it. The potash has a pronounced gneissosity and sharp, partially slickensided contacts, with the Boulby Shale which is internally slickensided and cross-cut by recrystallized sylvinite veins.

There is little doubt these rocks have been subject

to extensive lateral movement and that this roadway has been driven through the nose of an almost horizontal overfold.

(b) Interpretation and discussion

The tight fold closure observed in No. 5 cross-cut between R and T strongly suggests that the rocks from the upper part of the Boulby Halite to the Boulby Shale have been overfolded. The mirroring of the beds about the Boulby Halite at the end of roadway B in the East Spearhead (Figure 2.10) can also readily be interpreted as a section through an overfold. Figure 2.10B illustrates the probable mode of development of an overfold in these rocks and indicates the part of the succession that is observed at the end of roadway B in the East Spearhead.

The repetition of the Boulby Halite and the Boulby Potash in roadway G of the East Spearhead is compatible with the upper part of the Boulby Halite being thrust over the Boulby Potash (Figure 2.11E). A very low angle overthrust such as is shown in Figure 2.11E would cause the Boulby Halite to first overstep the Boulby Potash and then the Boulby Shale as is observed in roadway G (Figure 2.11A).

Although there are numerous signs of extensive movement along the contact between the lower bed of the

Boulby Potash and the overlying Boulby Halite (i.e. the thrust plane) it is surprising that no large scale slickensides have developed such as occur in the Boulby Shale in Panel No. 1. This might indicate recrystallization subsequent to movement. In the Neuhoef-Ellers Mine, in the Werra-Fulda region of West Germany, halite and sylvinite rocks are similarly extensively overfolded and their contacts are also rarely slickensided (Roth, 1972; and personal observations).

It was neither possible to determine how the overfolds and overthrusts grade into one another laterally nor to measure the orientation of the axes of these structures. However the disposition of the overfolds and overthrust and direction of slickensiding (north-east to east) suggest that the axes are approximately orientated north north-west to south south-east and that they lie in an almost horizontal plane. Further development of the Mine should help to clarify these points.

(3) Swells and depressions in the top of the Boulby Potash

Small swells and depressions occur in the top of the Boulby Potash which have axes orientated at $024^{\circ} \pm 10^{\circ}$ from true north (see Plate II). The swells usually have an amplitude of 1 to 2 metres but amplitudes up to 5 metres are occasionally recorded. The distance between

crests of adjacent swells, observed by the writer, varied from 15 to 25 metres although Talbot (1975) has recorded swells with wavelengths of 30 metres. There are minor undulations in the base of the Boulby Potash where swells and depressions are developed in the top of the bed. Figure 2.14 shows a typical swell observed in the South Spearhead.

Slickensides are frequently extensively developed on the slopes of the swells normal to the swell axes and these are sometimes superimposed on pre-existing slickensides. However in a number of depressions slickensides occur parallel aligned with, or at a shallow angle to the swell axes ($024^{\circ} \pm 10^{\circ}$) and these override the slickensides which are normal to the crest of the swells.

On the basis of the evidence available by 10th January, 1977, it is not possible to conclusively prove whether these small scale swells and basins developed at the same time as the overfolds and overthrusts or some time afterwards. The fact that the slickensides normal to the crests of the swells override pre-existing slickensides, some of which are orientated in a north-easterly direction, suggest that the swells post-date the overfolding and overthrusting. It is also unlikely that swells would develop only in the top of the Boulby Potash at the same time as overfolds and overthrusts.

Talbot (1977) has examined the workings developed

since January, 1977. He has suggested, by comparison with experimentally developed gravitational structures (Ramberg, 1972), that where the Boulby Potash is overlain by Boulby Shale the latter has sunk into the Boulby Potash because of its greater density. This has caused the Boulby Potash to move laterally and upwell into these small ridges and in some cases migrate up and through the Boulby Shale. This is true for the Boulby Potash in both lower and upper limbs of the overfolds. These observations confirm the suggestion that the swells must have developed after overfolding.

(4) Monoclines

The monoclines are gently dipping structures (5°) at the base of the Boulby Potash which have an east-west orientation. They are separated by approximately 300 metres in a north-south direction (Plate II).

In the area of the Shafts and in the South Spearhead, where the monoclines are most extensively developed, the contact between the Boulby Halite and Boulby Potash is markedly slickensided and the rock types are often separated by a thin shale parting which may represent the remains of bed B.H.2 (Table 2.2) as shown in Figure 2.15. The slickensides indicate a north-south direction of movement perpendicular to the monoclinal axes.

The monoclines in the Boulby Halite and the Boulby Potash were probably formed in response to overthrusting,

along an east-west axis, in the underlying Upper Magnesian Limestone and Billingham Main Anhydrite. Such an overthrust is shown diagrammatically in Figure 2.3 and in detail in Figure 2.16.

The time of formation of the monoclines is uncertain. However slickensides parallel aligned to the crests of the swells at the top of the Boulby Potash are similarly orientated to the slickensides developed along the contact between the Boulby Halite and the Boulby Potash in the areas of the monoclines. This suggests that the monoclines were formed after the swells and depressions in the top of the Boulby Potash.

(5) Summary of the structural history

The sequence of structural events which have resulted in the present disposition of the beds in the sequence examined will be related to regional tectonic events in the integrated geological history of the beds towards the end of the thesis. The suggested sequence of events is as follows:-

At an unknown depth the rocks from the Boulby Shale to the Upper Anhydrite were stressed and they developed fissures in which sylvite and halite crystals grew as the fissure dilated; the saturated solutions being derived from the Boulby Potash. The beds from the upper part of the Boulby Halite to the Rotten Marl were then overfolded and overthrust as a result of lateral movement

in a north-east to easterly direction. Subsequently small swells and depressions developed along the contact between the Boulby Potash and the Boulby Shale as these units attained gravitational equilibrium. The last phase of movement recognized resulted in the formation of E-W trending monoclines in the base of the Boulby Potash in response to overthrusting in the Upper Magnesian Limestone and the Billingham Main Anhydrite.

The borehole interpretations in Appendix 2 show that the beds of the Boulby Shale have been cross-cut by sylvinite veins and the rocks of the sequence examined have been overfolded in the C.P.L. concession area. It seems probable, therefore, that these beds have undergone the same structural history as those in the Mine. It has not been possible to provide a stratigraphic correlation between boreholes because of the variation in the sequence of beds in individual boreholes.

CHAPTER 3

THE UPPER PART OF THE BOULBY HALITE

The upper part of the Boulby Halite is composed of beds B.H.1 and 2. The character of these beds in the boreholes and the Mine is very similar. It has been possible to deduce much about the reactions which have occurred within them during and since deposition.

I Bed B.H.1

(1) General features

This bed is generally a massive crystalline coarse grey-brown halite rock (Figure 3.1). The unit, which is sometimes poorly colour banded, contains well developed pink-white halite bands near its upper contact with bed B.H.2, variable proportions of shale laminae and white patches of halite rock and sylvinite.

The colour bands, caused by variations in the clay and hematite content of the rock, are poorly developed and vary in colour from white - grey - orange - brown. Their general characteristics are described in Figure 3.2. They differ from the pink-white halite bands because they are of the same composition as the host rock. However Figure 3.3 shows an unusual variety of colour banding

in roadway H of the East Spearhead. The parallel planar grey laminae are connected by inclined laminae, both of which are composed of clay. The halite in the bands between the clays is granular. It was originally thought that these rocks might be tightly overfolded. However in the area of overfolding in the Mine (Plate II) some of the halite crystals are elongate. It is probable that these laminae represent cross-sections through mud cracks which have been slightly tilted by subsequent movement. Polygonal structures, similar to desiccation cracks, were observed in the Boulby Halite by Mr. P.J.E. Woods (pers. comm.) during shaft sinking.

The pink-white halite bands, which occur near the top of this bed throughout the Mine, take the form of 2 to 5 parallel aligned bands 5-10 cm. thick or one thicker band up to 1 metre thick (Figure 3.4). They are often of limited lateral extent and make sharp or diffuse contacts with the host rock. Occasionally these bands contain thin layers (2 cm. thick) of laterally impersistent sylvite crystals which enclose hematite platelets.

Shale laminae, up to 5 mm. thick, form 2 to 10% of this bed. Many of these laminae are crenulated (Figure 3.5) or have been so disrupted by recrystallization of the rock that they occur in interstices between halite crystals (Figure 3.6).

In the South Spearhead patches of white halite rock

and sylvinite, normally occurring in groups of 5 or 6, cross-cut this bed (Figure 3.7). The individual patches, which are irregular in outline and up to 1 metre in maximum dimension, are either almost entirely composed of euhedral halite crystals with accessory sylvite or vice versa. The composition of the patches within a group is random. In some cases the shale laminae in the adjacent rock stop abruptly at the contact with these patches which themselves contain no inclusions of shale laminae. Others, however, contain disrupted fragments of shale laminae.

(2) Petrography

This bed, excluding the pink-white halite bands and the shale laminae, contains halite, sylvite, anhydrite and hematite. The proportions and general characteristics of these minerals are shown in Table 3.1.

The halite crystals in much of this bed define an irregular granular fabric (Figures 3.5 and 3.8) although gneissoze textures do occur in some of these rocks in the area of overfolding in the Mine (Plate II). Halite crystals are frequently elongate where the bed is directly overlain by Boulby Potash. Sylvite grains occur in the interstices between halite crystals (Figures 3.5 and 3.8). Euhedral equant anhydrite crystals, frequently enclosing anhydrite granules, line the boundaries between halite crystals, project from shale into halite crystals, and

Table 3.1 Composition and mineral characteristics of bed B.H.1 excluding shale laminae, pink-white halite bands and patches of halite rock and sylvinite

<u>Mineral</u>	<u>Volume percentage of mineral*</u>		<u>Colour</u>	<u>Grainsize</u>	<u>Crystal shape and form</u>	<u>Comments</u>
	<u>Average</u>	<u>Range</u>				
Halite	85	70-90	White-red-brown	0-20 cm.	Well formed cubes to rounded or elongate crystals	The red halite crystals contain tiny randomly orientated inclusions of hematite platelets whilst those coloured brown contain clays. The majority of the crystals range in size from 0-3 cm. and are granular. They tend to be euhedral towards shale.
Sylvite	10	0-12	Milky white to red	0-3 mm.	Rounded to angular crystals	The red coloration is caused by tiny hematite inclusions which are either evenly distributed or concentrated around the edges of the crystals.

Table 3.1 (cont.)

<u>Mineral</u>	Volume percentage of mineral*		<u>Colour</u>	<u>Grainsize</u>	<u>Crystal shape and form</u>	<u>Comments</u>	
	<u>Average</u>	<u>Range</u>					
Anhydrite	4	0-5	Grey-white	0.0-0.1 mm.	Either euhedral equant crystals or anhedral granules	The euhedral equant crystals are 0.05- 0.1 mm. in grain size and frequently exhibit undulose extinction. The granules are always smaller and often included in the equant crystals.	45
Hematite	tr [†]	-	Red-brown	up to 0.05 mm.	Hexagonal platelets on (0001)	Present as inclusions in sylvite and halite.	

* The composition is based on a modal analysis of 20 thin sections.

† tr = trace.

Table 3.2 Composition and mineral characteristics of the pink-white halite bands in bed B.H.1

<u>Mineral</u>	Volume percentage of mineral*		<u>Colour</u>	<u>Grainsize</u>	<u>Crystal shape and form</u>	<u>Comments</u>
	<u>Average</u>	<u>Range</u>				
Halite	93	85-100	White	0.0-2.5 cm.	Rounded to elongate	
Sylvite	7	0-15	Milky white to red	0.0-2.0 cm.	Rounded to elongate	The red coloration is caused by tiny randomly orientated hematite platelets in the crystals.
Anhydrite	tr [‡]	-	Grey-white	0.0-0.2 mm.	Euhedral equant crystals	The crystals frequently occur in isolation in the halite.
Hematite	tr	-	Red-brown	0.0-0.05 mm.	Hexagonal platelets on (0001)	Present as inclusions in sylvite

* The compositions are based on a modal analysis of 10 thin sections.

‡ tr = trace.

Table 3.3

Evidence for the recrystallization of halite and anhydrite
in bed B.H.1

1. Halite

- (a) Contortion and abrupt termination of the laminae by halite crystals;
- (b) Fragmentation of shale laminae into patches in the interstices amongst halite crystals.
- (c) The development of elongate halite crystals defining gneissoze textures in the area of overfolding (Plate II) and where the bed is in direct contact with the Boulby Potash;
- (d) The inclusion of stringers of euhedral anhydrite crystals which appear to define former outlines of halite crystals.

2. Anhydrite

- (a) Euhedral equant anhydrite crystals containing inclusions of anhydrite granules, project from the edges of shale laminae into halite crystals of the host rock. The euhedral crystals appear to have formed by the recrystallization of the granules.
- (b) The euhedral equant anhydrite crystals which line the boundaries between halite grains often contain inclusions of clay and anhydrite granules.

form stringers which cut across halite grain boundaries.

Comparison of Tables 3.1 and 3.2 shows that the mineral characteristics of the pink-white halite bands are similar to the host rock except that these bands are relatively enriched in halite.

Table 3.3 presents abundant evidence for recrystallization of halite in the pink-white halite bands and the host rock. The majority of the recrystallized halite crystals have a granular habit, despite the fact that extensive development of crenulated shale laminae indicates that lateral movement has been widespread in this bed. This observation together with the fact that slickensides are absent along the thrust plane between the Boulby Halite and the Boulby Potash in roadway G (East Spearhead) strongly suggests that the halite has recrystallized since the phase of maximum movement. The elongate nature of sylvite crystals in some pink-white halite bands testifies to its recrystallization.

The evidence for recrystallization of anhydrite adjacent to, or enclosed in halite, is presented in Table 3.3. Schaller and Henderson (1932), Dunham (1948) and Stewart (1949) have all commented on similar features in halite rocks from Texas, New Mexico and north-east England. Schaller and Henderson (1932) and Dunham (1948) have suggested that these textures indicate recrystallization of anhydrite next to invading halite. However at Boulby there is no evidence that halite has invaded

this bed. The present observations suggest that it is much more likely that the anhydrite recrystallized at the same time as the halite. That the halite grains contain stringers of recrystallized anhydrite crystals suggests that the halite has recrystallized at least twice; the first time forming anhydrite crystals around the halite grain boundaries and a second time in which the halite crystals adopt new grain boundaries, the former halite outlines being preserved as anhydrite stringers.

It is interesting that a gneissoze fabric is sometimes developed in the pink-white halite bands when it does not occur in the adjacent host rock. This presumably reflects the compositional differences between the rocks (compare Tables 3.1 and 3.2). There is no evidence to suggest that the pink-white halite bands are secondary.

In the South Spearhead sylvite crystals containing many randomly orientated hematite platelets are set in a matrix of clays and hematite along the boundary with the clay laminae which contain small granules of carnallite (Table 3.4). The abundance of hematite, which is associated with potassium and magnesium minerals in most other salt deposits, suggests that sylvite might have been formed by the breakdown of carnallite in which iron, in diadochic substitution for magnesium cations, would have been released into solution and precipitated as hematite under oxidizing conditions. If this is the

Table 3.4 Composition and mineral characteristics of the shale laminae in bed B.H.1

<u>Mineral</u>	<u>Volume percentage of mineral*</u>		<u>Colour</u>	<u>Grainsize</u>	<u>Crystal shape and form</u>	<u>Comments</u>
	<u>Average</u>	<u>Range</u>				
Clays	50	40-70	Green-brown	0.00- 0.05 mm.	Elongate platelets	The clay minerals are predominantly illites. They may be parallel aligned or randomly orientated and are intergrown with anhydrite.
Anhydrite	30	15-40	Colourless- grey	0.0- 0.05 mm.	Elongate laths and euhedral equant crystals	The laths are intergrown with clays in the matrix of the laminae. The euhedral equant crystals project into chlorides of the host rock.
Halite	17	15-20	White	0.0-0.5 mm.	Rounded to elongate crystals	These crystals form small porphyroblasts in the clay-anhydrite matrix. They are larger in laminae enriched in anhydrite.

Table 3.4 (cont.)

<u>Mineral</u>	<u>Volume percentage of mineral*</u>		<u>Colour</u>	<u>Grainsize</u>	<u>Crystal shape and form</u>	<u>Comments</u>
	<u>Average</u>	<u>Range</u>				
Camallite	3	1-5	Red	0.0-0.5 mm.	Rounded granules	The mineral occurs in nests (1-2 mm. in width) and is intergrown with hematite and clays. Because of the friable nature of the host clays it was not possible to cut a thin section of the mineral. It was recognized by its astringent taste and R.I.'s.
Magnesite	tr [‡]	-	White-grey	0.0-1.0 mm.	Euhedral to subhedral hexagonal plates tabular on (0001)	3 R.I. measurements gave ω in the range 1.700-1.702, i.e. almost pure $MgCO_3$. The mineral cross-cuts anhydrite and clays to project into the cleavages of chloride minerals in the host rock.



Table 3.4 (cont.)

<u>Mineral</u>	<u>Volume percentage of mineral*</u>		<u>Colour</u>	<u>Grainsize</u>	<u>Crystal shape and form</u>	<u>Comments</u>
	<u>Average</u>	<u>Range</u>				
Quartz	tr	-	White-grey	0.00- 0.05 mm.	Rounded to euهدral	It is euهدral towards chloride minerals but anhedral towards anhydrite and clays. These crystals generally project from the edges of the laminae in the host halite rock.
Hematite	tr	-	Red-brown	0.00- 0.05 mm.	Hexagonal platelets on (0001)	Occurs as inclusions in camallite

* The composition is based on the modal analysis of 15 laminae.

† tr = trace.

Table 3.5Partial analysis of a brine from bed B.H.1*

<u>Constituent</u>	<u>Wt. %</u>
NaCl	6.5
KCl	10.2
CaCl ₂	30.1
MgCl ₂	42.7

* analysis by the staff of the Chemistry Laboratories, C.P.L.

case carnallite was formerly more abundant in this rock type than at the present moment. Alternatively the hematite might have been derived from the clays by extensive leaching by brines.

Small numbers of euhedral quartz and magnesite crystals project from the clay laminae into halite crystals in the host rock. They often contain inclusions of clays, suggesting they formed by the breakdown of clays possibly by reaction with brines.

On the basis of the available evidence, the origin of the white halite rock and sylvinite patches is uncertain. They may originally have formed in the rock at the time of deposition and recrystallized at depth disrupting the shale laminae. Alternatively they may have formed as a result of recrystallization of the bed at depth; the shale laminae being disrupted at the same time as the patches formed.

(3) Residual brines

Small quantities of residual brines have been collected from shot holes and roof bolt holes in this bed. Table 3.5 shows that these brines are enriched in MgCl_2 and CaCl_2 relative to NaCl . The fact that the halite crystals do not contain many fluid inclusions suggests that these brines occur in small cavities in the rocks. It will be shown in Chapter 7 that the composition of these brines is compatible with them being evolved in

this evaporite cycle.

II Bed B.H.2

The majority of thin sections of this bed came from boreholes, particularly S-20, because of the very limited exposure of the bed in the Mine.

The bed is a grey-green halite-clay rock composed of halite porphyroblasts set in a matrix of clays and minor proportions of magnesite and anhydrite (Figure 3.8). The composition of the rock and mineral characteristics are shown in Table 3.6.

It seems most probable that the halite porphyroblasts (Figure 3.9) formed within the clay sediment at the time of deposition or during early diagenesis. They have been slightly flattened by subsequent movement.

Deep red sylvite porphyroblasts occur in the uppermost 0.3 metres of this bed. These porphyroblasts frequently enclose clay matter and halite crystals (Figure 3.10) indicating that they grew contemporaneously or after the halite. This suggests that the sylvite crystals grew by displacement of the host rock. The timing of the displacement is uncertain, although the fact that many of the sylvite porphyroblasts are elongate indicates that they formed before movement of the beds. It seems likely that the displacement reaction would have occurred more easily prior to lithification.

Table 3.6 The composition and mineral characteristics of bed B.H.2

<u>Mineral</u>	<u>Volume percentage of mineral*</u>		<u>Colour</u>	<u>Grainsize</u>	<u>Crystal shape and form</u>	<u>Comments</u>
	<u>Average</u>	<u>Range</u>				
Clays	50	35-70	Green-brown	0.00- 0.05 mm.	Elongate platelets	The clays are dominantly illites which are intergrown in parallel alignment. Where associated with small quantities of carbonaceous matter the clays are black.
Halite	40	20-60	White- pale brown	0.0-5.0 mm.	Cubic to sub-rounded	The majority of the crystals have a maximum dimension of 3 mm. and form porphyroblasts set in the clay matrix.
Sylvite	19	15-21	Red-brown	0.0-6.0 mm.	Subhedral to anhedral crystals	The red-brown coloration is caused by inclusions of tiny randomly orientated hematite platelets. Sylvite only occurs in the uppermost 0.3 metres of the bed.
Anhydrite	10	3-12	Grey-white	0.0-0.1 mm.	Euhedral equant crystals	Anhydrite forms small pockets of crystals in the clay matrix.

Table 3.6 (cont.)

<u>Mineral</u>	<u>Volume percentage of mineral*</u>		<u>Colour</u>	<u>Grainsize</u>	<u>Crystal shape and form</u>	<u>Comments</u>
	<u>Average</u>	<u>Range</u>				
Magnesite	tr [†]	-	White-grey	0.0-1.0 mm.	Euhedral to subhedral hexagonal platelets tabular on (0001)	3 R.I. measurements gave ω in the range 1.703-1.705, i.e. almost pure MgCO ₃ . The mineral projects from the clays into the cleavages of the halite porphyroblasts. It probably formed by the breakdown of clays.
Quartz	tr	-	White-grey	0.00-0.05 mm.	Rounded to euhedral crystals	The crystals are euhedral towards the halite porphyroblasts and anhedral towards clays. They often contain inclusions of clays suggesting they formed by the breakdown of clays, possibly by reaction with brines.
Pyrite	tr	-	Black	0.01 mm.	Well to poorly formed octohedra	The mineral occurs singly or in small aggregates (0.05 mm.) associated with carbonaceous material.

Table 3.6 (cont.)

<u>Mineral</u>	Volume percentage of mineral*		<u>Colour</u>	<u>Grainsize</u>	<u>Crystal shape and form</u>	<u>Comments</u>
	<u>Average</u>	<u>Range</u>				
Hematite	tr	-	Red-brown	0.00- 0.05 mm.	Hexagonal platelets on (0001)	The mineral surrounds inclusions of clay in the sylvite porphyro- blasts, suggesting it has been derived by the breakdown of clays.
Carbona- ceous Matter	tr	-	Black	-	-	The substance forms discontinuous black stringers. A sample of organic matter was dissolved out of the rock, but it contained no algal filaments.

58

* The composition is based on the modal analysis of 10 thin sections.

† tr = trace.

Table 3.7

Summary of the replacement and recrystallization reactions
in the upper part of the Boulby Halite

<u>Subzone</u>	<u>Replacement and recrystallization reactions*</u>	<u>Scale of reaction†</u>	<u>Timing of reaction</u>
B.H.2	C→Hem,M	both S	Probably early→ late diagenesis
B.H.1	Recryst. of H	Maj.	During movement at depth
	Recryst. of Sy	S	During movement at depth
	Recryst. of A	S	late diagenesis to at depth
	C→M,Q,Hem	all S	Probably early → late diagenesis

* H = halite; Sy = sylvite; A = anhydrite; C = clays;
M = magnesite; Q = quartz; Hem = hematite.

† Maj. = large scale reaction; S = small scale reaction.

III Summary and Conclusions

The mineralogy of bed B.H.1 appears to be essentially primary, although carnallite may originally have been more abundant. The pink-white halite bands are probably a primary feature and their enrichment in halite suggests they were precipitated from a brine relatively depleted in CaSO_4 . The shale laminae represent small influxes of detrital matter at the time of deposition. Movement at depth resulted in the recrystallization of halite and anhydrite and the disruption of the shale laminae. The replacement and recrystallization reactions are summarized in Table 3.7. It is uncertain whether the white halite rock and sylvinite patches formed during deposition, in early diagenesis, or at depth.

The mineralogy of bed B.H.2 appears to be primary and early diagenetic and the elongate nature of many of the crystals testifies to deformation as a result of movement. The high proportion of clays in this bed indicates a major influx of detrital material at the time of deposition.

The probable environment of sedimentation of these beds will be discussed later in the thesis.

CHAPTER 4

THE BOULBY POTASH

I General features

This bed is a sylvinite rock which exhibits much lateral variation in thickness in the Mine because of the ease with which potash salts flow. It is generally thickest and least tectonically deformed in the area of the Mine enclosed by roadways 2E, 3S, 5W and 3N (see Figure 2.4) where it is about 3 metres thick. In the South and East Spearheads it is normally 1 to 2 metres thick but in the area of overfolding (Plate II) it is frequently less than 1 metre in thickness.

The bed varies in colour from grey to red. The rocks of the upper and lower contacts are deep red because they contain many hematite crystals derived from small rounded tectonic inclusions of Boulby Shale and of bed B.H.2 (Figure 2.6). There are also internal deep red bands which are associated with thin layers of small rounded shale inclusions (2 cm.). These layers probably represent former shale laminae which have been disrupted by movement.

However this unit often contains pink, grey and orange colour bands (Figure 4.1) in the absence of shale inclusions. Some of these bands are parallel aligned

with, or inclined to, the upper and lower contacts of the bed whilst others resemble cross-bedding or are isoclinally overfolded. The fact that three bands, occurring in vertical succession at the locality in Figure 4.1, contained 0.11, 0.18 and 0.21% Fe_2O_3 respectively indicates that they are also caused by variations in the hematite content of the rock. They often cease abruptly in a lateral direction or merge gradually into more massive sylvinite. The possible origins of these bands will be considered later in the chapter.

II Petrography

This bed has a very simple mineralogy consisting of sylvite, halite, anhydrite, clays and minor quantities of magnesite and hematite. Excluding clay matter, the unit has a remarkably uniform composition and contains on average 52% sylvite and 44% halite. Tables 4.1 and 4.2 give the mineral characteristics of the sylvinite and the shale fragments believed to represent former shale laminae.

The sylvinite displays granular to schistose textures with ragged to curved boundaries developed between sylvite and halite crystals (Figure 4.2). The latter texture is predominant in the areas of most intense movement (East Spearhead and Panel No. 1) with some sylvite crystals

Table 4.1 Composition and mineral characteristics of the Boulby Potash

<u>Mineral</u>	<u>Volume percentage of mineral*</u>		<u>Colour</u>	<u>Grainsize</u>	<u>Crystal shape and form</u>	<u>Comments</u>
	<u>Average</u>	<u>Range</u>				
Sylvite	52	40-60	Grey-red	0.0-5.0 mm.	Rounded to elongate crystals	The red coloration is caused by inclusions of hematite platelets, usually evenly dispersed except when concentrated round shale inclusions.
Halite	44	30-50	White-grey	0.0-2.0 cm.	Rounded to elongate	The majority of these crystals are up to 5 mm. in width. Rare porphyroblasts attain diameters of 2 cm. There are fewer hematite inclusions than in sylvite
Anhydrite	4	0-6	White-grey	0.0-0.1 mm.	Euhedral equant crystals	These crystals line the boundaries between some sylvite and halite crystals and project from clay laminae.
Hematite	tr [‡]	-	Red-brown	0.00- 0.05 mm.	Hexagonal platelets and rods	Inclusions in sylvite and halite crystals

* The composition is based on the modal analysis of 30 thin sections.

‡ tr = trace.

Table 4.2 Composition and mineral characteristics of shale laminae in the Boulby Potash

<u>Mineral</u>	<u>Volume percentage of mineral*</u>		<u>Colour</u>	<u>Grainsize</u>	<u>Crystal shape and form</u>	<u>Comments</u>
	<u>Average</u>	<u>Range</u>				
Anhydrite	60	40-100	White-grey	0.00- 0.05 mm.	Elongate laths	These elongate laths are usually intergrown with parallel aligned clays.
Clays	25	15-30	Green-brown	0:00- 0.05 mm.	Elongate platelets	The clay minerals are predominantly illites.
Halite	10	7-12	White	0.0-4.0 mm.	Rounded anhedral crystals	These crystals form porphyroblasts in the anhydrite-clay matrix.
Sylvite	3	0-5	Red-brown	0.0-5.0 mm.	Poorly formed cubes which are sometimes elongate	The red coloration in these crystals is caused by hematite crystals which are closely associated with clays. The hematite has probably been leached from the clays.

Table 4.2 (cont.)

<u>Mineral</u>	<u>Volume percentage of mineral*</u>		<u>Colour</u>	<u>Grainsize</u>	<u>Crystal shape and form</u>	<u>Comments</u>
	<u>Average</u>	<u>Range</u>				
Magnesite	2	0-4	White-grey	0.0-1.0 mm.	Hexagonal plates, tabular on (0001)	5 R.I. measurements gave \bar{w} in the range 1.701-1.705, i.e. almost pure $MgCO_3$. These crystals project into cleavages in sylvite and halite crystals within the laminae and in the host rock.
Hematite	tr [‡]	-	Red-brown	0.00- 0.05 mm.	Hexagonal plates on (0001)	This mineral occurs as inclusions in the sylvite described above.
Pyrite	tr	-	Brass metallic	0.00- 0.01 mm.	Well - poorly formed octohedra	These octohedra occur singly or in small aggregates associated with "mucous-like" carbonaceous material.
Carbonaceous material	tr	-	Grey	-	-	See pyrite and Figure 4.4.

* Composition based on the modal analysis of 8 thin sections. ‡ tr = trace.

being up to 4 times as long as wide. Halite crystals are not so elongate. In the areas of least deformation in the Mine a schistose texture is frequently developed in the lower and upper 25 cm. of the bed. Otherwise the texture varies between granular and gneissoze in a random manner.

The marked schistosity of much of the sylvinite testifies to the wholesale recrystallization of pre-existing sylvite and halite crystals as a result of movement at depth. Occasional colourless halite porphyroblasts, up to 2 cm. in maximum dimension, cross-cut elongate sylvite and halite crystals indicating that they formed by the recrystallization of halite after movement. The presence of individual halite grains spanning the boundary between mud fragments and the surrounding sylvinite indicates small scale displacement or replacement of mud by halite.

Euhedral equant anhydrite crystals sometimes line the boundaries between sylvite and halite crystals and project from interstitial clay (Figure 4.3). It is likely that they formed by recrystallization in a manner similar to those in the Boulby Halite. Occasional magnesite laths project from clays into the cleavages of sylvite and halite.

The presence of pyrite octohedra associated with mucous-like carbonaceous matter (Figure 4.4) in the remnant fragments of shale laminae testify to reducing

conditions at the time of their deposition.

III The origin of the sylvite

There is no petrographic evidence in this bed to indicate that sylvite has been derived from another mineral. However French geologists from the Holle Mine in the Congo have performed bromine analyses on co-existing sylvite and halite crystals from Boulby and suggested that the sylvite formed by the breakdown of carnallite (Mr. P.J.E. Woods; pers. comm.). They have not presented their analyses for examination. They also pointed out that the colour banding in the Boulby Potash, not attributable to shale inclusions, is very similar to colour bands in sylvinite lenses in the carnallite-halite beds of lower Cretaceous age in the Congo. The sylvite in the Congolese sylvinite lenses has formed by the breakdown of carnallite (Belmonte et al., 1965). The French geologists regard the colour banding in the Boulby Potash as representing the former positions of fronts of MgCl_2 brines rising upwards. The writer sees no reason why these brines could not have been migrating downwards.

The bromine method depends on the fact that bromine present in seawater does not form bromine salts on evaporation but substitutes into the chlorine site in chloride minerals (i.e. sylvite, carnallite, halite).

As evaporation proceeds the bromine content of the chloride salts increases with different salts containing different proportions of bromine. Braitsch (1972) showed that if the amount of bromine in solid solution in halite is taken as unity then the amount substituted in primary carnallite is 7.2 whilst that in primary sylvite is 10. If a chloride salt then reacts with a brine which is undersaturated in that salt its bromine content is reduced. Under these circumstances carnallite breaks down to sylvite; the secondary sylvite crystals having bromine values akin to carnallite. Presumably the French geologists found the $\text{Br}_{\text{KCl}}/\text{Br}_{\text{NaCl}}$ ratio for the Boulby Potash is approximately 7.2.

However according to Mr. P.J.E. Woods 2 co-existing sylvite and halite crystals in this bed contain 1670 ppm Br and 280 ppm Br respectively; giving a $\text{Br}_{\text{KCl}}/\text{Br}_{\text{NaCl}}$ ratio of 5.96. This ratio could be interpreted as indicating that the sylvite was derived by the breakdown of carnallite by reaction with solutions undersaturated in carnallite but, equally, the present sylvite could have formed by recrystallization of primary sylvite after reaction with brines. Such a brine could have come from above or below the bed. However if the brine came from above it could have leached small quantities of iron from the clays in the Boulby Shale and precipitated the element as hematite in variable proportions in this bed, whether the original mineralogy was sylvite or carnallite, hence

giving rise to the colour banding.

If the sylvite is derived from carnallite it is probable that the carnallite broke down by reaction with NaCl rich brines. The timing of such a reaction is uncertain although it would have occurred prior to the migration of KCl-NaCl brines which formed the fibrous sylvinite veins in the Boulby Shale and overlying rocks.

The true origin of the sylvite in this bed will only be revealed by the combined determination of the bromine content of the sylvite and halite crystals together with the rubidium content of the sylvite; the rubidium content of primary sylvite being much less than that in crystals derived from carnallite. The complexities of this type of chemical analysis are such that it would form the basis for further study.

IV Summary and Conclusions

This bed is primarily composed of sylvite and halite. The sylvite may be primary or have formed by the breakdown of carnallite by reaction with brines prior to the formation of the sylvinite veins in the Boulby Shale. The extensive lateral migration of the bed has caused wholesale recrystallization of sylvite and halite.

The shale laminae in the bed were deposited under reducing conditions.

CHAPTER 5

THE BOULBY SHALE

The Boulby Shale is composed of beds B.S.1 to 6 (Table 2.2). Units B.S.1, 4, 5 and 6 are shale beds of variable character, whilst B.S.2 is an anhydrite-halite rock and B.S.3 is a borate nodule bed. The geology of the latter bed is the most interesting and complex of all the units examined in the C.P.L. concession area and consequently it dominates this chapter. This does not diminish the importance of the other beds; a sound knowledge of which is essential to the stratigraphic and structural interpretation of the rocks (Chapter 2 and Appendix 2).

These beds differ markedly from their normal character in the area of the Mine enclosed by roadways 2E, 2S, 5W and 3N and in certain of the boreholes. Consequently they are considered separately at the end of the chapter.

I Beds B.S.1, 4, 5 and 6

These shale beds, which vary in colour from black (clay rich) to grey (anhydrite rich), have very similar textures, but are of different mineral compositions (Table 5.1). The characteristics of each mineral are

similar in the majority of units and are described in Table 5.2.

These beds are generally composed of small anhedral halite (all beds) and sylvite (only B.S.1 and 4) crystals set in a matrix of variable proportions of randomly orientated or parallel aligned anhydrite and clay laths (see Tables 5.1 and 5.2). However in many of the rocks of bed B.S.4 in the East Spearhead and occasionally in the South Spearhead, granular and euhedral equant anhydrite crystals enclose and separate areas of clays (Figures 5.1 and 5.2). The anhydrite crystals flanking these areas of clays contain clay inclusions indicating that they are replacive or displacive in origin. Figure 5.1 shows numerous corroded relicts of sylvite and halite which have also been partially replaced or displaced by anhydrite. There is little evidence to suggest the timing of this reaction. However if it is a displacement reaction it is likely to have occurred during diagenesis.

Small halite crystals in B.S.1 and the basal rocks of B.S.4 frequently have hexagonal or pseudo-hexagonal outlines (Figure 5.3). Hexagonal cross-sections through cubic minerals are not uncommon, although it is unusual that so many should occur in close proximity. This strongly suggests that halite has pseudomorphed a mineral which commonly adopts this habit and which might be expected to form in this type of environment. Such a mineral is carnallite. The close association of these

Table 5.1

Mineral compositions, in percentages, of beds
B.S.1, 4, 5 and 6 of the unaltered theoretical sequence

<u>Minerals</u>		<u>Beds</u>			
		B.S.1 ¹	B.S.4 ²	B.S.5 ³	B.S.6 ⁴
Anhydrite	Average Range	13 0-15	41 20-50	8 5-12	15 10-20
Halite	Average Range	20 14-26	15 10-25	35 29-40	40 25-50
Sylvite	Average Range	26 15-30	15 10-90	- -	- -
Iron-boracite/ ericaite	Average Range	- -	0.5 0-1	- -	- -
Clays	Average Range	40 30-70	24 12-50	55 45-60	40 25-50
Quartz	Average Range	1 0-2	3 0-6	- -	2 0-3
Magnesite	Average Range	1 0-3	2 0-3	2 1-3	2 0-4
Hematite	Average Range	tr [‡] -	tr -	tr -	tr -
Pyrite	Average Range	- -	tr -	tr -	- -

1. Composition determined by the modal analysis of 10 thin sections.
2. Composition determined by the modal analysis of 40 thin sections.
3. Composition determined by the modal analysis of 5 thin sections.
4. Composition determined by the modal analysis of 3 thin sections.

‡ tr = trace.

Table 5.2 Characteristics of the minerals of beds B.S.1, 4, 5 and 6

<u>Mineral</u>	<u>Colour</u>	<u>Grainsize</u>	<u>Crystal shape and form</u>	<u>Comments</u>
Anhydrite	Grey-white	0.0-0.5 mm.	Elongate laths or euhedral equant crystals	The mineral occurs as elongate laths, usually up to 0.1 mm. in length, in all these beds. Euhedral equant crystals (up to 0.5 mm.) occur in small numbers projecting from the anhydrite and clay matrix into sylvite and halite crystals. In B.S.4 euhedral equant crystals form part of the matrix (see text).
Halite	White to pale brown to rusty red	0.0-2.0 cm.	Subhedral to rounded crystals	The majority of the halite forms small anhedral colour- less crystals (0.5 mm.) in all these beds. In B.S.1 many of these small crystals have hexagonal outlines (see text and Figure 5.3. The halite in B.S.5 is rusty red due to numerous inclusions of randomly orientated hematite platelets. In B.S.1 and 4 large subhedral to anhedral pale brown porphyroblasts enclose anhydrite and clays. Their coloration is caused by the inclusions of clays.

Table 5.2 (cont.)

<u>Mineral</u>	<u>Colour</u>	<u>Grainsize</u>	<u>Crystal shape and form</u>	<u>Comments</u>
Sylvite	Colourless to milky-white to deep red	0.0-2.0 cm.	Subhedral to anhedral	Sylvite only occurs in B.S.1 and 4. It is of 2 types, (i) anhedral colourless to white elongate crystals (up to 4 mm.) enclosed in a matrix of clays and anhydrite, and (ii) large (up to 2 cm.) subhedral to anhedral milky white - red porphyroblasts which enclose anhydrite and clay. Their red coloration is caused by inclusions of randomly orientated hematite platelets which often surround clays. Many of these crystals have only red rims. In B.S.4 these porphyroblasts sometimes coalesce to form discontinuous bands.
Iron boracite	Blue-green	0.0-1.0 mm.	Euhedral to subhedral cubes	These only occur in B.S.4 as single isolated crystals usually associated with sylvite.

Table 5.2 (cont.)

<u>Mineral</u>	<u>Colour</u>	<u>Grainsize</u>	<u>Crystal shape and form</u>	<u>Comments</u>
Clays	Green-brown	0.00-0.05 mm.	Elongate platelets	Clays occur in all these beds and are frequently intergrown in parallel alignment with anhydrite laths. They form the matrix of the rocks. The clay minerals are chlorites and chlorite-smectites.
Quartz	White-grey-red	0.0-1.0 mm.	Euhedral to anhedral	The mineral occurs in all the beds and is usually 0.3 mm, or less, in width. The crystals project from the clays and anhydrite of the matrix into sylvite and halite crystals; particularly the large porphyroblasts of these minerals. Quartz is euhedral towards the chloride minerals but anhedral towards others.
Magnesite	White to grey	0.0-0.5 mm.	Euhedral to subhedral hexagonal plates, tabular on (0001)	This mineral occurs in all the beds. 10 R.I. measurements gave w in the range 1.700-1.707, i.e. almost pure $MgCO_3$. The mineral usually projects from the matrix into the cleavages of sylvite and halite. Magnesite rosettes occur in B.S.6 (see text).

Table 5.2 (cont.)

<u>Mineral</u>	<u>Colour</u>	<u>Grainsize</u>	<u>Crystal shape and form</u>	<u>Comments</u>
Hematite	Red-brown	0.00-0.05 mm.	Euhedral to anhedral hexagonal plates, tabular on (0001).	The mineral occurs as inclusions in sylvite porphyroblasts, particularly adjacent to clay inclusions. These platelets are also intergrown with clays in the matrix of B.S.6. The mineral occurs in all beds.
Pyrite	Black	0.00-0.05 mm.	Euhedral to anhedral octohedra	The mineral only occurs in beds B.S.4 and 5 where it forms single crystals or small clusters intergrown with clays.

halite crystals with secondary sylvite in B.S.3 (see later text) suggests that carnallite might have broken down to sylvite by reaction with brines saturated in halite.

Large subhedral sylvite porphyroblasts (Figure 5.4) are sporadically developed in B.S.1 and the lower rocks of B.S.4 where they have sometimes coalesced into thin laterally impersistent bands (Plate III). Similar isolated halite porphyroblasts also occur in these beds. These sylvite and halite crystals frequently contain inclusions of clays and anhydrite of the host rock (Figures 5.4 and 5.5), suggesting they have grown by replacement or recrystallization.

Quartz, magnesite and hematite are more abundant in these rocks than in the shale laminae in the Boulby Halite and Boulby Potash (compare Tables 3.4, 4.2 and 5.1). Small numbers of euhedral to subhedral quartz crystals are evenly distributed in the majority of these beds excluding B.S.5 (Figure 5.3). However Figure 5.5 shows that quartz and hematite crystals are particularly abundant along the contacts between clays and large sylvite and halite porphyroblasts in B.S.1 and 4. The fact that these quartz crystals are frequently of undamaged euhedral form and contain inclusions of hematite indicates that these minerals are of authigenic origin. The presence of sylvite inclusions in these quartz crystals (Figure 5.5) suggests they were formed by reaction of the brines, which precipitated the sylvite

and halite porphyroblasts, with the clays during diagenesis. A combination of a higher clay content in the beds and more highly concentrated brines presumably accounts for the greater abundance of quartz and hematite in these beds than in the Boulby Halite and Boulby Potash.

In beds B.S.1, 4 and 5 minor magnesite plates cross-cut the matrix in a random manner and project into the cleavages of sylvite and halite crystals (Figures 5.3 and 5.4). However, in contrast, single magnesite plates in B.S.6 are usually parallel aligned to the bedding; suggesting that they grew when the rock was under stress. Small aggregated rosettes of this mineral also form occasional nodules along the contacts between the matrix and halite crystals in B.S.6 (Figure 5.6). The fact that the magnesite crystals in rosettes are randomly orientated suggests that they grew prior to, or after, the stress field which directed the growth of the single plates. It is, therefore, likely that this mineral formed by the breakdown of submicroscopic carbonate matter over a prolonged period of time in these units.

II Bed B.S.2

This bed is a grey-white anhydrite or anhydrite-halite rock of variable character. It is usually 5 - 6 mm. thick, but sometimes it pinches and swells, varying in thickness from 0.5 - 7.0 mm., even in areas

of little apparent tectonic activity. In the south of the East Spearhead in No. 1 cross-cut south off L between roadways P and Q it forms two tightly overfolded, parallel aligned bands, each 2 mm. thick, and separated by 2 mm. of shale. However the single bed is never observed to split into 2 bands in the Mine.

The bed occurs in two characteristic petrographic forms:-

- (i) as an almost pure anhydrite rock (Figure 5.7), and
- (ii) as an anhydrite-halite rock (Figure 5.8).

However they have never been observed merging into one another. The composition and mineral characteristics of the bed are described in Table 5.3.

Where the bed is of petrographic type (i) it is a laminated rock composed almost entirely of elongate parallel aligned or, less frequently, randomly orientated anhydrite laths. Occasional euhedral equant anhydrite crystals, which have probably formed by recrystallization, cross-cut the laths. Rare, small, partial rosettes of parahilgardite were found in a fragment of the bed in a breccia in Panel No. 1. These crystals have partially developed well formed faces, suggesting they grew at the same time as the anhydrite rather than by replacement or recrystallization. Rare trails of clay minerals, parallel to the top and bottom of the bed, are enclosed within and sometimes cross-cut by anhydrite laths. This suggests that the clays have been replaced or displaced

Table 5.3 The composition and mineral characteristics of bed B.S.2

<u>Mineral</u>	<u>Volume percentage of mineral</u>		<u>Colour</u>	<u>Grainsize</u>	<u>Crystal shape and form</u>	<u>Comments</u>
	<u>Average</u>	<u>Range</u>				
<u>Type (i)*</u>						
Anhydrite	98	95-100	Grey-white	0.00- 0.03 mm.	Elongate laths or euhedral equant crystals	The majority of these crystals are parallel aligned or randomly orientated laths. They are cross-cut by a few euhedral equant crystals.
Magnesite	1	0-2	Grey-white	0.0-0.5 mm.	Euhedral to subhedral platelets, tabular on (0001)	These crystals cross- cut the anhydrite laths.
Clays	1	0-3	Green-brown	0.00- 0.05 mm.	Elongate platelets	These crystals occur in occasional trails enclosed in anhydrite.
Para- hilgardite	tr [†]	-	Grey	0.00- 0.05 mm.	Wedge shaped crystals	The crystals occur in small partially developed rosettes in the anhydrite matrix.

by anhydrite. The former extent of the clays is unknown.

The anhydrite-halite rock (type (ii)), on the other hand, contains halite (Table 5.3) and exhibits a greater variety of textures than type (i). The matrix anhydrite forms elongate and granular crystals which grade into one another randomly. Halite forms anhedral porphyroblasts, and occasionally thin layers in the anhydrite matrix. Figure 5.8 shows that the halite porphyroblasts frequently enclose, and have boundaries lined with, euhedral anhydrite crystals. The presence of inclusions of anhydrite granules in these euhedral anhydrite crystals suggests the latter grew by recrystallization, although there is no indication of the timing of this reaction.

It is uncertain whether the differences in petrographic character of this bed represent a primary lateral facies variation or if they are secondary in nature; possibly resulting from an influx of halite into the unit. If the clay trails enclosed in the type (i) variety of the bed are all that remain of a former clay horizon, then the whole unit may be of secondary origin.

III Bed B.S.3

(1) General

This bed contains many nodules containing dominant iron-boracite and ericaite (both of formula

$(\text{Fe,Mg,Mn})_3\text{B}_7\text{O}_{13}\text{Cl}$) or parahilgardite $(\text{Ca}_2[\text{B}_5\text{O}_8(\text{OH})_2]\text{Cl})$.

It comprises the most extensive development of borate minerals found in the English Zechstein and, as far as the writer is aware, the largest concentration of iron-boracite and parahilgardite discovered in the world.

Parahilgardite and iron-boracite were first recorded in the U.K. from this bed by J.F. Watt (in 1965; pers. comm.) and Milne et al. (1977; as part of the work for this thesis) respectively. This thesis provides the first recorded occurrence of ericaite in the U.K. Small quantities of other borate minerals have been recorded from the English Zechstein and these are summarized in Table 5.4.

The exposures of this bed in the Mine, up until 10th January, 1977, are shown in Figure 5.9. It is only sporadically developed in the area of overfolding (East Spearhead and Panel No. 1) due to brecciation of the strata.

Figure 5.9 shows that the iron-boracite and parahilgardite nodules are exposed in different areas of the Mine. The zone of transition is not exposed but has been inferred (see Figure 5.9). It is, therefore, not known whether these different types of nodules merge into one another laterally or whether they are distinct provinces within the same bed.

Parahilgardite nodules occur in borehole B, whilst iron-boracite nodules are present in boreholes A, C and V. Small numbers of iron-boracite crystals, which have been

Table 5.4

The Borate Minerals of the English Zechstein

<u>Mineral</u>	<u>Occurrence and brief description</u>	<u>Source</u>
Boracite	E2 boring: as single crystals and in aggregates in well cuttings from the Boulby Potash.	Guppy (1944) and Stewart (1951a)
"	F1 borehole: as rare crystals in halite from the Boulby Potash.	Stewart (1965)
"	E5 borehole: in radiating nodules in halite from the Staintondale Group.	Sabine (1953)
Sulphoborite	Fordon borehole: replacing anhydrite in the Fordon Evaporites.	Stewart (1963a)
p-Veachite	E2 borings: as single crystals from well cuttings from the Fordon Evaporites.	Stewart et al. (1954) and Beevers and Stewart (1960)
Iron-boracite	Boulby Mine: in nodules in a borate nodule bed overlying the Boulby Potash.	Milne et al. (1977) and this thesis
Ericaite	" "	This thesis
Parahilgardite	" "	This thesis and v. Hodenberg and Kühn (1977)

replaced by halite, are all that remain of this bed in borehole S-20.

The iron-boracite nodules are ellipsoidal in shape with major axes varying in length from 1 to 15 cm. Minor axes are approximately half the major ones. They are frequently very tightly packed in the bed such that there are often almost no gaps between them (Plate III). The host rock is a grey-black shale.

The parahilgardite nodules are also ellipsoidal with major axes ranging in length from 0.5 to 10.0 cm. Minor axes are approximately half the major ones. Occasionally many small nodules of this type coalesce to give a large composite nodule which may range up to 0.3 metres in length and 0.2 metres in width. The small nodules (3x2x1 cm.) tend to be tightly packed, whereas the larger ones (10x6x5 cm.) may be separated by up to 12 cm. of parahilgardite-anhydrite-clay shale. Typical parahilgardite nodules are shown in Figure 5.10.

Both iron-boracite and parahilgardite nodules frequently have slickensided contacts with the host rock.

(2) Mineralogy of the Borates

(a) Iron-boracite and ericaite

Iron-boracite (orthorhombic) and ericaite (monoclinic) are members of the boracite group of minerals

($[\text{Mn,Fe,Mg}]_3\text{B}_7\text{O}_{13}\text{Cl}$) in which divalent iron is the predominant cation. A complete solid solution is known to exist between pure iron and magnesium boracites (v. Hodenberg and Kühn, 1974). In this thesis this group of minerals is named according to the classification of Drs. R. Kühn and M. Hey (pers. comm.), shown in Table 5.5, and approved by the IMA Commission on New Minerals and New Mineral Names.

These minerals occur in aggregates or as single crystals, in nodules and to a lesser extent in the host rock. Iron-boracite is always dominant with ericaite frequently being absent. These minerals are occasionally minor accessories in parahilgardite nodules.

(a) General characteristics, lattice parameters and optical properties

The iron-boracite crystals are either large euhedral blue-green pseudocubic crystals (up to 3 mm. edge) with well developed faces of the form $\{100\}$ and subsidiary faces of the forms $\{110\}$ and $\{111\}$ or anhedral blue-purple grains up to 0.5 mm. in width. Ericaite forms large pseudocubic crystals similar to those of iron-boracite. These minerals do not have a cleavage but sometimes develop a conchoidal fracture.

The lattice parameters of a single iron-boracite crystal are given in Table 5.6. Table 5.7 shows that they vary, reflecting the different chemical compositions

Table 5.5

The classification of boracite group minerals used in this thesis¹

<u>Chemical Formula³</u>	<u>Symmetry²</u>	<u>Mineral Name</u>	<u>Useful sources of data on these minerals</u>
(<u>Mg</u> , Fe, Mn) ₃ B ₇ O ₁₃ Cl	Orthorhombic	Boracite	Palache, Berman & Frondel (1951)
(<u>Fe</u> , Mg, Mn) ₃ B ₇ O ₁₃ Cl	Orthorhombic	Iron-boracite	Milne et al. (1977)
(<u>Fe</u> , Mg, Mn) ₃ B ₇ O ₁₃ Cl	Monoclinic	Ericaite	v. Hodenberg and Kühn (1974)
Fe ₃ B ₇ O ₁₃ Cl	Trigonal	Congolite	Wendling et al. (1972)
Mn ₃ B ₇ O ₁₃ Cl	Orthorhombic	Chambersite	Honea and Beck (1962)

1. This classification has been proposed by Drs. R. Kühn and M. Hey (see text).
2. All these minerals invert to cubic symmetry at temperatures of 265°C and above.
3. Fe indicates that iron is the principal cation in the mineral.

Table 5.6

The lattice parameters, optical properties and hardness of
iron-boracite and ericaite crystals from iron-boracite
nodules in bed B.S.3

	<u>Iron-boracite</u>	<u>Ericaite</u>
<u>Lattice parameters</u>		
a	8.62 \AA ¹	- ²
b	8.63 \AA	-
c	12.17 \AA	-
Unit cell volume	905.33 \AA^3	-
Symmetry	Orthorhombic	Monoclinic
<u>Optical properties</u>		
n_α	1.715 \pm 0.002	1.715 \pm 0.002
n_β	- ³	1.720 \pm 0.002
n_γ	1.728 \pm 0.002	1.727 \pm 0.002
$n - n_\alpha$	0.013	0.012
$2V_\gamma$	80-90 $^\circ$ ³	82 $^\circ$ \pm 1 $^\circ$
<u>Hardness</u> ⁴	7	7

1. The lattice parameters and symmetry of iron-boracite were determined from 3 single crystal rotation photographs using a Pye Unicam camera and CuK_α radiation.

2. The writer was unable to interpret single crystal photographs of ericaite due to the extremely complicated array of spots caused by twinning. Dr. R. Kühn has shown the mineral to be monoclinic (pers. comm.).

3. The turbidity of iron-boracite precluded the measurement of n_β and an accurate determination of $2V_\gamma$.

4. The hardness is presented on the Moh's scale.

Table 5.7

Comparison of the properties of English and German boracites and iron-boracites

Type and locality	Wt. %			Cation. %				a	b	c	T ^{††}
	MgO	FeO	MnO	Mg ²⁺	Fe ²⁺	Mn ²⁺					
Small anhedral grains from Boulby [†]	12.44*	28.38	4.34	40.34	51.65	8.00		8.63	8.63	12.19Å	287°C
Large crystals from Boulby [†]	16.82*	22.11	2.85	54.53	40.21	5.25		8.59	8.59	12.15	297
Riedel, Hånigsen//	8.55	38.69	0.46	28.71	70.44	0.85		8.58	8.69	12.17	310-315 °C
Niedersachsen, Wathlingen//	29.90	1.68	-	96.94	3.06	-		8.53	8.60	12.15	-
Segeberg//	30.84	-	-	100	-	-		8.53	8.53	12.12	265
Stassfurt**	30.84	-	-	100	-	-		8.54	8.54	12.07	265
E2 borehole, Yorkshire ^{††}	31.00	-	-	100	-	-		8.56	8.56	12.10	272

* Calculated by difference, knowing FeO and MnO%.

† Orthorhombic to cubic inversion temperature.

†† Cell dimensions determined using a Haag-Guinier camera of 200 mm equivalent diameter and Cu-Kα radiation and orthorhombic to cubic inversion temperature determined using a Du Pont differential thermal analyser.

// Kühn and Schaacke, 1955 ** Ito, Morimoto and Sadanaga, 1951 †† Guppy, 1944

of the individual crystals. Dr. R. Kühn of the Kaliforschung Institute in Hannover has shown the ericaite crystals to be monoclinic (pers. comm.).

The optical properties of these minerals are given in Table 5.6. Figure 5.11 shows that the ericaite crystals display complicated sector and multiple twinning. However others display cross-hatched twinning, similar to that observed in microcline, in each quadrant. Because of the complex nature and overlapping of twin lamellae few of these crystals extinguish. Figures 5.12 and 5.13 show that iron-boracite crystals have a highly turbid appearance.

(β) Optical evidence for a relationship between iron-boracite and ericaite

Ericaite crystals in the nodules usually occur singly (Figure 5.11), whilst the majority of the iron-boracite crystals occur in aggregates (Figure 5.13). However, rare iron-boracite crystals exhibit remnant sector twinning characteristic of ericaite. Figure 5.12 also shows rare ericaite crystals which have partially broken down to much smaller euhedral to anhedral crystals; the majority of which show no sign of having formed from ericaite. These optical observations indicate that some of the iron-boracite crystals have formed by the breakdown of ericaite.

(X) Mineral Chemistry

(i) General:- Table 5.8 presents a chemical analysis of iron-boracite from a nodule in which these crystals only occurred as anhedral grains. The analysis gives a formula for the mineral of $(\text{Mn}_{0.24}\text{Fe}_{1.50}\text{Mg}_{1.30})\text{B}_{6.90}\text{Si}_{0.04}\text{O}_{13.07}\text{Cl}_{0.93}$ based on fourteen anions (oxygen and chlorine).

However Table 5.9 shows that the iron-boracite crystals within individual nodules exhibit considerable variation in bulk composition with the pseudocubic and granular crystals having the same range in composition.

(ii) Electron microprobe analyses:- The electron microprobe was used to determine the apparent concentrations¹ of MgO, MnO and FeO in co-existing iron-boracite

1. In order to determine the true weight percentage of any elemental oxide in a mineral, using the electron microprobe, it is necessary to know the apparent concentrations of all the oxides present in the mineral. However it is not possible to analyse for boron using the electron microprobe because boron has a very low atomic number and little is known of its absorption coefficient. Using the computer it was possible to back calculate the apparent concentrations of boron and
(continued on next page)

and ericaite crystals in three iron-boracite nodules, one parahilgardite nodule and remnant crystals of iron-boracite in the S-20 borehole in order to:-

- (i) evaluate the extent of the variation in the bulk MgO, MnO and FeO content amongst and within the iron-boracite crystals (Table 5.9) and,
- (ii) determine if co-existing ericaite and iron-boracite crystals have the same compositions.

Only those crystals with square outlines were analysed in order that the position of the analysis points within the crystals were accurately known. Figures 5.14 to 5.18 show the variation in composition of these crystals in the nodules. The composition of the individual

(continued from previous page)

chlorine in the iron-boracite crystal for which a full chemical analysis is given in Table 5.8. The apparent concentrations of boron and chlorine were then combined with those of MgO, MnO and FeO of the individual crystals analysed with the electron microprobe, and fed back into the computer to be converted into weight percentages. However the correlation coefficient for boron, which should be unity, was very low and extremely variable even amongst separate analyses of the same crystal. For this reason, it was decided to express the proportions of MgO, MnO and FeO in terms of their apparent concentrations.

Table 5.8

Mineral analyses of iron-boracite and parahilgardite from
nodules in bed B.S.3¹

<u>Wt. %</u>	<u>Iron-boracite</u>	<u>Parahilgardite</u>
CaO	0.27	33.15
SrO	-	0.82
MnO	3.82	0.01
MgO	11.75	0.10
FeO	24.05	-
Fe ₂ O ₃	-	0.02
Al ₂ O ₃	-	0.03
Na ₂ O	0.10	0.03
K ₂ O	0.01	0.02
B ₂ O ₃	53.80	51.83
SiO ₂	0.55	0.03
Cl	7.38	10.66
Br	0.01	0.01
H ₂ O	-	5.50
Total (less 0 \equiv Cl)	100.07	99.79

1. The mode of separation and chemical analysis of these minerals are given in Appendix 3.

Table 5.9

Bulk FeO, MnO and MgO contents of iron-boracite crystals from various iron-boracite nodules

Wt. % cation oxide	Iron-boracite crystals*†											
	1	2	3	4	5	6	7	8	9	10	11	12

FeO	21.12	8.31	21.58	24.10	19.68	20.11	20.24	24.45	21.62	20.35	23.68	17.29
MnO	1.82	0.87	2.19	2.72	1.78	1.55	1.85	2.80	2.29	2.64	3.64	2.15
MgO	17.85	25.67	17.44	15.71	18.74	18.63	18.39	15.48	17.36	17.88	15.43	19.88

- * 1. Large pseudocubic iron-boracite crystal from the centre of nodule 1.
 2. Fine grained anhedral iron-boracite crystal from the centre of nodule 1.
 3. " " " " edge " " "
 4. Small anhedral iron-boracite crystal from the middle of an iron-boracite aggregate in the centre of nodule 2.
 5. Large euhedral pseudocubic iron-boracite crystal surrounding 4. from nodule 2.
 6. Isolated large euhedral pseudocubic iron-boracite crystal from the interior of nodule 2.
 7. Small anhedral iron-boracite crystal from the outer edge of nodule 2.
 8. " " " " interior of nodule 3.
 9. " " " " outer edge of nodule 3.
 10. Large pseudocubic iron-boracite crystal from the centre of nodule 4.
 11. Small anhedral iron-boracite crystal from the edge of nodule 4.
 12. " " " " " 18.

- † FeO determined colourmetrically
 MnO determined by atomic absorption spectroscopy
 MgO " " "

Table 5.10

Possible polymorphic reactions relating iron-boracite and ericaite in nodules in bed B.S.3

<u>Process Number</u>	<u>Reaction</u>
1*	$\begin{array}{c} \text{Metastable cubic polymorph} \swarrow \searrow \\ \text{iron-boracite (stable)} \\ \text{ericaite (metastable)} \longrightarrow \text{iron-boracite (stable)} \end{array}$
2*	Metastable cubic polymorph \longrightarrow ericaite (metastable) \longrightarrow iron-boracite (stable)
3*	Ericaite (metastable) \longrightarrow iron-boracite (stable)
4	$\begin{array}{c} \text{Iron-boracite (stable)} \\ + \\ \text{Ericaite (metastable)} \longrightarrow \text{iron-boracite (stable)} \end{array}$
5	$\left. \begin{array}{c} \text{Metastable cubic polymorph} \\ \text{OR} \\ \text{Iron-boracite (stable)} \end{array} \right\} \begin{array}{c} \text{inversion} \\ \text{as a} \\ \text{result} \\ \text{of burial} \end{array} \longrightarrow \begin{array}{c} \text{stable} \\ \text{polymorph} \\ \text{at depth} \end{array} \longrightarrow \text{iron-boracite (stable)}$ <p style="text-align: right;">on uplift</p>

* The iron-boracite polymorphs are most likely to be related by one of processes 1-3 (see text).

analysis points is given in Appendix 4.

Figures 5.14 to 5.16 show that the individual iron-boracite and ericaite crystals exhibit a wide range in composition in all the nodules examined (see Figure 5.18). Some of these crystals become depleted in MnO and FeO (in the parahilgardite nodules, see Figure 5.16) or enriched in these elements (Figure 5.14(B)) towards their edges, whilst others exhibit no systematic internal variation in composition (ericaite crystal B.18; Figures 5.14(E) and (F)). However the iron-boracite crystals from the S-20 borehole (Figure 5.17) and an ericaite crystal from iron-boracite nodule 2 (Figure 5.15(B)) are all of almost constant composition. The individual crystals are thus of very variable character.

The similarity in composition of iron-boracite and ericaite crystals also strongly suggests that there is a relationship between the minerals.

(J) The nature of the relationship between iron-boracite and ericaite

The X ray, optical and chemical data indicate that iron-boracite and ericaite are polymorphs, and that some, if not all the iron-boracite crystals formed by the breakdown of ericaite. The widespread occurrence of iron-boracite suggests that it is the stable polymorph at the present time. Table 5.10 shows that there are a number of possible hypotheses which might relate the

minerals.

Boracite group minerals invert to cubic symmetry at temperatures from 265°C (Mg rich) to 340°C (Fe rich; see Table 5.7) because of repositioning of the cations and chlorine atoms in the crystal structure (Ito et al., 1951; Heide et al., 1951; v. Hodenberg and Kühn, 1974). Below the inversion temperature these minerals are of monoclinic, orthorhombic or trigonal symmetry (Table 5.5) and are frequently characterized by extremely complicated sector and multiple twinning. Table 5.7 shows that the iron-boracite crystals at Boulby invert to cubic symmetry at temperatures from 287°C upwards depending upon their composition.

The cubic morphology of the iron-boracite and ericaite crystals at Boulby suggests that they were originally of cubic symmetry. The nodules are of diagenetic origin (see later text) and the rocks of the English Zechstein have almost certainly never been heated to 265°C or above. Heide, however, in a personal communication to Braitsch (1972), said that he had synthesized pseudocubic crystals well below 265°C. At Boulby, therefore, it is quite possible that the iron-boracite and ericaite crystals may have formed from an original early diagenetic metastable cubic polymorph by either of process 1 or 2 in Table 5.10.

However Braitsch (1972) has suggested that where boracite minerals have obviously formed well below 265°C

their cubic morphology may be the result of mimetic twinning. Should this be the case at Boulby then the ericaite, and perhaps iron-boracite, are original early diagenetic minerals and they may be related by either of processes 3 or 4 in Table 5.10.

Since deposition this bed has been buried to 2 - 3 kms. in depth and subsequently uplifted (see Chapter 9). It seems unlikely that ericaite is a high pressure polymorph of iron-boracite, as suggested in process 5 of Table 5.10, as although there is no data on the effect of pressure on boracite minerals, iron-boracite crystals from Riedel-Hänigsen in Germany (Kühn and Schaacke, 1955), which have been buried to depths of 3 - 4 kms. (Trusheim, 1960), do not appear to have inverted to ericaite at any time in their history.

The similarity in the variations of the chemical composition of the iron-boracite and ericaite crystals from Boulby indicates that either they are both derived from the same pre-existing polymorph (process 1; Table 5.10) or that all the iron-boracite was formed by the breakdown of ericaite (process 2 or 3; Table 5.10). The variations in bulk composition of these minerals are also compatible with any of these metastable origins. They are less likely to have formed by process 4 (Table 5.10) as if iron-boracite was a stable primary mineral one would expect it to have a relatively constant composition, which is rarely observed, and be twinned.

Therefore, although it is not possible to distinguish which of processes 1 to 3 led to the formation of the iron-boracite and ericaite crystals, it is evident that these minerals were originally metastable and have been attaining equilibrium since the late Permian.

(b) Parahilgardite

Parahilgardite is a member of the hilgardite group of minerals which have general formula $\text{Ca}_2[\text{B}_5\text{O}_8(\text{OH})_2]\text{Cl}$ (Palache, Berman and Frondel, 1951). The mineral has been named according to a classification of this group of minerals proposed by the writer in Appendix 5 and shortly due to be presented to the IMA Commission on New Minerals and New Mineral Names for ratification. This scheme of classification has been constructed in order to simplify and clarify the naming of the minerals. A comparative study of the properties of the hilgardite group of minerals is also given in Appendix 5.

The mineral, which occurs in rosettes, is the principal constituent of these nodules (Figure 5.19). It is also present in a similar form in the host rock. Prior to the discovery of this bed hilgardite minerals have only been described from insoluble residues in salt deposits in Louisiana (Hurlbut and Taylor, 1937; Hurlbut, 1938) and north Germany (Braitsch, 1959).

(α) General characteristics

The crystals vary in length from 0.1 - 15.0 mm. and in width from 0.05 - 8.0 mm. and are always much larger in the nodules than in the host rock. The dominant tabular euhedral crystal form is $\{010\}$ although the subsidiary forms $\{100\}$ and $\{01\bar{1}\}$ are present. The morphology of these crystals resembles that of the triclinic pedial class described for other hilgardite minerals by Hurlbut and Taylor (1937), Hurlbut (1938) and Braitsch (1959). In most cases the crystals display well developed (010) and (001) cleavages and a few crystals show simple twinning. The mineral has a hardness of 5 - 7 cm. Moh's scale.

Left and right handed crystals of the mineral are also suspected because some crystals appear to be mirror images of one another. Many enantiomorphic minerals are optically active (Wooster, 1938) but the mineral in thin section was too thin to show rotation of the plane of polarized light and in sections 1 mm. thick, there was inadequate light transmission. The existence of enantiomorphs cannot, therefore, be conclusively proved.

(β) Optics, lattice parameters and chemical composition

The optical properties, lattice parameters, and chemical composition of the mineral from a nodule are given in Tables 5.11, 5.12 and 5.8 respectively. The

Table 5.11

The optical properties and optical orientation of
parahilgardite from nodules in bed B.S.3

Optical orientation¹

	ϕ	ρ
n_{α}	114°	79°
n_{β}	-2°	28°
n_{γ}	-115°	64°

Optical properties

n_{α}	1.630
n_{β}	1.636
n_{γ}	1.664
$2V_{\gamma}$	$34.8 \pm 0.58^{\circ}$ and $37.2 \pm 0.01^{\circ}$
$n_{\gamma} - n_{\alpha}$	0.034

1. The optical orientation is given following the conventions given in Walstrom (1969, p. 446).

Table 5.12

The lattice parameters of parahilgardite from nodules in
bed B.S.3

	<u>1^a</u>	<u>2^b</u>	<u>3^b</u>
Unit cell parameters			
a	6.273Å ^c	6.297Å	6.297Å
b	6.491Å	6.464Å	11.335Å
c	6.570Å	6.565Å	11.541Å
α	73.50°	74.14°	93.33°
β	64.67°	61.58°	89.78°
γ	60.66°	61.26°	90.43°
Space Group	P1	P1	- ^c
Unit cell volume	203.58Å ³	205.73Å ³	822.34Å ³
No. of molecules in the unit cell	1	1	4
Measured density	2.60g/cm ^{3d}	2.58g/cm ³	2.58g/cm ³
Calculated density	2.69g/cm ³	2.69g/cm ³	2.69g/cm ³

a. These lattice parameters were determined by the writer.

b. These lattice parameters were determined by v. Hodenberg and Kühn (1977).

c. These lattice parameters were determined by the analysis of single crystal rotation, Weissenberg, and precession photographs using CuK_α radiation.

d. The density of the mineral was measured on a single crystal using a pycnometer at 20°C.

e. Not given, but either P1 or P1̄.

chemical analysis gives the mineral a formula of $(\text{Ca}_{1.97}\text{Sr}_{0.03}\text{Mg}_{0.01})\text{B}_{4.97}\text{O}_{7.96}(\text{OH})_{2.04}\text{Cl}_{1.00}$ based on eleven anions (O, OH, Cl).

The lattice parameters of a sample of this mineral from one of these nodules have also recently been determined by v. Hodenberg and Kühn (1977). Table 5.12 shows that they found the mineral to have two different sets of lattice parameters; one similar to those determined by the writer and another quite different set. They were unable to account for these two sets of parameters.

However the parahilgardite in the nodules is highly turbid and displays many unusual mineralogical features when compared with those crystals in the host rock. These features are a consequence of the mode of growth of the mineral and are, therefore, important in the genesis of the nodules. In addition they provide a plausible explanation for the different sets of lattice parameters observed by v. Hodenberg and Kühn (1977).

(8) The nature and origin of the turbidity in the parahilgardite of the nodules

(i) Optical characteristics:- The majority of these crystals have a turbid appearance characterized by undulose extinction, extinction bands, and lamellae with subgrains. Many crystals exhibit only undulose extinction. Other crystals, however, show random areas

of irregular outlines, often having diffuse boundaries with the host, and different birefringence colours. Extinction bands (maximum thickness 0.05 mm.) are common. In (010) sections these bands frequently form V shapes with the head of the V pointing towards the centre of the rosette (Figure 5.20). In other mineral sections they resemble ostrich plumes (Figure 5.21) with sharp or diffuse boundaries. Individual extinction bands may themselves exhibit undulose extinction.

The lamellae, which do not transgress grain boundaries, are closely spaced features (up to 0.01 mm. apart; see Figure 5.22) being either parallel or inclined (maximum of 16°) to the (001) cleavage. The lamellae may be straight or curved and have a maximum individual thickness of 0.003 mm. This thickness may vary where lamellae rapidly narrow or terminate (Figures 5.22 and 5.23). Boundary walls of the lamellae are well defined and may be smooth or corrugated with interiors being composed of small anhedral elongate to subrounded subgrains frequently exhibiting undulose extinction. The host parahilgardite crystal surrounding a lamella may have normal or undulose extinction (Figure 5.22). Where simultaneous extinction of subgrains occurs the lamellae extinguish with, or up to 22° of rotation from, the host mineral. In some crystals, lamellae have coalesced and produced turbid areas composed of very small subgrains (Figure 5.23).

(ii) Chemical variations:- The parahilgardite crystals have been analysed for calcium, strontium, iron, magnesium and manganese using an electron microprobe analyser in order to determine if the turbidity of the mineral is caused by variations in the cation content. Little variation was found in the magnesium, manganese and iron contents and values were frequently below the detection limit of the electron microprobe.

The strontium content within crystals and between crystals, however, is variable (see Table 5.13). Some of the crystals contained nearly sixty times as much SrO as others, but within an individual crystal the SrO content varied by a factor of up to three. The ranges in weight percent SrO are also presented in Table 5.13 and show that there are similar variations in the SrO content of the lamellae and the host crystal. There is no relationship between the CaO and SrO values in the parahilgardite crystals.

(iii) Possible causes of strain:- There is a close similarity in the optical characteristics of this mineral, aluminium deformed by creep (Kelly and Gifkins, 1953) and naturally deformed quartz crystals (Carter and Friedman, 1965; Carter, 1965). Kelly and Gifkins (1953) showed that when stress was applied to aluminium the first sign of deformation was the development of extinction bands which on further application of strain broke down

Table 5.13

Variation in the SrO and CaO in the lamellae and host
crystals of the parahilgardite in the
parahilgardite nodules

Host/ lamellae*	No. of analyses	SrO (Wt%)		CaO (Wt%)	
		Range	Average	Range	Average
H	1	0.03	0.03	30.65	30.65
L	2	0.12	0.12	31.91- 32.90	32.40
H	1	0.19	0.19	32.18	32.18
L	1	0.03	0.03	32.21	32.21
H	2	0.13- 0.42	0.28	31.18- 32.50	31.84
L	1	0.12	0.12	32.68	32.68
H	6	0.08- 0.73	0.34	30.85- 32.11	32.46
H	3	0.18- 0.87	0.62	31.74- 32.83	32.13
H	3	0.19- 0.23	0.21	31.53- 32.52	32.16
H	2	0.09- 0.13	0.11	32.06- 32.13	32.10
L	2	0.08- 0.25	0.17	31.21- 32.13	31.67
H	2	0.10- 0.24	0.17	32.21- 32.15	32.18
L	2	0.18	0.18	31.56- 31.81	31.68
H	2	0.17- 0.44	0.33	31.59- 32.10	31.88
H	3	0.27- 0.52	0.42	32.09- 32.39	32.24
L	2	0.41- 0.48	0.45	32.10- 32.11	32.15

Table 5. 13 (cont.)

Host/ lamellae	No. of analyses	SrO (Wt%)		CaO (Wt%)	
		Range	Average	Range	Average
H	4	0.06- 0.24	0.13	30.13- 32.57	31.86
L	1	0.09	0.09	32.03	32.03
H	3	0.00- 0.06	0.03	30.90- 32.18	31.65
H	2	0.09- 0.16	0.13	32.96- 33.08	33.02
L	1	0.05	0.05	32.45	32.45
H	3	0.04- 0.51	0.25	31.38- 32.83	32.31
L	1	0.17	0.17	32.80	32.80

*H = host crystal

L = lamella

and developed subgrains (cells) both along and across the bands. The deformed aluminium of Kelly and Gifkins and parahilgardite are similar in the following respects:-

Both display undulose extinction and parallel extinction bands which vary in width and optical orientation.

Both exhibit closely spaced lamellae with sharp boundaries.

In both cases these lamellae have broken down internally to form randomly orientated subgrains.

The turbid features of parahilgardite also resemble those of naturally and experimentally deformed quartz. Comparison between parahilgardite and deformed quartz shows that the lamellae are closely spaced features which do not transgress grain boundaries; the lamellae are often composed of subgrains and lenticles which may be in different optical orientations; and the lamellae are usually sharp. However none of the lamellae contain cavities or inclusions as is sometimes the case with naturally and experimentally deformed quartz crystals.

As the lamellae and host crystals of parahilgardite have similar chemical composition it is probable that chemical variation is not the cause of the turbidity. Thus by comparison with aluminium and quartz it seems most likely that this turbidity is a result of strain applied to the crystals.

(iv) Possible origins of the stress in the parahilgardites:- The small parahilgardite crystals which have grown in the host rock rarely show strain features, suggesting that the process producing the strain acted within, or on, only the nodules. There are a number of possible hypotheses which could have caused the strain features to develop.

The nodules are always dominantly composed of aggregated rosettes of parahilgardite (see Figure 5.19). Morse et al. (1932) have shown that substances of almost any chemical class and crystallizing in any chemical system may be prepared in spherulitic form. Rapid competitive growth of primary crystals in a sediment could account for the strain features and the size of these crystals when compared with those in the host rock.

However according to Spry (1969) spherulitic structures also frequently form as a result of reorganization of disordered material by the rotation of small units of that material which are subsequently added to a nucleus. A combination of difficult nucleation and slow growth promotes the development of spherulites with the kinetics being governed largely by the rate of nucleation. When spherulites are imperfectly formed individual crystals exhibit undulose extinction and lineage features. It is possible, therefore, that the parahilgardite crystals in the nodules grew by recrystallization and re-ordering of those crystals in the host rock. The

strain features observed could result from imperfect crystal growth possibly caused by a large number of crystals competing for a limited volume in the sediment or rock.

As the nodules sharply truncate the parahilgardite rosettes in the host rock and spherulitic structures generally form by slow rather than rapid growth, it is much more likely that the parahilgardite in the nodules formed by recrystallization of those crystals in the host rock.

Within an individual crystal the lamellae resulting from the strain correspond to areas of different orientation and structure. That v. Hodenberg and Kühn (1977) observed two sets of cell dimensions for this mineral (see Table 5.12) might suggest the lamellae are of different structure but this has not been proved because of the difficulty in X-raying lamellae. Alternatively the spherulitic growth might have caused two different polymorphs to grow simultaneously and the lamellae represent strained areas of the crystals in different orientations. Hurlbut (1938) and Braitsch (1959) obtained different sets of lattice parameters for parahilgardite (see Appendix 5; Table A5.2) in insoluble residues from the Choctaw salt dome, Louisiana, although nothing could be said of their origins.

(3) The area of iron-boracite nodules

(a) The petrography of the host rock

This rock is a grey-black shale which is frequently interstitial to the iron-boracite nodules. It is principally composed of clays, sylvite and halite with subsidiary anhydrite, magnesite and iron-boracite. The composition and mineral characteristics of the rock are given in Table 5.14.

The rock is generally composed of small anhedral sylvite and halite crystals enclosed in a matrix of parallel aligned clays. Anhydrite laths are occasionally intergrown with clays.

Hematite, magnesite and quartz crystals are similar to those in the other shale beds and formed by the reaction of brines with the clays during diagenesis.

(b) Petrography of the nodules

These nodules are of very variable composition (see Table 5.15) and contain:-

(i) iron-boracite, sylvite, magnesite and halite, each of which range from being minor minerals to principal constituents, and

(ii) ericaite, clays, talc, and hematite which are always accessory minerals.

There is no systematic variation in the composition of

Table 5.14

Composition and mineral characteristics of the host rock of the iron-boracite nodules in bed B.S.3

<u>Mineral</u>	<u>Volume percentage of mineral*</u>		<u>Colour</u>	<u>Grainsize</u>	<u>Crystal shape and form</u>	<u>Comments</u>
	<u>Average</u>	<u>Range</u>				
Anhydrite	10	7-14	White-grey	0.0-0.2 mm.	Elongate laths	They occurred intergrown with clay platelets.
Halite	15	11-22	White	0-4 mm.	Anhedral crystals	They generally form small, frequently elongate, porphyroblasts enclosed in the clay matrix.
Sylvite	35	20-40	Milky white to deep red brown	0-2 cm.	Anhedral	They form small elongate crystals (4 mm.) enclosed in the matrix.
Iron-boracite/ Ericaite	5	0-8	Blue-green to purple	0.0-2.0 mm.	Euhedral	These crystals form isolated cubes in the clay matrix.
Clays	30	20-50	Green-brown	0.00-0.05 mm.	Elongate platelets	This mineral defines the matrix of the rock and is sometimes intergrown with anhydrite laths and small quantities of black carbonaceous matter.

Table 5.14 (cont.)

<u>Mineral</u>	Volume percentage of mineral*		<u>Colour</u>	<u>Grainsize</u>	<u>Crystal shape and form</u>	<u>Comments</u>
	<u>Average</u>	<u>Range</u>				
Magnesite	5	0-8	White-grey	0.0-0.5 cm.	Euhedral to subhedral hexagonal plates, tabular on (0001)	Single plates cross- cut the clay matrix and project into the cleavages of sylvite and halite crystals.
Quartz	1	0-3	White-grey	0.0-0.2 mm.	Euhedral to anhedral	It occurs along the contact between the clay matrix and chloride minerals towards which it is euhedral.
Hematite	tr	-	Red-brown	0.00- 0.05 mm.	Euhedral to subhedral hexagonal plate- lets, tabular on (0001)	It occurs as inclusions around clay in the large red sylvite porphyroblasts.
Pyrite	tr [†]	-	Brass- metallic	0.00- 0.05 mm.	Euhedral to anhedral octohedra	It occurs as single crystals or in small aggregates intergrown with clays.

* Composition determined from the modal analysis of 10 thin sections.

† tr = trace.

Table 5.15

Compositions (in volume percent of minerals) of three adjacent nodules in an area of iron-boracite nodules in bed B.S.3

Nodule Type	<u>Volume percentages of minerals</u>				
	Iron-boracite	Sylvite	Magnesite	Halite	Clays
1. Iron-boracite nodule	96	2	-	-	2
2. Iron-boracite- sylvite-magnesite nodule	55	20	20	4	1 114
3. Sylvite-magnesite nodule	4	50	40	3	3

Table 5.16 The composition and mineral characteristics of the nodules in the iron-boracite
nodule area of bed B.S.3

<u>Mineral</u>	<u>Volume percentage</u> of mineral*		<u>Colour</u>	<u>Grainsize</u>	<u>Crystal shape</u> <u>and form</u>	<u>Comments</u>
	<u>Average</u>	<u>Range</u>				
Iron-boracite	54	0-100	Blue-green to purple	0.0-3.0 mm.	Euhedral to anhedral	It occurs in aggregates many of which may coalesce to give a wholly iron-boracite nodule.
Ericaite	1	0-2	Blue-green to purple	0.0-3.0 mm.	Euhedral	It usually occurs as single crystals, but occasionally is observed to have broken down to iron-boracite.
Sylvite	30	0-98	Red	0.0-4.0 mm.	Subhedral to anhedral crystals	The red coloration is caused by inclusions of hematite platelets many of which are concentrated around clays. Sylvite is usually intergrown with magnesite. It encloses iron-boracite aggregates in many nodules.

Table 5.16 (cont.)

<u>Mineral</u>	<u>Volume percentage of mineral*</u>		<u>Colour</u>	<u>Grainsize</u>	<u>Crystal shape and form</u>	<u>Comments</u>
Halite	5	0-98	White	0.0-2.0 mm.	Anhedral	This is a replacive mineral which is absent from many nodules. Where present it has replaced all other minerals.
Magnesite	10	0-50	Grey-white	0.0-1.5 cm.	Euhedral to subhedral hexagonal plates, tabular on (0001)	10 R.I. measurements give ω in the range 1.700-1.705, i.e. almost pure magnesite. The plates are much larger in these nodules than in the other rocks. They are intergrown with sylvite and are of primary and secondary origin.
Clays	tr [†]	0-2	Green-brown	0.00-0.05 mm.	Elongate platelets	These occur as inclusions in iron-boracite and sylvite crystals and are often surrounded by haloes of hematite.

Table 5.16 (cont.)

<u>Mineral</u>	<u>Volume percentage of mineral*</u>		<u>Colour</u>	<u>Grainsize</u>	<u>Crystal shape and form</u>	<u>Comments</u>
	<u>Average</u>	<u>Range</u>				
Talc	1	0-2	Green-brown	0.0-0.5 mm.	Euhedral to subhedral plate- lets, tabular on (0001)	It has R.I.s of $n_{\alpha} = 1.540 \pm 0.002$; $n_{\beta} = 1.591 \pm 0.002$; $n_{\gamma} = 1.593 \pm 0.002$. The mineral occurs projecting from clays into the cleavages of sylvite. This is the only occurrence of the mineral in the sequence examined.
Hematite	tr	-	Red-brown	0.00- 0.05 mm.	Euhedral to subhedral hexagonal plates, tabular on (0001)	It occurs as randomly orientated inclusions in sylvite, particu- larly adjacent to clays.

* The compositions were determined by the modal analysis of 20 nodules.

† tr = trace.

Table 5.17

B₂O₃ and total iron analyses of iron-boracite and
parahilgardite nodules

<u>Nodule Type</u>	<u>Sample</u>	<u>Locality</u>	<u>Wt%B₂O₃</u>	<u>Total iron</u>
Fe boracite nodules	2S1	Roadway 2S, 34m east of 2E	1.27	1.93
"	2S2	" " "	31.41	17.32
"	ED1	Roadway L, 21m east of 3E	33.58	15.84
"	ED2	" " "	23.21	12.36
"	ED5	" " "	27.11	12.53
"	ED6	" " "	44.01	21.15
"	A	?	1.27	- ¹
"	B	?	1.33	-
"	201	S. Spearhead in No. 2 cross-cut between D and E	0.88	-
"	202	" " "	13.87	-
"	203	" " "	2.44	-
Parahilgardite nodules	274	East Spearhead in Roadway K, 10m east of No. 6 cross-cut	31.85	-
"	290	East Spearhead in No. 7 cross-cut between K and L, 30m south of K	43.27	-
"	295	East Spearhead, 10m east of the junc- tion of L and No. 8 cross-cut north	39.35	-
"	311	East Spearhead along No. 8 cross- cut between K and L	40.35	-
"	327	East Spearhead opposite the junc- tion of P and No. 5a cross-cut north	44.58	-

1. - = not determined.

these nodules. The characteristics of these minerals are summarized in Table 5.16. Table 5.17 shows that the B_2O_3 and total iron content of the nodules is very variable, reflecting the differences in their iron-boracite content.

Iron-boracite and ericaite commonly occur in aggregates or, occasionally, as single crystals. Almost pure iron-boracite nodules occur where large numbers of these aggregates have coalesced (Figures 5.24C and 5.25). However in the majority of nodules iron-boracite aggregates are set in a matrix of anhedral red sylvite crystals which are intergrown with single plates or sheaves of magnesite (Figures 5.13 and 5.24B). Sylvite-magnesite nodules with minor iron-boracite, usually in the form of single crystals, are moderately abundant (Figure 5.24A).

Figure 5.25 shows that in nodules principally composed of iron-boracite the mineral usually has a granular habit. However, where enclosed in sylvite, the iron-boracite crystals around the perimeter of these aggregates are frequently of pseudocubic form, whilst those in the centres are anhedral and granular (Figure 5.13). The anhedral grains may have formed by the breakdown or recrystallization of the euhedral crystals or, alternatively, both types may be "primary" with those adjacent to sylvite adopting euhedral form. Many of the iron-boracite and sylvite crystals contain inclusions

of clay (Figures 5.25 and 5.26).

Table 5.18 and Figures 5.27 and 5.28 show that the disposition of stringers of hematite crystals and the orientations of secondary talc and magnesite plates indicate that there is abundant evidence for the recrystallization of sylvite at least twice.

In some nodules the magnesite plates and sheaves cut across sylvite grain boundaries and neither bear any relationship to the sylvite cleavage nor define misorientated cubic grids which would indicate that sylvite had recrystallized. This indicates that at least some of the magnesite crystals grew at the same time as sylvite. There is, therefore, evidence for at least three generations of magnesite crystals; the first which formed at the same time as the sylvite; a second which grew in the cleavages of sylvite (Figure 5.28); and a third which grew after the recrystallization of sylvite (Figure 5.28).

Sylvite has replaced magnesite, iron-boracite and ericaite in some but not all of the nodules. In some cases it has only replaced magnesite on a small to medium scale (Figure 5.29) but in others magnesite is only present as remnant inclusions. The same is true of iron-boracite and ericaite (Figure 5.30). However sylvite is enriched in hematite inclusions, over and above those derived from clays, where it has partially or completely replaced iron-boracite and ericaite. It is interesting

Table 5.18

Evidence for the recrystallization of sylvite in the
iron-boracite nodules

1. Figure 5.27 shows stringers of tiny hematite crystals, which appear to define former crystal outlines, cross-cutting anhedral sylvite crystals. This indicates that sylvite crystals with hematite rims have recrystallized.
2. Figure 5.28 shows talc and magnesite crystals which appear to define the cubic cleavage in a sylvite crystal. However the present cleavage direction is defined by the large magnesite plates which cross-cut the similarly orientated talc and magnesite crystals. This strongly suggests that the talc grew in the sylvite cleavage by the breakdown of the associated clays possibly at the same time as the first generation of magnesite plates formed. The sylvite then recrystallized and adopted new cleavages into which a second generation of magnesite grew.
3. In some nodules sylvite crystals enclose magnesite plates which define a cubic grid bearing no relation to the present cleavages. This almost certainly indicates that the sylvite has recrystallized.

that in a few nodules sylvite has almost entirely replaced iron-boracite whilst in equilibrium with magnesite and vice versa. However in numerous cases both of these minerals have been partially replaced by sylvite. In a few nodules it has almost completely replaced iron-boracite and magnesite; resulting in occasional almost pure sylvite nodules. The timing of these reactions is uncertain, but they are likely to have occurred during diagenesis and burial.

Halite is present in variable proportions in some of these nodules (see Tables 5.15 and 5.16). It usually contains inclusions of sylvite, magnesite and iron-boracite (Figures 5.26 and 5.31); the individual fragments of each mineral being of similar orientation. This indicates that the halite is a replacement mineral. On occasion it has almost completely replaced all the other minerals; giving rise to rare halite nodules. The timing of these reactions is also uncertain. However halite has occasionally been observed replacing sylvite which is in reaction with iron-boracite. This suggests that solutions saturated in NaCl percolated into some of the nodules after many of the other reactions were in progress.

As a consequence of these replacement and recrystallization reactions adjacent nodules often have very different mineral compositions (Table 5.15 and Figure 5.26). In addition, nodules of similar composition may

Table 5.19

The original mineral assemblages of nodules in the area of
iron-boracite nodules in bed B.S.3

1. An iron-boracite polymorph (see Table 5.10)
2. An iron-boracite polymorph - sylvite - magnesite
3. Sylvite - magnesite

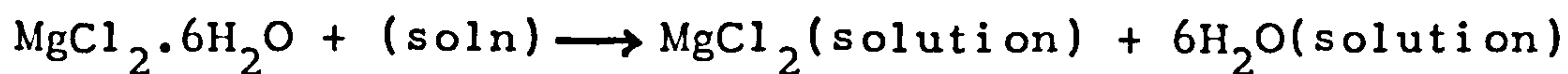
Table 5.20

The breakdown reactions of carnallite and bischofite
by reaction with brines undersaturated in these minerals

1. Carnallite



2. Bischofite



have formed by different processes; for example a sylvite-magnesite nodule of "primary" origin may have a similar composition to a "primary" iron-boracite-sylvite-magnesite nodule in which the iron-boracite has subsequently been replaced by sylvite.

(c) Mode of formation of the nodules

The mineralogical studies of iron-boracite and ericaite and the petrographic analysis suggest that these nodules were originally composed of the mineral assemblages shown in Table 5.19. The presence of clay inclusions in the iron-boracite (Figure 5.26) and sylvite crystals indicates that the nodules grew in a clay sediment.

The average bromine contents of three sylvite crystals from three iron-boracite-sylvite-magnesite nodules and three halite crystals from the host rock are 1448 ppm and 222 ppm respectively; giving a $\text{Br}_{\text{KCl}}/\text{Br}_{\text{NaCl}}$ ratio of 6.5. This indicates that the sylvite crystals of these nodules are secondary and have either formed by the breakdown of carnallite by reaction with a solution undersaturated in carnallite or by the recrystallization of pre-existing sylvite after reaction with brines (see Chapter 4 for the theoretical basis for these conclusions). However the presence of abundant small hexagonal halite crystals, which can most readily be interpreted as

pseudomorphs after carnallite, in beds B.S.1 and 4, below and above this unit, strongly suggests that the sylvite crystals in these nodules have been formed by the breakdown of carnallite on reaction with brines saturated in halite (see Table 5.20; reaction 1).

Iron-boracite and ericaite both have compositions approximating to $(\text{Mn}_{0.24}\text{Fe}_{1.50}\text{Mg}_{1.30})\text{B}_{6.90}\text{Si}_{0.04}\text{O}_{13.07}\text{Cl}_{0.93}$. As borate minerals accurately reflect the chemical environment of their formation (Van't Hoff, 1909) the original metastable iron-boracite polymorph (Table 5.10) must have formed by the reaction of magnesium chloride, iron and boron in the clay sediment. The magnesium chloride would almost certainly have been derived from the pore solutions in the sediment which would have been partly composed of MgCl_2 released by the breakdown of carnallite and also very possibly bischofite (see Table 5.20).

The iron content of the iron-boracite and ericaite crystals (15-25% FeO; see Table 5.9) is far in excess of that which would be expected from the evaporation of normal seawater (0.17 ppm Fe at the beginning of carnallite precipitation; Bratisch, 1972). However six samples of the host clays have an average total iron content of 4.7%, and this suggests that they were almost certainly the source of iron for the original iron-boracite (polymorph) crystals.

The boron of these minerals could have been derived

from the eutonic brines, the clays (which are known to absorb boron from solutions; Porrenga, 1967) or both of these sources. However the aggregated nature of these minerals (Figures 5.13 and 5.24) in the bed strongly suggests that the first crystals to nucleate in the sediment attracted boron rich solutions towards them from which further crystals formed by reaction with the clays. Otherwise one would have expected iron-boracite and ericaite to be evenly distributed in the rock. The former being the case the boron was probably principally present in the pore solutions of the sediment although some could have been released into solution by the clays at an earlier date.

The "primary" magnesite crystals intergrown with sylvite in many of the nodules probably formed by the reaction of MgCl_2 rich brines with carbonate matter in areas of the host sediment locally relatively depleted in boron. This would account for the variation in the initial composition of adjacent nodules.

The evidence, therefore, indicates that the initial minerals of these nodules (an iron-boracite polymorph, sylvite and magnesite) are all secondary and grew in a clay sediment by displacing and replacing the clays during diagenesis. The first crystals of the iron-boracite polymorph grew metastably (Table 5.10) in separate nucleation sites by the reaction of brines enriched in MgCl_2 and B_2O_3 with iron rich clays. The growth of these

crystals attracted boron from the surrounding solutions and more of them formed by a similar reaction; resulting in the formation of aggregates of the iron-boracite polymorph. In some cases these aggregates coalesced to form nodules. However, simultaneously, magnesite grew by the reaction of MgCl_2 solutions with carbonate matter in areas of the sediment locally relatively depleted in boron, and sylvite crystals, resulting from the breakdown of carnallite, grew by displacement. Aggregates of the iron-boracite polymorph, sylvite and magnesite coalesced to form nodules composed of variable proportions of these minerals. This resulted in the simultaneous growth of iron-boracite (polymorph) nodules, iron-boracite (polymorph)-sylvite-magnesite nodules and sylvite-magnesite nodules in close proximity to one another.

Since the time of formation of the nodules the original iron-boracite polymorph has attempted to attain equilibrium by one of processes 1 to 3 in Table 5.10 and the other minerals have been involved in an extensive series of replacement and recrystallization reactions summarized in Table 5.24.

(4) The area of parahilgardite nodules

(a) Petrography of the host rock

The rock is pale grey and less friable than the host rock of the iron-boracite nodules. It is principally composed of clays and parahilgardite with subsidiary anhydrite, sylvite and halite and accessory quartz, magnesite, iron-boracite and ericaite. The composition and mineral characteristics of the rock are given in Table 5.21.

The rock is generally composed of small rosettes of parahilgardite (Figure 5.32) and small anhedral halite crystals set in a matrix of parallel aligned to randomly orientated clay platelets which are intergrown with small numbers of anhydrite laths. Occasional deep red sylvite porphyroblasts cross-cut and enclose the clays.

The parahilgardite crystals range from 5 volume percent of the rock distant from the nodules to over 80 volume percent adjacent to the nodules (Figure 5.19). Table 5.22 shows that the B_2O_3 content of the rock rises markedly towards the nodules. Many of the parahilgardite rosettes have kernels of clays, sylvite, dolomite and carbonaceous matter (Figures 5.19 and 5.32). However the individual crystals rarely contain inclusions of these minerals. This suggests that the parahilgardite crystals grew within a sediment by displacing the other minerals.

Table 5.21 Composition and mineral characteristics of the host rock of the parahilgardite nodules in bed B.S.3

<u>Mineral</u>	<u>Volume percentage of mineral*</u>		<u>Colour</u>	<u>Grainsize</u>	<u>Crystal shape and form</u>	<u>Comments</u>
	<u>Average</u>	<u>Range</u>				
Anhydrite	13	10-15	Grey-white	0.0-0.1 mm.	Elongate laths or euhedral equant crystals	The majority of the crystals form elongate laths intergrown with clays. The euhedral equant crystals cross-cut the laths and are formed by recrystallization.
Halite	11	6-15	White	0-5 mm.	Anhedral crystals	These crystals are usually up to 3 mm. in maximum dimension and set in a matrix of anhydrite and clays. Occasional larger crystals have sometimes partially replaced iron-boracite.

Table 5.21 (cont.)

<u>Mineral</u>	<u>Volume percentage of mineral*</u>		<u>Colour</u>	<u>Grainsize</u>	<u>Crystal shape and form</u>	<u>Comments</u>
	<u>Average</u>	<u>Range</u>				
Sylvite	10	5-12	Red	0-1 cm.	Anhedral crystals	It forms anhedral porphyroblasts, some of which are enclosed in the anhydrite-clay matrix; others cross-cut and enclose clays. The red coloration is due to hematite inclusions derived from the clays.
Iron boracite/ ericaite	1	0-3	Blue-green	0.0-1.0 mm.	Euhedral cubes	Occasional crystals, usually associated with sylvite, are evenly dispersed in the rock.
Para- hilgardite	22	5-80	White- pale grey	0.0-0.5 mm.	Tabular, wedge shaped crystals	The mineral occurs in rosettes intergrown with clays, anhydrite and sylvite; see Figure 5.32.
Clays	40	35-42	Green-brown	0.00- 0.05 mm.	Elongate platelets	These crystals form the matrix of the rock and may be parallel aligned or randomly orientated.

Table 5.21 (cont.)

<u>Mineral</u>	Volume percentage of mineral*		<u>Colour</u>	<u>Grainsize</u>	<u>Crystal shape and form</u>	<u>Comments</u>
	<u>Average</u>	<u>Range</u>				
Magnesite	2	0-3	White-grey	0.0-1.0 cm.	Euhedral to subhedral hexagonal plates, tabular on (0001)	It cross-cuts the clay- anhydrite matrix of the rock and projects into the cleavages of chloride minerals.
Dolomite	tr [†]	-	Grey- pale brown	0.00- 0.01 mm.	Rounded granules	It occurs at the centres of a few para- hilgardite rosettes.
Hematite	tr	-	Red	0.00- 0.05 mm.	Euhedral to subhedral hexagonal plates, tabular on (0001)	It occurs as randomly orientated inclusions in hematite.
Quartz	1	0-2	White-grey	0.0-0.5 mm.	Euhedral to subhedral crystals	The mineral occurs along the contacts between the clay matrix and chloride minerals. It is euhedral towards sylvite and halite.

* The composition was determined from the modal analysis of 10 thin sections.

† tr = trace.

Table 5.22

B₂O₃ analyses of shale adjacent to and distant from
parahilgardite nodules

<u>Sample</u>	<u>Locality</u>	<u>Distance from parahilgardite nodules</u>	<u>Wt.% B₂O₃</u>
256	East panel in Road- way J, 20m east of No. 8 cross-cut	0 cm	27.81
"	"	3 cm	18.36
"	"	6 cm	7.85
131	East panel in Road- way K, 10m east of No. 8 cross-cut north	0 cm	18.58
"	"	3 cm	8.98
"	"	6 cm	4.14
274	East panel in Road- way K, 10m east of No. 6 cross-cut	Nearest nodule 12 cm	0.15
"	"		0.62
"	"		0.19

Table 5.23 Composition and mineral characteristics of the parahilgardite nodules in bed B.S.3

Volume percentage of minerals*					
<u>Mineral</u>	<u>Average</u>	<u>Range</u>	<u>Colour</u>	<u>Grainsize</u>	<u>Crystal shape and form</u>
Para- hilgardite	90	70-100	White to pale grey	0.0-1.5 cm.	Tabular wedge shaped crystals
This mineral forms rosettes and has a highly turbid appearance (see text).					
Sylvite	5	2-15	Red	0.0-3.0 mm.	Anhedral
It occurs as wedges between adjacent para- hilgardite rosettes. The red coloration is caused by inclusions of hematite.					
Iron- boracite/ ericaite	3	0-12	Blue-green	0.0-1.0 mm.	Euhedral cubes
The minerals occur as single crystals in the centre of the nodules or as small aggregates of crystals around the edge.					
Magnesite	2	0-3	Grey-white	0.0-0.2 mm.	Euhedral to subhedral hexagonal plates, tabular on (0001)
They only occur in the cleavage of replacive halite.					
Halite	1	0-5	White	0.0-4.0 mm.	Anhedral crystals
This mineral occurs in a few nodules where it has replaced the other minerals.					

Table 5.23 (cont.)

<u>Mineral</u>	Volume percentage of minerals*		<u>Colour</u>	<u>Grainsize</u>	<u>Crystal shape and form</u>	<u>Comments</u>
	<u>Average</u>	<u>Range</u>				
Hematite	tr [‡]	-	Red	0.00- 0.05 mm.	Euhedral to subhedral hexagonal plates, tabular on (0001)	It occurs as randomly orientated inclusions in the sylvite.

* The composition of these nodules was determined by the modal analysis of 25 nodules.

‡ tr = trace.

Iron-boracite and ericaite are evenly dispersed in the rock and are usually associated with sylvite. The quartz and magnesite crystals have similar parageneses to those in bed B.S.4 except that in this rock quartz occasionally contains inclusions of iron-boracite and parahilgardite; suggesting that it has replaced these minerals or grew at the same time as them.

(b) Petrography of the nodules

These nodules are principally composed of aggregated rosettes of parahilgardite (Figures 5.19 and 5.33) with smaller quantities of iron-boracite, ericaite, sylvite, halite and magnesite. The composition and mineral characteristics of these nodules are given in Table 5.23. Table 5.17 presents typical B_2O_3 contents for these nodules.

The parahilgardite crystals have been described earlier in the chapter. When present, ericaite forms isolated cubes in the centre of the nodules, whilst iron-boracite tends to occur in small aggregates around the edges. Sylvite forms red wedge shaped crystals in the interstices between parahilgardite rosettes.

Anhedral colourless halite crystals occur around the outside edges of a few nodules. They commonly contain many orientated inclusions of parahilgardite and penetrate the lamellae of these crystals (Figure 5.34).

This indicates that the halite has replaced the parahilgardite in these instances.

A few nodules are truncated by sylvinite veins.

(c) The mode of formation of the nodules

The parahilgardite ($\text{Ca}_2[\text{B}_5\text{O}_8(\text{OH})_2]\text{Cl}$) crystals in this bed must have precipitated from boron rich calcium chloride solutions which were present within the clay sediment. They grew by displacing the other minerals in the sediment during diagenesis.

They are unevenly disseminated in the bed and this suggests that those to crystallize first attracted boron rich solutions from the surrounding sediment from which further crystals precipitated. This led to the formation of aggregates of small parahilgardite rosettes. The mineral may originally have been metastable, as it is intergrown with very small quantities of iron-boracite and ericaite of known metastable origin.

At some time later, but prior to sylvinite veining, these parahilgardite crystals recrystallized into much larger crystals which again formed rosettes. These aggregated rosettes of larger crystals now compose the nodules. The strain features of these crystals result from imperfect crystal growth during recrystallization. The initial cause of the recrystallization is uncertain, but it may have been compaction of the sediment as burial commenced.

(d) Comparison of the iron-boracite and parahilgardite nodules

The parahilgardite, iron-boracite and ericaite crystals all appear to have grown by displacement in a clay sediment. The original iron-boracite polymorph formed by the reaction of B_2O_3 rich $MgCl_2$ brines with clays and combined with secondary sylvite and magnesite to form nodules during early diagenesis. However the parahilgardite crystals precipitated from a brine rich in B_2O_3 and $CaCl_2$ but without reaction with the clays. The parahilgardite nodules formed later by recrystallization of the mineral, very possibly during late diagenesis. The iron-boracite nodules are, therefore, "original" but are composed of a secondary mineral assemblage, whilst the parahilgardite nodules are "secondary" but have formed by the recrystallization of a primary or early diagenetic mineral assemblage which formed without reaction with the host rock.

Iron-boracite and ericaite are polymorphs which are derived from an original metastable polymorph by one of processes 1 to 3 in Table 5.10. Similarly two parahilgardite polymorphs occur in the parahilgardite nodules but they almost certainly result from the recrystallization, under local stress, of the small crystals of the mineral in the host rock.

The proportions of the original minerals in the

iron-boracite nodules are much more varied than those in the parahilgardite nodules. In addition, the minerals of the iron-boracite nodules have undergone a much more complex series of replacement and recrystallization reactions than those in the parahilgardite nodules.

The origin of the MgCl_2 and CaCl_2 brines which precipitated the original iron-boracite polymorph and parahilgardite in different areas of a clay sediment to form this bed will be considered in Chapter 7. As far as the writer is aware, no other marine borate deposit has, as yet, been located in the world bearing any resemblance to this bed.

IV The rocks of the Boulby Shale in the area of the Mine enclosed by roadways 2E, 2S, 5W and 3N and boreholes S-20, X, Y, D, V, V-D1 and M

(1) General

The Boulby Shale overlies the roofs of the majority of the roadways in this area of the Mine, but it can be observed in the S-20 borehole (drilled on the site of No. 2 shaft) and also where it and the Rotten Marl have downbulged into the Boulby Potash.

Comparison of Figure 5.35 and Tables 5.1 and 5.11 show that these beds are enriched in halite relative to those in the other areas of the Mine. Beds B.S.3 and 4 in the S-20 borehole are halite-anhydrite-clay rocks which

consist of anhydrite and clay laminae set in a matrix of colourless halite. The clay laminae are often abruptly terminated by halite (Figure 5.36) which composes up to 80% of some rocks. Figure 5.36 shows typical remnant crystals of iron-boracite which have been partially replaced by halite in bed B.S.3. Patches of bed B.S.5 exhibit the typical textures of the unit, but these are frequently enclosed or pervaded by colourless halite (see Figure 5.37). Similar features also occur in this bed in boreholes X, Y, D, V, V-D1 and M and in bed B.S.4 in borehole X.

Red fibrous sylvinite veins, which usually cross-cut the beds of this unit, are conspicuously absent in the S-20 borehole and the downbulges into the Boulby Potash. However during shaft sinking Mr. P.J.E. Woods (pers. comm.) observed remnant fibrous sylvinite veins, which had been almost completely replaced by halite, in the upper beds of the Boulby Shale. A number of these veins, iron-boracite and parahilgardite nodules have also been partially replaced by colourless halite in the South and East Spearheads in the Mine (Figures 5.21, 5.26 and 5.38). In addition, these veins are rare in the other boreholes in which this type of halite occurs.

The colourless halite in this area of the Mine, the South and East Spearheads and in these boreholes is, therefore, almost certainly of the same origin and is a secondary replacement mineral. However the extent

to which it has replaced the minerals of this bed is very variable. In this area of the Mine and these boreholes it has transformed the mineralogy and characteristics of the beds to the point where they are almost unrecognizable, whereas in the South and East Spearheads it has done little to modify the rocks.

As this halite has replaced sylvinite veins, it probably replaced the other minerals of these beds during burial. However as these are the least brecciated beds of the Boulby Shale in the Mine, and halite is known to deform plastically during movement, it is likely that these replacement reactions occurred prior to the widespread lateral migration of the Boulby Potash.

The brine which precipitated this halite could result from the dissolution of a pre-existing halite bed near the top of the Boulby Shale, but equally it could have been produced by the dehydration of the overlying Rotten Marl (Carnallitic Marl). In either case it is obvious that this occurred over a wide area and that the brine percolated unevenly downwards.

(2) Discussion of the economic importance of the secondary halite in the Boulby Shale

The effects of this halite on the rocks of this unit are of considerable economic importance. In the area of the Mine enclosed by roadways 2E, 2S, 5W and 3N the

secondary halite rocks of this unit provide an excellent roof for the roadways driven in the Boulby Potash. Therefore if new roadways are driven into a similar geological environment elsewhere in the C.P.L. concession area, it should be possible to extract all the Boulby Potash rather than leaving some of it in place to help support the overlying rocks.

The brines which precipitated this halite must have been unsaturated with respect to sylvite as halite has replaced sylvite in both the beds and the veins. Up to 10th January, 1977, these brines had only modified the beds of the Boulby Shale. However it is quite possible that they might have percolated into the Boulby Potash elsewhere in the C.P.L. concession area. If this has occurred, sylvite will have been dissolved out of the bed and halite precipitated. It is, therefore, possible that zones of impoverishment may be found in the Boulby Potash, although it is not possible to predict where these might occur.

V Summary and Conclusions

This unit is composed of a series of shale beds of variable composition (Table 5.1). The petrographic character of these beds indicates that the majority of the minerals grew within an original clay sediment or that clays were brought into the area at the time these

minerals precipitated.

The most important and interesting of these beds is B.S.3, which contains separate areas of iron-boracite and parahilgardite nodules. The iron-boracite nodules are principally composed of variable proportions of iron-boracite, sylvite and magnesite (Table 5.13). Mineralogical studies indicate that the present iron-boracite crystals formed from a pre-existing metastable polymorph (Table 5.10) which grew by the reaction of boron rich MgCl_2 brines with iron rich clays during early diagenesis. The sylvite formed by the breakdown of carnallite and magnesite grew by the reaction of MgCl_2 brines with carbonate matter in areas locally relatively deficient in boron. During late diagenesis and burial numerous replacement and recrystallization reactions have occurred within these nodules (summarized in Table 5.24).

The parahilgardite nodules are principally composed of aggregated rosettes of parahilgardite. Mineralogical studies indicate that they formed by the recrystallization of pre-existing parahilgardite crystals which had originally been precipitated in the host rock by boron rich calcium chloride solutions. Nodule formation is likely to have occurred during late diagenesis or early burial. Table 5.24 summarizes the subsequent replacement and recrystallization reactions.

In random areas throughout the C.P.L. concession area various of these beds have been modified by secondary

Table 5.24 Summary of the replacement and recrystallization reactions recorded in the

Boulby Shale

<u>Bed</u>	<u>Replacement and recrystallization reactions₁</u>	<u>Scale of reaction₂</u>	<u>Timing of the reaction</u>
B.S.6	Recryst. of A C → Q C → M	S S S	Late diagenesis and during burial Early → late diagenesis "
B.S.5	Recryst. of A C → M C → C.H A → C.H	S S I → Maj S → I	Late diagenesis and during burial Early → late diagenesis During burial at depth "
B.S.4	Recryst. of A ?C → A Carn → H C → M, Hem, Q M → Sy ?Sy → A A → C.H C → C.H Sy → C.H M → C.H and I.B → C.H	S ?I I all S S ?I S → Maj S → Maj I both S	Late diagenesis and during burial " Early diagenetic Early → late diagenesis Probably late diagenesis Late diagenesis and during burial During burial at depth " " "
B.S.3	Parahilgardite nodules	Maj S → I S	During diagenesis or early burial During burial at depth "

Table 5.24 (cont.)

<u>Bed</u>	<u>Replacement and recrystallization reactions₁</u>	<u>Scale of reaction₂</u>	<u>Timing of the reaction</u>
B.S.3 (cont.)			
Parahilgardite	C→A	S	Late diagenesis or at depth
nodule	P→A	S	" " "
host rock	P→Q	S	During diagenesis or early burial
	I.B→Q	S	" " "
	I.B→C.H	S	During burial at depth
Iron-boracite			
nodules	Er→I.B	S but poss. Maj	Since formation
	Recryst. of sy	Maj	During late diagenesis and burial
	M→Sy	S→Maj	" " "
	Er→Sy	S	" " "
	I.B→Sy	S→Maj	" " "
	Er→C.H	S	During burial at depth
	I.B→C.H	S→Maj	" " "
	Sy→C.H	S→Maj	" " "
	M→C.H	S→Maj	" " "
	T→C.H	S	" " "
	?M→T	S	" " "
Iron-boracite			
nodule	B→?	?Maj	Early diagenesis
host rock	Cam→syl	?Maj	" "
	C→Hem,M,Q	all S	Early→late diagenesis
	C→C.H	S→Maj	During burial at depth
	Sy→C.H	S→Maj	" " "
	A→C.H	S	" " "
B.S.2			
	Recryst. of A	I	Late diagenesis and during burial

Table 5.24 (cont.)

<u>Bed</u>	<u>Replacement and recrystallization reactions¹</u>	<u>Scale of reaction²</u>	<u>Timing of the reaction</u>
B.S.1	?recryst. of H Carn→H C→M and Q	S→I I both S	Probably during burial Early diagenesis Early→late diagenesis
<p>1. B = bischofite; Carn = carnallite; Sy = sylvite; H = halite; C.H = colourless replacive halite; A = anhydrite; M = magnesite; Q = quartz; Hem = hematite; T = talc; P = parahilgardite; Er = ericaite; I.B = iron-boracite; C = clays.</p>			
<p>2. Maj = a major replacement reaction; I = a replacement reaction of intermediate scale; S = small scale replacement reaction.</p>			

brines saturated in halite. In the area of the Mine enclosed by roadways 2E, 2S, 5W and 3N this secondary halite has replaced the majority of the minerals of these beds; converting them into halite-anhydrite-clay rocks. It is believed this brine originated by the dehydration of the Rotten Marl or the dissolution of a halite bed near the top of the Boulby Shale.

CHAPTER 6BORON GEOCHEMISTRYI General

Boron is contained in borate minerals, clay minerals (Porrenga, 1967), anhydrite (Ham et al., 1961) and in fluid inclusions in minerals in salt deposits. The exact boron content of the solutions which precipitated these minerals and solutions is unknown. Braitsch (1972), however, used the simplified Boeke equation to calculate the B_2O_3 content of evaporating seawater at the beginning of gypsum, halite, carnallite and bischofite precipitation (see Table 6.1).

Van't Hoff (1909) and Jänecke (1915) predicted that small quantities of primary or early diagenetic magnesium borates would form together with potash salts and bischofite ($MgCl_2 \cdot 6H_2O$) during the final stages of evaporation of seawater as only then would boron be sufficiently concentrated in the residual magnesium chloride brines to combine with other elements and precipitate. Nikolaev and Chelishcheva (1940a) were unsuccessful in an attempt to crystallize boracite from brines collected from Lake Inder (which were very similar in composition to evaporated seawater) despite the fact that, after isothermal evaporation, they were highly

Table 6.1

The B_2O_3 content of seawater during progressive
evaporation¹

<u>Onset of precipitation of:-</u>	<u>ppm B_2O_3</u>
Gypsum	40
Halite	120
Carnallite	1190
Bischofite	1610

1. After Braitsch (1972)

Table 6.2

B₂O₃ content of insoluble residues from the rocks of the
sequence examined

<u>Location of insoluble residues</u>	<u>No. of samples</u>	ppm B ₂ O ₃	
		<u>Range</u>	<u>Average</u>
Parahilgardite area of the Borate Nodule Bed	3	1500-6200	3200
Boulby Potash	9	400-5500	1977
Boulby Halite	4	1400-1800	1650

Table 6.3Boron analyses from the rocks of the sequence examined

<u>Locality Number</u>	<u>Sample Number</u>	<u>Sample description and position</u>	<u>ppm B₂O₃</u>
23	114	Red sylvinite 25 cm. below the Boulby Shale	300
"	115	Grey sylvinite 40 cm. below the Boulby Shale	800
"	116	Grey sylvinite 70 cm. below the Boulby Shale	2000
"	117	Grey sylvinite 1.4 m. below the Boulby Shale	600
60	119	Purple-brown coarse grained Boulby Halite 80 cm. below the Boulby Potash	1000
"	120	Thin white banded Boulby Halite 60 cm. below the Boulby Potash	200
"	121	Banded sylvinite immediately above the Boulby Halite	70
"	122	Banded sylvinite 50 cm. above the Boulby Halite	800
45	61	White banded Boulby Halite 50 cm. below the Boulby Potash	700
"	62	Grey-brown Boulby Halite with a slight enrichment in potash 20 cm. below the Boulby Potash	600
"	63	Banded sylvinite 20 cm. above the Boulby Halite	1800
41	49	Red sylvinite	700
"	50	Purple-grey sylvinite	2600
"	51	Purple-grey sylvinite	400
79	174	Boulby Halite 20 cm. below the Boulby Potash	270
"	175	Boulby Halite from the base of the Boulby Potash	600

Table 6.3 (cont.)

<u>Locality Number</u>	<u>Sample Number</u>	<u>Sample description and position</u>	<u>ppm B₂O₃</u>
79	176	Sylvinite 10 cm. above the Boulby Halite	3000
"	177	Sylvinite 90 cm. above the Boulby Halite/Potash contact	200
"	178	Sylvinite 1.2 m. above the Boulby Halite	2600
"	179	Sylvinite 1.9 m. above the Boulby Halite	800
"	180	Basal Boulby Shale	500
50	71	Boulby Halite 23 cm. below the Boulby Halite/Potash breccia	500
"	72	Boulby Halite/Potash breccia 43 cm. below the sylvinite	500
"	73	Boulby Halite/Potash breccia 11 cm. below the sylvinite	500
"	74	Sylvinite 14 cm. above the base of the Boulby Potash	250
"	75	Sylvinite 74 cm. above the base of the Boulby Potash	300
"	76	Purple sylvinite 1.04 m. above the base of the Boulby Potash	450
51	77	Boulby Halite 20 cm. below the Boulby Halite/Potash breccia	800
"	78	Boulby Halite/Potash breccia 34 cm. below the Boulby Potash	200
"	79	Sylvinite 5 cm. above the base of the Boulby Potash	5000
"	80	Banded sylvinite 26 cm. above the base of the Boulby Potash	2150
"	81	Banded sylvinite 94 cm. above the base of the Boulby Potash	350

Table 6.4

The average B_2O_3 content of the bulk samples
of Boulby Halite and Boulby Potash

<u>Bed</u>	No. of <u>samples</u>	ppm B_2O_3	
		<u>Average</u>	<u>Range</u>
Boulby Halite	10	584	270-1000
Boulby Potash	22	954	70-2600

enriched in MgCl_2 and contained 8% boric acid. However according to Valyashko (1972b), various Russian researchers (unnamed) have since precipitated boracite ($\text{Mg}_3\text{B}_7\text{O}_{13}\text{Cl}$) from these brines by following the same procedure and then leaving the residual solutions to stand, undisturbed, for at least three years.

The presence of borate minerals in bed B.S.3, overlying and associated with potash salts, accords with theoretical predictions and experimental results. However the extensive development of these minerals throughout the C.P.L. concession area caused the writer to consider whether an external source (solutions from fumaroles or a reworked borate deposit) was contributing boron to the brines precipitating these salts. The object of analysing these rocks for boron was, therefore, to determine if they are enriched or depleted in boron relative to evaporated seawater (Table 6.1). Comparison with the boron content of other salt deposits is made in Chapter 11.

II Results and discussion

Analyses of 10 halite and 10 sylvite crystals from the Boulby Halite and Boulby Potash were all below the detection limit of the analytical method (i.e. less than 20 ppm B_2O_3 ; same method as used to analyse iron-boracite and parahilgardite; see Appendix 3).

Analyses of 16 water insoluble residues (chiefly clay minerals) from these same units and bed B.S.3 contain from 400 to 6200 ppm B_2O_3 (see Table 6.2).

Analyses of 32 bulk samples (Table 6.3) from seven sections through these beds (see Figures 6.1 and 6.2) show variability between and within sections which is primarily the result of variations in the proportions of clays and anhydrite.

The insoluble residues and bulk samples from the potash clearly contain, on average, more B_2O_3 than those from the halite (Tables 6.2 and 6.4) and this is in accordance with the former being precipitated from a more concentrated brine.

Comparison of Tables 6.1 and 6.4 show that the average bulk boron content of the halite and potash rocks at Boulby is not in excess of the theoretical boron content of evaporated seawater during halite precipitation. The average boron content of the insoluble residues of these beds is slightly in excess of the probable concentration of the element in the host brines and this almost certainly results from the clays absorbing boron from the solutions over long periods of time. The boron in the minerals of the sequence examined has, therefore, been derived from seawater without large additions from extraneous sources.

CHAPTER 7THE CHEMICAL EVOLUTION OF THE THIRD ZECHSTEIN
EVAPORITE CYCLE IN THE BOULBY MINE

There is an enormous amount of literature dealing with the chemistry of seawater systems and these are summarized in Stewart (1963b), Borchert and Muir (1964) and Braitsch (1972). Experimental data have provided the basic details of the stable mineral assemblages in these systems over the temperature range 0 - 110°C.

The chemical evolution of evaporite deposits is best considered by comparison with physico-chemical models based on experimental data. It is impossible for conditions in nature to be duplicated in the laboratory and these models must, therefore, be regarded as idealizations. Nevertheless they are the only direct way of predicting the composition of the solutions of natural salt deposits.

I Comparison of this evaporite cycle with
experimental data

There are significant differences between the theoretical succession of minerals resulting from the evaporation by fractional crystallization, of a closed system of seawater at 25°C, and the present mineralogy

Table 7.1

The theoretical succession of minerals resulting from the
fractional crystallization of seawater at 25°C

<u>Zone</u>	<u>Minerals</u> ¹
Bischofite	Bischofite, carnallite, kieserite, Mg borates, halite, anhydrite.
Carnallite	Carnallite, kieserite, halite anhydrite, Mg borates.
Kainite	Kainite, kieserite, halite, anhydrite. Kainite, hexahydrite, halite, anhydrite. Kainite, epsomite, halite, anhydrite.
K-free magnesium sulphates	Epsomite, halite, polyhalite. Bloedite, halite, polyhalite.
Polyhalite	Halite, polyhalite.
Halite-anhydrite	Halite, anhydrite.
Calcium sulphate	Anhydrite, gypsum.
Carbonate	Carbonates of calcium and perhaps magnesium.

1. Bischofite = $\text{MgCl}_2 \cdot 6\text{H}_2\text{O}$.
- Carnallite = $\text{KMgCl}_3 \cdot 6\text{H}_2\text{O}$.
- Kieserite = $\text{MgSO}_4 \cdot \text{H}_2\text{O}$.
- Hexahydrite = $\text{MgSO}_4 \cdot 6\text{H}_2\text{O}$.
- Epsomite = $\text{MgSO}_4 \cdot 7\text{H}_2\text{O}$.
- Kainite = $\text{KMgClSO}_4 \cdot \frac{11}{4}\text{H}_2\text{O}$.
- Bloedite = $\text{Na}_2\text{Mg}(\text{SO}_4)_2 \cdot 4\text{H}_2\text{O}$.
- Polyhalite = $\text{Ca}_2\text{MgK}_2(\text{SO}_4)_4 \cdot 2\text{H}_2\text{O}$.

Table 7.2 The primary and present mineralogy of the beds from the Upper Magnesian Limestone to bed B.S.3 in the Mine¹

<u>Zone</u>	<u>Original mineralogy and composition of co-existing solutions where important</u>	<u>Present mineralogy</u>
Bed B.S.3	c ² , n, cl, ?bi, ?sy; MgCl ₂ and CaCl ₂ solns. containing B ₂ O ₃	sy, n, mg, I.B, Er, p.h, cl, q, h.
Boulby Shale	?a	a, n, mg.
Bed B.S.2		
Bed B.S.1	c, n, cl	sy, n, cl, mg, q, h.
Boulby Potash	sy, n, a and/or g, cl	sy, n, a, cl.
Boulby Halite	n with minor a and/or g, cl	n and minor a, cl.
Billingham Main Anhydrite	g and possibly a	a
Upper Magnesian Limestone	ca and/or ar	dol.

1. The beds of the Boulby Shale above B.S.3 are enriched in anhydrite and clays; representing dilution of the brines and increased terrestrial influence. They form the regressive phase of the cycle and are, therefore, not considered in comparisons with the theoretical succession for progressive evaporation (Figure 7.1).

2. C = carnallite; n = halite; sy = sylvite; bi = bischofite; ta = tachyhydrite; cl = clays; a = anhydrite; g = gypsum; ca = calcite; ar = aragonite; dol = dolomite; I.B = iron-boracite; Er = ericaite; ph = parahilgardite; mg = magnesite; q = quartz; h = hematite.

Table 7.3 Comparative evaporite component profiles*

Components	Thickness in a 100 metre evaporite section				
	Theoretical † for seawater	Zechstein	3rd Zechstein evaporite cycle at Boulby	Other marine evaporites (and potash)	Gypsum-halite deposits
MgCl ₂	9.4	0.5	0 ⁺	0.1	0
KCl	2.6	1.5	3.3	1.4	0
MgSO ₄	5.7	1.0	0	0.2	0
NaCl	78	78	47.3	66	23.5
CaSO ₄	3.6	16	18.7	26	58
CaCO ₃ and CaMg(CO ₃) ₂	0.4	3	30.8 ^x	6.3	18.5

* After Borchert and Muir (1964) with the addition of column 3.

† Column 1 calculated from phase equilibria data; column 2 based on the whole Zechstein profile (4 cycles) from the lowest anhydrite to the highest halite; column 3 based on data from the S-20 borehole and observations in the Mine; column 4 is an average value for many other marine evaporites which exhibit a distinct MgSO₄ deficiency, but an excess of anhydrite; column 5 is for gypsum-halite deposits which exhibit excess gypsum but magnesium sulphate deficiency.

+ The MgCl₂ component at Boulby originally occurred in beds B.S.1 and 3 and is in part preserved in iron-boracite.

x The abnormal thickness of the carbonate layer at Boulby is due to a large part of it being of shelf sea origin.

of the Boulby cycle (compare Tables 7.1 and 7.2). These are:-

(i) The Upper Magnesian Limestone is composed of dolomite rather than calcium carbonate; it is, therefore, enriched in magnesium. Table 7.3 (cols. 1 and 3) also shows that it is much thicker than the theoretical carbonate layer of evaporite cycles.

(ii) The upper beds of the cycle do not contain polyhalite, bloedite, epsomite, hexahydrate, kieserite and kainite, indicating that they are depleted in MgSO_4 .

(iii) Sylvite is prevalent in this cycle rather than carnallite, although some carnallite was originally present in the basal rocks of the Boulby Shale.

(iv) A calcium-chloro-borate (parahilgardite) occurs in bed B.S.3 in addition to the magnesium borates predicted from the theoretical succession. Bed B.S.3, representing complete desiccation of the cycle, is, therefore, enriched in CaCl_2 .

(v) The clay beds above bed B.S.3 are not present in the theoretical succession.

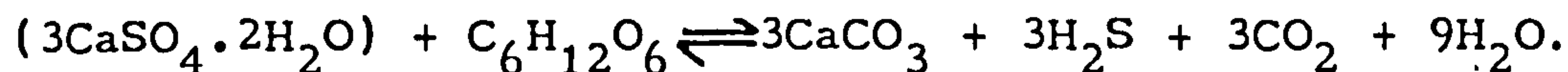
Much of the Upper Magnesian Limestone is fossiliferous and it was probably deposited on a shallow shelf sea. This accounts for its abnormal thickness relative to the theoretical succession. In addition the clay beds above bed B.S.3 represent the "retrogressive phase" of the cycle after final desiccation and therefore need not be considered here.

II Origins of MgSO_4 depletion and/or CaCl_2 enrichment in brines

Possible reasons for the MgSO_4 depletion and/or CaCl_2 enrichment in the upper beds at Boulby are:-

- (i) Reduction of (SO_4^{2-}) by bacteria.
- (ii) Release of calcium during dolomitization.
- (iii) An influx of calcium bicarbonate solution in continental waters.
- (iv) An influx of CaCl_2 solutions.

(i) Borchert and Muir (1964) suggested that evaporite sequences of the type at Boulby are not deficient in MgSO_4 but in (SO_4^{2-}) as a result of bacterial reduction to H_2S . In the Dead Sea, at the present time, gypsum crystals which precipitate at the surface are completely redissolved by the time they reach the bottom sediments because of bacterial reduction (Neev and Emery, 1967). The process occurs as follows:-



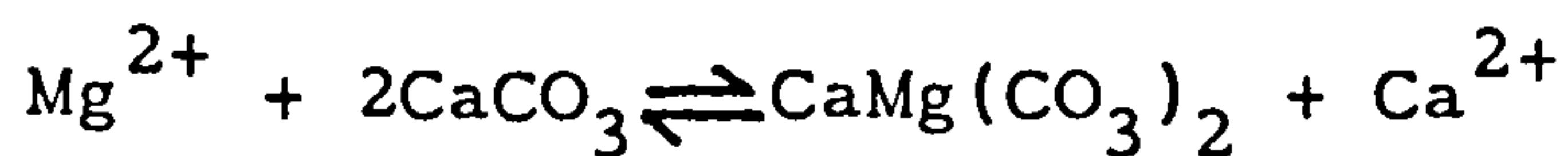
The calcium carbonate is sometimes precipitated as calcite and the H_2S rises to the surface waters where it is oxidized to (SO_4^{2-}) and reprecipitated as gypsum. Under these conditions the (SO_4^{2-}) anion is recycled but not removed from the system.

Should bacteria succeed in reducing (SO_4^{2-}) to H_2S , without recycling as above, then the system will become

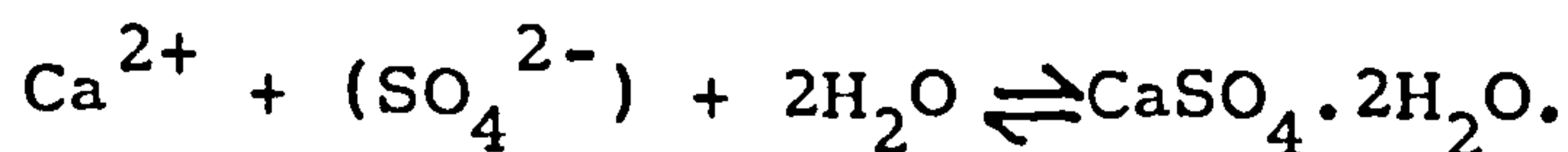
depleted in (SO_4^{2-}) . Therefore in the Jänecke ternary diagram for the normal seawater system $\text{MgCl}_2\text{-KCl-NaCl-Na}_2\text{SO}_4\text{-H}_2\text{O}$ (Figure 7.1) the composition of the brines at the end of halite precipitation, will lie on a straight line from S.W. to X, projected from the (SO_4) apex. If (SO_4^{2-}) is completely removed from the system the brine will have the composition of point X and precipitate the sequence of beds shown in Table 7.4(a). Notice that as SO_4 depletion occurs, the brines are enriched in MgCl_2 .

It is difficult to assess the role of bacterial reduction in the genesis of evaporite deposits, but Correns (1960) and Braitsch (1972) regard it as minimal because hematite, rather than pyrite, is the principal iron bearing mineral in halite and potash deposits.

(ii) Experiments (summarized, with references in Bathurst, 1976) indicate that it is extremely difficult to crystallize dolomite as a primary precipitate. However it commonly forms by the reaction of brines, of high Mg/Ca ratio, with primary calcite or aragonite (Shearman, 1966; Kinsman, 1969) according to the following equation:-

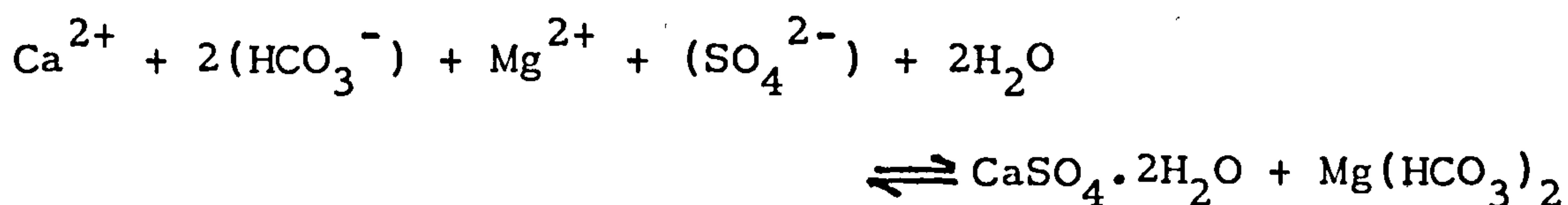


The brines become depleted in Mg^{2+} and relatively enriched in Ca^{2+} which reacts with the (SO_4^{2-}) anion in solution to precipitate gypsum as follows:-



The combined effect of these two reactions is to deplete the brine in MgSO_4 . Consequently, after formation of the halite layer, the composition of the MgSO_4 deficient brines lies on the straight line from the MgSO_4 composition point through and beyond the seawater point S.W. If the brine is completely depleted in MgSO_4 it will have composition IV and precipitate the sequence of beds in Table 7.4(a). The brines are enriched in MgCl_2 as MgSO_4 depletion occurs.

(iii) An influx of calcium bicarbonate in continental waters of arid regions causes existing brines to become depleted in MgSO_4 (Valyashko, 1956; Hermann, 1977) according to the following equation:-



The composition of the brines at the end of precipitation of the halite layer is as for (ii). The hypothetical magnesium bicarbonate may remain in solution, precipitate as magnesite, or become involved in the dolomitization processes stated above. Valyashko (1958) regards this process as the principal cause of MgSO_4 deficiency and dolomitization in evaporite deposits.

(iv) An influx of CaCl_2 solutions into seawater during evaporation prevents precipitation of MgSO_4 minerals (Hermann, 1977) in the following manner:-

Table 7.4

Sequence of beds produced by the fractional crystallization
of solutions in Figures 7.1, 2 and 3

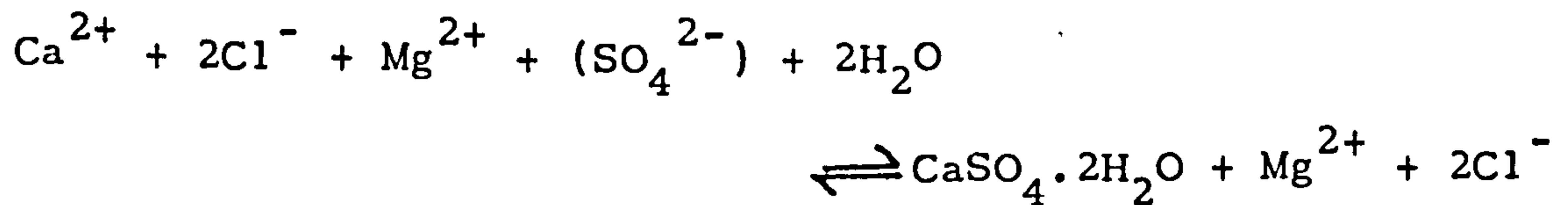
	(a) [‡]	(b)	(c)
WAY ↑	bi* + c + n	bi + c + ta + n	Ca + cc + ta + n
UP	c + n	c + ta + n	cc + ta + n
	sy + n	c + n	c + ta + n
		sy + n	c + bi + n
			c + n
			sy + n

‡ (a) Sequence of beds produced by the fractional crystallization of solutions of composition X or IV in Figure 7.1.

(b) Sequence of beds produced by the fractional crystallization of solution L in the CaCl_2 rich system at 93°C (Figure 7.2).

(c) Sequence of beds produced by the fractional crystallization of solution L in the CaCl_2 rich system at 35°C (Figure 7.3).

* bi = bischofite; c = carnallite; n = halite;
 sy = sylvite; ta = tachyhydrite; cc = chlorocalcite;
 Ca = $\text{CaCl}_2 \cdot 4\text{H}_2\text{O}$.



Only the (SO_4^{2-}) anion is removed from solution by this reaction. Complete depletion in (SO_4^{2-}) results in the brines having composition X at the end of precipitation of the halite layer (see (i)).

However should the brines become enriched in calcium over and above that which causes complete depletion in MgSO_4 or (SO_4) they will migrate out of the normal seawater system (Figure 7.1) and into the system MgCl_2 - CaCl_2 - KCl - NaCl - H_2O (see Figure 7.2). In theory the composition of the brine will lie on the line joining X or IV to the CaCl_2 apex or in the area between these lines (see Figure 7.2). The presence of primary or early diagenetic parahilgardite ($\text{Ca}_2 \text{ B}_5\text{O}_8(\text{OH})_2 \text{ Cl}$) in bed B.S.3 and CaCl_2 rich brines in the Boulby Halite are compatible with this hypothesis.

Little is known of the CaCl_2 rich system (Figure 7.2) at temperatures below 93°C . The lowest temperature at which tachyhydrite can co-exist with bischofite is 22°C when they precipitate from a solution of specific composition 34.6 mole % MgCl_2 and 65.4 mole % CaCl_2 (D'Ans, 1961). Therefore as the temperature falls below 93°C the stability field of bischofite expands and moves towards the CaCl_2 apex of the CaCl_2 rich system. Figure 7.3 illustrates the position of the bischofite-

tachyhydrite boundary curve at 35°C (calculated after D'Ans, 1961).

At 93°C (Figure 7.2) a brine of composition L would follow the crystallization path LABD, whilst at 35°C (Figure 7.3) it would migrate along the path LMNOPQ before final crystallization. Table 7.4(b) and (c) gives the sequence of beds that would be precipitated in each of these cases under conditions of fractional crystallization. In the former case the final solutions are rich in MgCl_2 , whilst in the latter they are enriched in CaCl_2 .

The exact position of the carnallite-sylvite boundary curve is uncertain at temperatures below 93°C. If this boundary curve migrates towards the K_2Cl_2 apex in Figure 7.3 then the basal layer, as a result of fractional crystallization of solution L, will be a carnallite-halite rock rather than a sylvite-halite rock.

Nikolaev and Chelishcheva (1940b) examined the system MgCl_2 -KCl-NaCl- Na_2SO_4 - B_2O_3 - H_2O at 25°C (Figure 7.1) by taking a sample of Lake Inder brine which had a composition almost exactly the same as evaporated seawater but with a slight enrichment in boron. They found that, except for slight differences in the final stages of evaporation, the position of the univariant points (since we are dealing with isothermal sections) of this brine were the same as for the boron free system. It is probable, therefore, that boron has little effect on the

positions of the univariant points in the CaCl_2 rich system (Figures 7.2 and 7.3).

III Discussion of the sequence at Boulby¹

Any hypothesis for the chemical evolution of this evaporite cycle must attempt to account for as many of the chemical features of the rocks as possible; particularly the separate areas of iron-boracite and parahilgardite nodules in bed B.S.3. It is only possible to discuss the chemical evolution of these rocks qualitatively as we neither know the stability fields of all the minerals in the CaCl_2 rich system accurately nor the exact bulk composition of the brine at the end of halite precipitation.

The complete absence of MgSO_4 minerals from the

1. This discussion is based on the assumption that the Billingham Main Anhydrite, Boulby Halite and Boulby Potash were deposited in a basinal/lagoonal rather than supratidal environment. The writer supports deposition of these beds in the former environment (see Chapter 8) because as far as the writer can see, evolution under supratidal conditions cannot account for the MgSO_4 depletion and CaCl_2 enrichment of the brines which formed these beds (see Chapter 8).

sequence at Boulby and almost all the other rocks of this cycle in north-east England (F.H. Stewart; pers. comm.) indicates that MgSO_4 and/or (SO_4) depletion has occurred on a large scale. There is no evidence for large scale bacterial reduction of the (SO_4^{2-}) anion to H_2S in any of these rocks in north-east England. It is also most improbable that large quantities of CaCl_2 solutions were flowing from the neighbouring low lying landmass into the brines which were precipitating these rocks.

However these rocks lie close to the coastline of that time. It is likely, therefore, that influxes of continental waters may have depleted the brines in MgSO_4 whilst simultaneously precipitating gypsum (see reaction (iii) in the previous section).

In addition, some, if not all, of the dolomite of the Upper Magnesian Limestone is of secondary origin (Stewart, 1965). Numerous studies (summarized in Milliman, 1974) have shown that dolomitization of calcite and/or aragonite is frequently a penecontemporaneous process. However this is not always the case. Defleyes et al. (1965) have proposed that seepage of dense lagoonal brines into the sea through porous limestones has dolomitized the pre-existing limestones on Bonaire. This process is analogous to the seepage refluxion theory that Adams and Rhodes (1960) used to account for dolomitization of Permian lagoonal limestones in Texas. In addition Loewengart (1962) observed that brines of

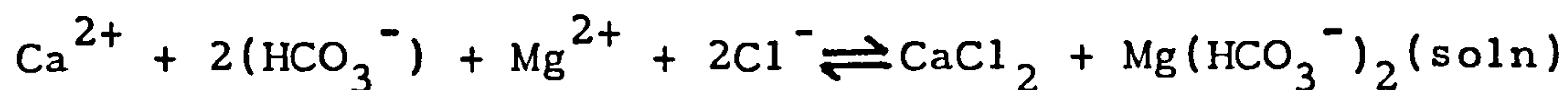
the Dead Sea have a high CaCl_2 content. He attributes this to the percolation of brines from the Dead Sea into adjacent limestones at times of high water level; these brines dolomitize the limestones and the calcium that is released by this reaction is returned to the Dead Sea in solutions from salt water springs. The Dead Sea brines are consequently becoming depleted in MgSO_4 and enriched in CaCl_2 .

It is likely, therefore, that dolomitization of the primary calcite and/or aragonite of the Upper Magnesian Limestone occurred over a long period of time; with the reaction proceeding in the lower beds as the upper ones were being deposited. The great thickness of this unit strongly suggests that this process continued as the overlying evaporite beds were being deposited. If the calcium cations released as a result of dolomitization were refluxed back into the overlying brines they would precipitate as gypsum and the brines would become depleted in MgSO_4 (see reaction (ii)). Such is the thickness of the Upper Magnesian Limestone that if this process occurred it could probably account for the CaCl_2 enrichment of the overlying brines without recourse to influxes of continental waters.

On the basis of the present evidence it is, therefore, suggested that the MgSO_4 depletion and CaCl_2 enrichment in these rocks was caused by influxes of continental waters (the hypothetical $\text{Mg}(\text{HCO}_3^-)_2$ may also have aided ,

dolomitization) or large scale dolomitization of the Upper Magnesian Limestone by the overlying brines or a combination of these processes.

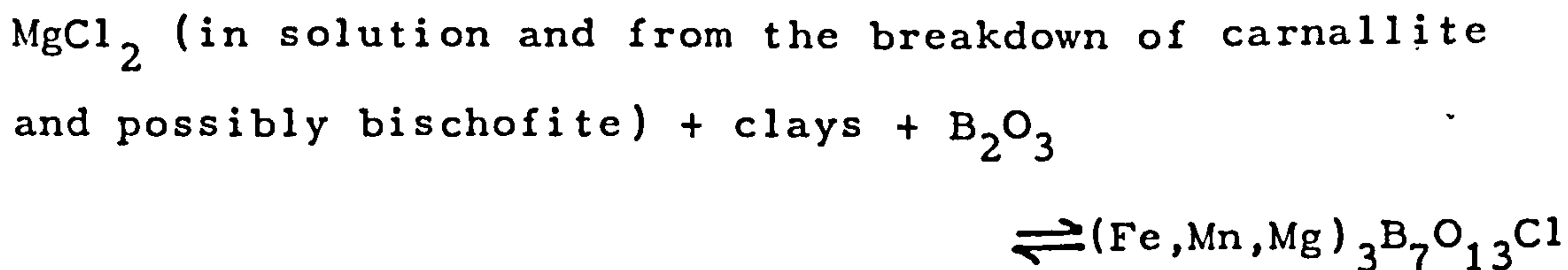
As NaCl is the most abundant constituent of seawater it would have precipitated as evaporation proceeded. The brines may have become completely depleted in MgSO_4 prior to or by the end of precipitation of the halite layer. It is theoretically possible that this could have occurred by the end of gypsum precipitation. Any further influxes of continental waters would have caused the brines to become enriched in CaCl_2 according to the following equation:-



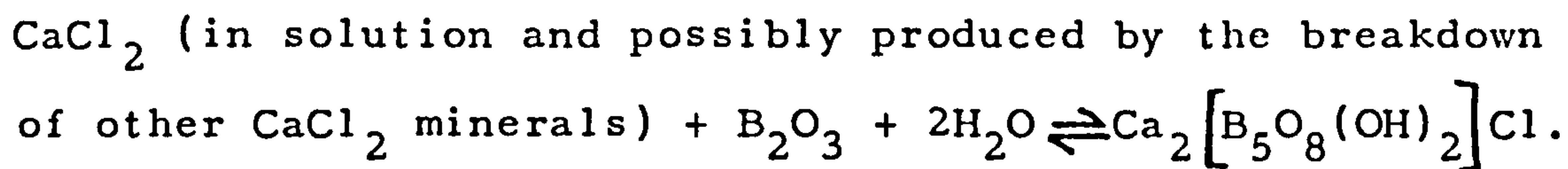
All subsequent calcium cations entering the system as a result of dolomitization of the Upper Magnesian Limestone below would effectively have enriched the brines in CaCl_2 and their composition would have migrated into the CaCl_2 rich system.

It seems unlikely that these CaCl_2 rich brines would all have had exactly the same composition when they began to crystallize, after precipitation of the halite layer, but, at temperatures of 35°C or below the final composition of the residual solution would be Q in Figure 7.3. The lower beds resulting from the crystallization of solution L in Figure 7.3 would be enriched in minerals containing MgCl_2 (see Table 7.4(c)) and they would be overlain by beds containing CaCl_2 rich minerals. If

gentle differential subsidence or earth movements of some sort occurred towards the end of precipitation of beds enriched in MgCl_2 the CaCl_2 brines would migrate laterally and precipitate CaCl_2 rich minerals elsewhere. The iron-boracite would have formed in those areas enriched in MgCl_2 minerals and brines by the following reaction:-



Parahilgardite would have formed in those areas of sediment enriched in CaCl_2 by the reaction:-



The presence of separate areas of iron-boracite and parahilgardite in bed B.S.3 implies that differential subsidence or earth movements of some sort must have occurred at this time. It is also generally regarded that subsidence occurred during the deposition of potash salts (see next chapter).

If the brines were markedly enriched in CaCl_2 at the end of deposition of the halite layer then they would have precipitated primary carnallite rather than sylvite (see Figure 7.3). The Boulby Potash may, therefore, be of primary or secondary origin (i.e. formed by the breakdown of carnallite).

It seems likely that the anhydrite in the Boulby Potash and bed B.S.3 reflect small quantities of sulphate which must have been brought in by influxes of seawater or terrestrial waters after the composition of the brines had entered the CaCl_2 rich system. Some of the anhydrite in bed B.S.3 may also be secondary, precipitating from brines percolating down during diagenesis.

CHAPTER 8POSSIBLE ENVIRONMENTS OF SEDIMENTATION

In recent years there has been much discussion on the environment of sedimentation of the potash deposits of the English Zechstein. Some authors support a basinal origin for these deposits (Richter-Bernburg, 1955; Borchert and Muir, 1964; Schmalz, 1969) whilst others believe some of them formed in a supratidal environment (Shearman, 1966; Smith, 1973).

It is intended to suggest a possible basinal origin for the Boulby Halite and Potash and review Smith's (1973) supratidal hypothesis for the origin of these rocks. These postulations will be discussed in the light of the data presented earlier in this study.

Throughout this chapter evaporite minerals deposited in a supratidal environment refers to minerals deposited on land adjacent to the sea, whilst those precipitated in a basinal environment formed in evaporating basins partially cut off from the sea. In the latter case towards the end of halite precipitation the beds may also become emergent (see later text).

I Basinal origin for the Boulby Halite and Boulby Potash

(1) General

In 1877 Ochsenius proposed that evaporite deposits formed in basins, partially but generally not completely cut off from the open sea by a bar, in areas of arid climate where evaporation exceeded precipitation plus runoff. This hypothesis has subsequently been modified by various authors (King, 1947; Scruton, 1953) to account for the features of individual evaporite cycles around the world.

The chemical and physical character of the rocks of this cycle in north-east England impose restraints on the nature of the basin/lagoon in which they may have been deposited. It is known that if a volume of seawater 1000 metres high were evaporated, only 1 metre of gypsum would result, clearly implying that the formation of chloride salts would require a basin of unreasonable depth. The necessary concentration must be achieved by continuous inflow of seawater into a subsiding basin or lagoon. However the rocks toward the top of the Upper Magnesian Limestone contain ripple marks; suggesting they were deposited in a shallow water environment. The presence of structures interpreted as mud cracks at the top of the Boulby Halite and abundant terrigenous material associated with halite and potassium salts in the Boulby Shale also indicates that these rocks were

deposited under similar conditions. The rocks of the Billingham Main Anhydrite and much of the Boulby Halite must, therefore, have been deposited during a period of very rapid subsidence.

Using the recalculated data of Usiglio (1849), Clarke (1924) calculated the absolute amounts of the chief minerals which will precipitate on evaporation of a litre of seawater. These are: 0.1172 g. of CaCO_3 ; 1.7488 g. of CaSO_4 ; and 29.6959 g. of NaCl . The excessive thickness of the Upper Magnesian Limestone is due to much of it being a shelf sea deposit. However comparison of the above data with Table 2.1 indicates that the Boulby Halite is thinner than would be expected by the direct evaporation of seawater. In theory this may be caused by incomplete evaporation of seawater, dissolution of the halite bed, or escape of the concentrated brines from the basin by downward percolation and lateral migration through or back over the bar and out to sea. Evaporation proceeded to near completion in this cycle and there is little evidence for large scale dissolution of the Boulby Halite. If dolomitization is the cause of MgSO_4 depletion and CaCl_2 enrichment in this cycle, then some of the brines escaped by downward migration, but it also seems very likely that some of them escaped by migration through or over the bar.

Whether the MgSO_4 depletion and CaCl_2 enrichment was caused by dolomitization or continental waters flowing

into the basin/lagoon, calcium cations must have been generated more rapidly than they were removed from the basin by reflux¹. It is possible that the bar may have cut the basin off from the ocean completely at some stage prior to precipitation of potassium minerals; thus allowing a build up of calcium cations in solution.

(2) Proposed Hypothesis

It is suggested that these beds were deposited in a basin/lagoon of the type shown diagrammatically in Figure 8.1 as a result of the rapid and probably continuous subsidence of the Upper Magnesian Limestone shelf. The lagoon was very large and the bar was probably situated towards the centre of the present southern North Sea as the area of subcrop of the strata representing the more concentrated brines offlap in that direction (see Figure 1.3) and subcrop offshore. The barrier may have been a carbonate reef or possibly a nearly emergent area of the sea floor behind which rapid subsidence occurred. Whether one could locate the barrier at the present time is uncertain, as much halokinesis has occurred in the southern North Sea basin since

1. The term "reflux" was introduced by King (1947) to describe brines which returned to the open sea either by overflowing the barrier or by percolating through it.

that time.

High evaporation rates would have removed water from the lagoon creating a slope in the water surface and a continuous inflow of relatively fresh water from the adjacent Zechstein Sea. At initial formation the basin water would have had a relatively low and even density, but progressive concentration of the surface water would have occurred. A current of dense water flowing to the sea would have commenced when the slope of the pressure surfaces at depth created a potential for flow which exceeded the hydrostatic head. The inflowing and outflowing waters at the barrier would almost certainly have mixed, thus increasing the concentration of the inflowing waters and diluting the outgoing brines.

The water entering the basin/lagoon may already have been preconcentrated due to evaporation which had occurred since the flooding of the Zechstein basin at the beginning of the third cycle. As the surface waters flowed towards the distal areas of the lagoon, it would have become more concentrated both by evaporation and continued mixing with more saline brines. Deposition of evaporite minerals was, therefore, initiated in these distal regions. Calcium carbonate would have been the first to precipitate. Further concentration would have caused calcium sulphate minerals (Billingham Main Anhydrite) to crystallize in the distal regions and an entrance-ward migration of the zone of calcium carbonate precipitation.

On further concentration halite would have precipitated first in the distal regions and with time towards the centre of the lagoon.

Towards the end of halite precipitation the lagoon was getting very shallow and may on occasion have become emergent; giving rise to mud cracks in the rocks. Sporadic influxes of detrital material must have occurred to give rise to bed B.H.2.

Valyashko (1956, 1972a) has observed this advanced stage of evaporation in various playa lakes in the U.S.S.R. and shown that at a certain point the volume of the brines becomes first equal to, and then less than, that of the salts precipitated from the brine; resulting in the level of the brine dropping below the salt surface. For the lakes of the Aral-Caspian region this happens before the onset of epsomite crystallization. However Valyashko (1972a) calculated that for brines of marine origin this point would be reached at the onset of potassium salt formation. If the region is completely stable, the brines will then sink through the halite. If, however, this stage is reached at the same time as gentle subsidence is occurring, the brines will migrate laterally into depressions and form lakes with halite shores in which potassium minerals will continue to precipitate in the correct order. Carnallite is observed precipitating under these conditions in the Tsarkhan playa lake in the unstable Tsaidam depression in Tibet at the present

time (Valyashko, 1972a).

It seems likely that the potassium salts of this cycle were deposited in lakes with halite shores of the type described by Valyashko (1972a). During the final stages of desiccation at Boulby further differential subsidence or an earth movement of some sort caused the CaCl_2 rich brines to migrate laterally into other depressions prior to crystallization.

Desiccation would have occurred in the distal areas of the basin/lagoon first and then migrated progressively towards the barrier. The beds of potassium salts would, therefore, be diachronous; precipitating first in the distal areas and finally in the centre of the lagoon and towards the barrier. These beds then became covered by shales and mudstones of detrital origin which will be discussed later in the chapter.

II Supratidal origin

After examination of the textural features of potash deposits in the Fordon borehole, Shearman (1966) suggested that it might be possible for soluble salts to be emplaced in near-shore intertidal and supratidal deposits after burial. Holliday (1967) thought this hypothesis feasible but saw no reason why potash minerals could not form by precipitation from marine groundwaters or by reaction within pre-existing minerals on coastal sabkhas. In 1973

Smith (1973) proposed an alternative supratidal origin for the Boulby Halite and the Boulby Potash based on a comparison with supratidal evaporite deposits presently forming in various parts of the world.

Currently layered halite deposits are forming in depressions in supratidal flats behind the Laguna Ojo de Liebre (Phleger, 1969; Kinsman, 1969) and in Salina Ometepec (Shearman, 1970) in the Baja Peninsula of Mexico. The surfaces of these supratidal deposits are only rarely flooded by seawater, although some is carried in by the wind. The halite layers of Salina Ometepec are composed of vertically orientated crystals with distinctive internal chevron patterns composed of fluid inclusions. Smith (1971) claims to have observed similar halite crystals in the lower rocks of the Boulby Halite in north-east England and suggested they may have formed in a similar manner to those in Salina Ometepec. However neither the writer nor F.H. Stewart (pers. comm.) have seen such crystals in this unit.

Phleger (1969) and S. Smith (1971) recorded high concentrations of potassium and magnesium in interstitial brines in the halite beds of Laguna Ojo de Liebre and Salina Ometepec respectively. Phleger further showed that little of the seawater arriving in the flats ever returns to the sea and that it thus becomes progressively more concentrated as it advances over the flats. Holser (1966) observed gypsum being replaced by polyhalite due

to reaction with these brines in the flats of Laguna Ojo de Liebre, proving that potassium minerals may form in this type of environment. Although potassium minerals are only rarely observed in marine supratidal environments at the present time, Valyashko (1972a) has shown that they are locally abundant in some inland playa lakes of Russia.

These observations of recent supratidal deposits and inland lakes show that highly concentrated brines and potassium and magnesium salts can form in the supratidal environment given the correct combination of circumstances. Smith (1973) believes that given favourable conditions and gentle subsidence over a long period of time, it was possible to form the potassium bearing salts of this cycle in a supratidal environment by the following process:-

At the time of formation of the Boulby Halite the environment of sedimentation was similar to that of the Laguna Ojo de Liebre and Salina Ometepe at the present day. Each inundation of normal seawater was followed by the precipitation of a new halite layer as a result of resolution and concentration of the brine on its passage inland. The most concentrated residual brines (potassium and magnesium rich) would have migrated towards shallow depressions where they would have sunk and concentrated below the halite surface as desiccation proceeded. The brines probably precipitated interstitial carnallite at this stage. Successive flooding of the

salt flats would have led to re-solution of these soluble salts; their place being taken by more halite. These brines would have become further concentrated and progressively larger quantities of late stage potassium and magnesium minerals and brines would have developed with time. As with many modern salt flats halite precipitation probably exceeded subsidence and the salt flats advanced seaward, resulting in the inland halite areas only rarely being flooded. Occasional rainfall probably further concentrated potassium and magnesium minerals in depressions.

After repeated reflooding of the halite over long periods of topographical stability accompanied by slow subsidence, considerable quantities of potassium and magnesium minerals and concentrated brines would have lain on or beneath the halite surface. Consequently water reflooding these flats would have very quickly become saturated with potassium and magnesium ions which it would have carried into depressions and precipitated. As these brines would have been saturated in potassium and magnesium, they could hardly have redissolved pre-existing K and Mg minerals and in this way a deposit of potassium bearing minerals would have begun to build up. This would have continued until such time as the cycle was broken by the influx of unsaturated brines or the deposit was covered by impermeable fine terrigenous sediment.

Few modern salt flats are more than 15 kms. wide, but those envisaged by Smith in the above hypothesis may have reached 100 to 200 kms. in width. Smith regards this disparity as purely a function of time, as Kinsman (1969) has shown that the Trucial Coast sabkhas are advancing seaward at an average of 1 to 2 metres per year. At this rate of advance a coastal plain 100 to 200 kms. would develop in only a million years.

Whether the brines, produced by the evaporation of seawater, evolved in a basinal or supratidal environment, the final stages of evaporation, leading to the formation of potassium bearing salts, are very similar in both cases. The fundamental difference between the hypotheses is that in the basinal environment the Billingham Main Anhydrite and the majority of the Boulby Halite formed in a subsiding lagoon adjacent to the sea, whilst in the supratidal environment the Boulby Halite and possibly some of the Billingham Main Anhydrite formed on land adjacent to the sea.

III Discussion

(1) Basinal versus supratidal hypothesis

In considering whether the Boulby Halite and associated potassium bearing salts were deposited in basinal or supratidal conditions it is important to

establish if MgSO_4 depleted and CaCl_2 enriched brines may develop in the latter environment. CaCl_2 rich brines have been recorded in coastal flat sediments of the Persian Gulf where calcium cations released as a result of dolomitization of aragonite by the brines are in excess of the sulphate anions in solution (Bush, 1970). There is, however, little additional sediment besides halite in the Boulby Halite from which CaCl_2 rich brines might have been derived; indicating this is a most unlikely source of these brines. There is also no evidence that these brines were derived from the clays associated with the parahilgardite in bed B.S.3.

If the potassium minerals crystallized in pools which lay on the surface of supratidal halite, these brines could have become enriched in calcium by influxes of calcium bicarbonate rich continental waters. This, however, does not explain the absence of MgSO_4 minerals from the Boulby Halite. There is little evidence for widespread bacterial activity in the Boulby Halite which could have caused depletion in these minerals.

According to Braitsch (1972) the calcium content of seawater influxes would permit only limited depletion of MgSO_4 in the brines in a roundabout way (early diagenetic) via polyhalite precipitation. However this would not cause MgSO_4 depletion on the scale observed in north-east England; neither is polyhalite recorded in these rocks.

Unfortunately the distribution of the Boulby Potash and the petrography of the sequence examined (see next section) do not provide a unique solution as to whether the beds of this cycle evolved in a supratidal or basinal environment. There appears to be continuous subcrop of this bed from the C.P.L. concession area to Whitby and possibly even further south (see Figure 1.1). The present lateral distribution of the bed at Boulby is secondary, resulting from lateral migration of the bed at depth, but this may not be the case around Whitby. There is evidence for the vertical movement of cations in all areas. Potash beds of this cycle have also been recorded in the North Sea by Brunstrom and Walmsley (1969) and Taylor and Colter (1974), but their distribution is not known in detail. If the present subcrop of this bed has not been dramatically altered from the original by secondary processes, then the potassium minerals appear to have been deposited in a large lake which extends into the North Sea. Such a lake would represent the final stages of desiccation of beds which formed in a basinal environment or on a supratidal coastal halite plain up to 200 km. in width.

The writer, therefore, prefers a predominantly basinal origin, of the type described, for the Billingham Main Anhydrite and the majority of the Boulby Halite, with emergence at the time of potassium salt precipitation, as this type of environment most readily accounts for

the chemical features of this bed. Should it be shown that brines can become depleted in MgSO_4 and enriched in CaCl_2 in a supratidal environment, then this would greatly strengthen the case for deposition of these beds in this type of environment.

(2) The origin of the clays in the Boulby Shale

The former carnallite crystals in beds B.S.1 and 4 (and presumably B.S.3) grew in association with clays. The proximity of these beds to the shoreline indicates the clays are almost certainly of terrestrial origin. They may be of wind-blown, fluvial or both of these origins. In the former case large quantities of detrital material must have been carried by the wind to produce up to 50% clays in a few of these rocks. Alternatively these beds may originally have contained smaller quantities of clays which have since become concentrated as a result of brines leaching out some of the more soluble salts. Both iron-boracite and parahalargardite would remain as they are relatively insoluble.

The fine grained character of these clays suggests that if they are of fluvial origin, they were deposited in the distal parts of a flood plain. The clays may have been carried into the area after the formation of small separate depressions containing the MgCl_2 and CaCl_2 brines and mineral assemblages respectively. The fresh waters associated with the clays may have washed away

much of the final stage brines.

The origin of the beds above the lower parts of B.S.4 is uncertain. The generally increased proportions of anhydrite indicate a marked dilution of the brines and the clays suggest prolonged terrestrial influence. One possibility is that repeated influxes of fluvial material onto a halite plain, resulting from the desiccation of a large basin/lagoon or a supratidal deposit, caused reworking of the halite around the depressions containing potassium bearing and borate minerals. In time these depressions would have become covered with halite and clay bearing beds. There must, however, have been influxes of less saline waters, from the land or sea, to account for the anhydrite in these beds.

Alternatively Richter-Bernburg (1955) proposed that beds of this type result from a very rapid influx of seawater over the beds representing complete desiccation. A relatively thin stream of this water flowing towards remoter areas would have evaporated quickly so that the more insoluble salts, i.e. the carbonates, would have precipitated on the way. Consequently solutions bearing only sulphates and chlorides would have flowed into the regions most distant from the source of fresh seawater (Boreal Sea). This process, accompanied by influxes of detrital material of fluvial or wind-blown origin, could also account for the upper beds of the Boulby Shale.

CHAPTER 9ESTIMATION OF THE DEPTH OF BURIAL OF THE BEDS IN THE
SEQUENCE EXAMINED.I Statement of the Problem

In the S-20 borehole these beds are overlain by 1167 metres of strata; the youngest being Upper Liassic in age (Table 9.1). However it is generally regarded that the Permian salt beds of north-east England were overlain by strata up to Upper Cretaceous in age (Ziegler, 1974) and these latter beds outcrop on the floor of the adjacent North Sea (Kent, 1967) and in the Fordon borehole (Falcon and Kent, 1960; see Figure 1.1 for locality). They have since been eroded onshore after uplift in the late Cretaceous and early Tertiary (Ziegler, 1974).

The thickness of Jurassic and Cretaceous rocks which have been eroded in the C.P.L. concession area is of considerable interest as it permits calculation of the likely maximum depth of burial of the beds in the sequence examined; this being the depth at which maximum deformation is likely to have occurred. There is, however, little published data on the depths of burial of the rocks of north-east England and that which is available is largely unsubstantiated but summarized in Table 9.3.

Table 9.1The stratigraphy of the S-20 borehole(No. 2 shaft, Boulby Mine; after Woods, 1973)

System	Formation		Depth (in metres)	Thickness (in metres)
<u>Recent</u>	Drift		0.00	36.67
			36.67	
<u>Jurassic</u>	Upper Lias		41.67	5.00
	Middle Lias		84.00	42.33
	Lower Lias		406.67	322.67
<u>Triassic</u>	Rhaetic		423.33	16.66
	Keuper		646.67	223.34
	Bunter		1003.33	356.66
<u>Upper Permian</u>	EZ 4-5	Eskdale and Staintondale groups		200.37
	EZ3	Boulby Shale	1203.70	1.30
		Boulby Potash	1205.00	3.30
		Boulby Halite	1208.30	43.40
		Billingham Main Anhydrite	1251.70	17.00
		Upper Magnesian Limestone	1268.70	28.30
			1297.00	

Table 9.2The stratigraphy of the Fordon borehole(after Falcon and Kent, 1960)

System	Formation		Depth (in metres)	Thickness (in metres)
<u>Cretaceous</u>	U P P E R	Chalk	0.00	174.33
			174.33	
	L O W E R	Red Chalk	204.67	30.34
		Speeton Clay	353.33	148.66
<u>Jurassic</u>	Kimmeridge Clay			426.67
	Corallian Beds		780.00	21.00
	Oxford Clays and Kellaway Beds		801.00	60.33
	Estuarine Series		861.33	64.34
	Upper Lias		925.67	29.33
	Middle Lias		955.00	8.67
	Lower Lias and Rhaetic		963.67	148.00
			1111.67	
<u>Triassic</u>	Keuper			109.33
	Bunter		1221.00	345.67
<u>Upper Permian</u>	Saliferous Marls		1566.67	189.33
	Upper Evaporites*		1756.00	52.33
	Rotten Marl		1808.33	25.34
	Middle Evaporites†		1833.67	53.66
	Upper Magnesian Limestone		1887.33	71.67
			1959.00	

Table 9.2 (cont.)

* Falcon and Kent (1960) do not subdivide this formation into rock units and the data is the property of The British Petroleum Company Ltd. However this formation comprises the Upgang Formation, Upper Anhydrite, Upper Halite and Upper Potash, Sleights Siltstone and the Top Anhydrite.

† Falcon and Kent (1960) do not subdivide this formation into rock units and the data is the property of The British Petroleum Company Ltd. This formation comprises the Billingham Main Anhydrite, the Boulby Halite, Boulby Potash and Boulby Shale.

Table 9.3

Published estimates of the depth of burial of beds in N.E. England and adjacent North Sea

<u>Unit</u>	<u>Depth (in metres)</u>	<u>Reference</u>	<u>Comments</u>
Billingham Main Anhydrite in the Billingham Mine	2000-2330	Raymond (1960)	No indication was given of how these values were determined.
Permian salt beds of the North Sea, north of latitude 54N.	2500	Brunstrom and Walmsley (1969)	No indication was given of how this value was determined, but it presumably involved seismic investigations.
Base of the Triassic in the Cleveland Hill High 20 km. offshore from Boulby	2000 metres below its present level	Marie (1974)	Marie determined the minimum uplift of these rocks since late Cretaceous by comparing the maximum palaeodepth derived from sonic velocities and the present depth of the basal Triassic Bunter Shale.

Unfortunately the general character of the beds of the sequence examined gives little indication of their former depth of burial. However it is possible to estimate an approximate value by considering the stratigraphy and thicknesses of the overlying rocks in the S-20 borehole (Woods, 1973) and in boreholes in adjacent regions.

II Calculations and Discussion

In Jurassic and Cretaceous times north-east England was an area of differential subsidence with the thickest sequences of sediments being deposited in the basins. Cimmerian earth movements also caused localized uplift and erosion which has resulted in breaks in the stratigraphic sequence in many boreholes (Ziegler, 1974). As the majority of these strata have been removed at Boulby it is neither possible to tell if similar breaks in the succession occurred nor if there was much variation in thickness of units between Boulby and other areas.

The approximate thickness of Jurassic and Cretaceous strata which have been eroded at Boulby has been derived by comparison with the beds of the Fordon borehole (see Table 9.2) and the type boreholes for these systems in the North Sea. In the S-20 borehole (Table 9.1) the Boulby Shale is overlain by 793 metres of rocks to the top of the Rhaetic. There is also a full sequence of

Lower and Middle Liassic rocks (365 metres) but those of the Upper Liassic have been partially eroded. However in the Fordon borehole there is an almost complete sequence of strata from the Upper Liassic to the Kimmeridge Clays (602 metres, Table 9.2) which, when added to the thickness of the Lower and Middle Liassic rocks in the S-20 borehole, gives an estimated thickness of 967 metres for the Jurassic rocks deposited at Boulby. An alternative possibility is to take the total thickness of Jurassic rocks (768 metres) in the Jurassic type wells (B.P. 48/6-5 and Phillips 47/15-IX; Rhys, 1974) in the North Sea as an approximation to the thickness of these strata deposited at Boulby. The whole Jurassic sequence must be considered as there is insufficient palaeontological data to distinguish between the Liassic subdivisions in the type succession (Rhys, 1974). The values of 967 and 768 metres have therefore been used as two possible thicknesses of Jurassic strata deposited in the C.P.L. concession area.

In the Fordon borehole the Lower Cretaceous beds are 179 metres thick (Table 9.2) but the Upper Cretaceous (Chalk) is incomplete because of erosion. There are 253 metres of Lower Cretaceous and 730 metres of Upper Cretaceous rocks (Chalk) in the Cretaceous type wells in the North Sea (Shell Esso 49/24-1 well and Burmah 48/22-2 well; Rhys, 1974). However Hancock and Scholle (1974), who have examined many confidential boreholes,

have indicated that the Chalk is not usually more than 500 metres thick in the North Sea. Therefore in calculating the depth of burial of the beds in the sequence examined we have possible values of 179 and 253 metres for the thickness of the Lower Cretaceous and 730 and 500 metres for the thickness of the Upper Cretaceous beds.

It is possible to permute the thicknesses of Jurassic and Cretaceous strata in a number of different ways to arrive at an estimate of the former depth of burial of the beds of the sequence examined. These permutations are given in Appendix 6 and the results are shown in Table 9.4. Based on the data above, these beds have been buried to depths of between 2240 and 2743 metres. The estimated average palaeodepth is 2492 metres.

The Billingham Main Anhydrite lies 50 metres below the Boulby Potash in the Mine, giving it an estimated former depth of burial of 2542 metres. This is not very different from Raymond's estimate (see Table 9.3).

In the S-20 borehole the top of the Boulby Shale is 200 metres below the base of the Triassic. Assuming that approximately the same amount of overburden has been removed at Boulby as in the Cleveland Hill High, then Marie's (1974) data indicates that the maximum palaeodepth of the sequence examined in the Mine is 3200 metres and this is in approximate agreement with the higher stratigraphic estimates in this thesis.

Table 9.4

Stratigraphic estimations of the maximum depth of burial
of the beds of the sequence examined¹

<u>Stratigraphic Depth</u> <u>(in metres)</u>	<u>Calculation No.</u> <u>in Appendix 6</u>
2743	1
2544	2
2513	3
2314	4
2439	5
2240	6
2669	7
2470	8

1. Calculations in Appendix 6.

The present stratigraphical estimates of the maximum depth of burial of the beds of the sequence examined are, therefore, in approximate agreement with those of Raymond (1960) and that derived using Marie's (1974) data and this strongly suggests that these beds were buried to between 2200 and 3200 metres towards the end of the Cretaceous, prior to uplift.

CHAPTER 10GEOLOGICAL HISTORY

The rocks of the third Zechstein evaporite cycle at Boulby may have been deposited in a basin/lagoon (as defined in Chapter 8), supratidal or possibly both of these types of environment. The chemical character of the beds, however, favours the first hypothesis.

Under basinal/lagoonal conditions these beds would have formed in a large rapidly subsiding lagoon which developed on the Upper Magnesian Limestone shelf. The barrier, which may have been a carbonate reef or topographic high, presumably lay somewhere in the middle of the present southern North Sea. It did not completely isolate the lagoon from the sea. Water entering the lagoon became progressively more concentrated as it migrated towards the distal areas due to evaporation and mixing with more concentrated brines. Consequently evaporite minerals precipitated in the distal regions first; initially as calcium carbonate minerals, followed by calcium sulphates and then halite. The relatively thin layer of halite, when compared with the sulphates and carbonates of the cycle, indicates the brines were, in part, refluxed back to sea. Over a prolonged period the brines became depleted in MgSO_4 and enriched in CaCl_2 because of influxes of calcium bicarbonate rich

continental waters or calcium cations released by the dolomitization of the Upper Magnesian Limestone by evaporite brines. Towards the end of halite precipitation the lagoon was very shallow and the halite probably became emergent. Gentle differential subsidence caused the K and Mg rich brines to migrate laterally into depressions and form lakes with halite shores where they precipitated potassium bearing minerals. During the final stages of desiccation the CaCl_2 brines migrated into small depressions because of further differential subsidence or an earth movement of some sort.

If the Boulby Halite and associated potassium bearing salts are of supratidal origin, then the environment at the end of precipitation of the Billingham Main Anhydrite, which is largely of subaqueous origin, probably resembled that of the salt flats in Baja California at the present day. Recurrent influxes of normal seawater onto the gently subsiding landsurface resulted in the precipitation of layers of halite and concentration of the remaining brines as they migrated inland into shallow depressions. These brines became progressively enriched in K and Mg ions due to evaporation and recurrent flooding over a prolonged period of time. Halite precipitation exceeded subsidence and the salt flats advanced seaward. After a long period of topographical stability accompanied by gentle subsidence, large quantities of K and Mg brines and minerals would have lain on or beneath the halite

surface. Evaporation of lakes of K-Mg rich brines enriched in CaCl_2 which lay on the surface of the halite accompanied by differential subsidence similar to that of the former hypothesis, would have given rise to the present sequence and distribution of rock types at Boulby. There is, however, no identifiable source of CaCl_2 in this hypothesis.

During the final stages of desiccation detrital material, of windblown or fluvial origin, was deposited on the halite plain. The fine grainsize of the clays suggests that if they are of fluvial origin, they accumulated on the distal portions of a flood plain. A marked dilution of the brines occurred after deposition of the lower parts of bed B.S.4; possibly reflecting reworking of the halite beds by terrestrial waters carrying detrital material and, probably, accompanied by occasional marine incursions. Equally a rapid transgression of seawater, which had deposited its carbonate component elsewhere, accompanied by influxes of terrestrial material from the adjacent landmass, would account for these beds.

During diagenesis numerous secondary reactions occurred in the rocks of the sequence examined; particularly in the lower beds of the Boulby Shale. They may have happened as the upper beds of the cycle were still being deposited.

Carnallite, which was originally present in many of

the rocks of beds B.S.1 - 4 was replaced by halite during early diagenesis, by reaction with brines saturated in NaCl. Sylvite, released by this reaction, occurs over approximately the same depth range as the halite pseudomorphs after carnallite, but is irregularly distributed in the vertical and lateral senses; suggesting there may have been considerable redistribution of secondary KCl rich brines. If the Boulby Potash was originally a carnallite-halite rock, then it is likely that the carnallite also broke down at this time.

In the area of iron-boracite nodules in bed B.S.3 an original metastable iron-boracite polymorph (see Table 5.10) formed by the reaction of MgCl_2 brines, partly released by the breakdown of carnallite and possibly bischofite, with iron-containing clays during diagenesis. These crystals coalesced into aggregates which frequently combined with sylvite (resulting from the breakdown of carnallite) and magnesite to form nodules. The proportions of iron-boracite, sylvite and magnesite in these nodules is very variable. Since diagenesis the metastable iron-boracite polymorph has been attaining equilibrium by inverting to other polymorphs. Since nodule formation the sylvite has replaced the other minerals to variable degrees (see Table 5.24).

In the area of parahilgardite nodules in bed B.S.3 small parahilgardite crystals formed from CaCl_2 rich brines which may themselves have resulted from the

breakdown of pre-existing calcium chloride minerals.

The parahilgardite crystals grew in small rosettes which displaced the host clays. At some stage later, possibly during late diagenesis, many of the small crystals of this mineral recrystallized into much larger crystals which also formed rosettes. The aggregates of larger rosettes constitute the present parahilgardite nodules. The small quantities of sylvite in these nodules and their host rock suggests that carnallite was originally much less abundant than in the area of iron-boracite nodules. This is in accordance with phase equilibria data.

The clays in the upper part of bed B.S.4 in the East Spearhead have been extensively displaced or replaced by anhydrite. The uneven lateral distribution of this reaction suggests it may result from the downward percolation of more dilute brines during diagenesis. The presence of authigenic quartz, magnesite and hematite lining the boundaries between clays and chloride minerals in the Boulby Shale testifies to the interaction of the clays with concentrated brines.

When the rocks of the sequence examined were buried to an unknown depth, they were stressed such that fissures developed from the base of the Boulby Shale to the Upper Anhydrite. As the fissures dilated, KCl-NaCl solutions from the Boulby Potash migrated upwards and sylvite and minor quantities of halite formed in the fissures as they opened. Crystal growth was in the direction of least

stress, resulting in the development of fibrous crystals. With each successive dilation new mineral fibres formed and the pre-existing fibres grew longer.

The fact that there is much lateral variation in the intensity of fissure development suggests that the stress field may have been inhomogeneous or that there may have been much lateral variation in the mechanical properties of the rocks at that time. The stress field changed with time as some of the mineral fibres in the veins are curved. It is possible that the stress field existed over a long period of time.

Subsequent to the formation of the fibrous sylvinite veins, but probably prior to the large scale lateral migration of the Boulby Potash, a brine saturated in NaCl percolated down into the rocks of the Boulby Shale. It has modified these beds, to varying degrees, throughout much of the C.P.L. concession area. In the area of the Mine enclosed by roadways 2E, 2S, 5W and 3N colourless halite has almost completely replaced all the minerals of beds B.S.3 - 5 and the majority of the sylvinite veins. However in the East Spearhead and in many of the boreholes it has replaced the minerals of these beds on a much more limited scale. The brine is believed to have formed by the dissolution of a halite bed, which no longer exists, in the upper part of the Boulby Shale, or by the dehydration of the Rotten Marl.

In north Germany salt beds have only undergone large

scale lateral migration when they have been buried by at least 1000 metres of overburden (Trusheim, 1960). Depths of this order would have been reached during the Jurassic at Boulby. Whilst it is possible that the large scale lateral migration of the beds of the sequence examined may have started during the late Jurassic and early Cretaceous earth movements (Kent, 1974) it seems most likely that they underwent maximum deformation, forming the overfolds and overthrusts, when they were buried at greatest depth (2200 - 3200 metres) towards the end of the Cretaceous and the early Tertiary. This is substantiated by Brunstrom and Walmsley (1969) who reported that the majority of halokinesis in the British Sector of the North Sea, north of latitude 54N (approximately Scarborough), took place in the Tertiary.

It is probable that the Boulby Potash was the first bed to start migrating because the critical boundary between the elastic and plastic conditions is lower for potassium salts than rock salt (Trusheim, 1960). In the areas of most intense lateral migration the basal beds of the Boulby Shale are frequently brecciated and highly sheared (in Panel No. 1), whereas in the less deformed areas (South Spearhead) the unit only has a slickensided base. This phase of movement is the principal cause of attenuation of the beds in the C.P.L. concession area.

Talbot (1977) has suggested that the overfolding

and overthrusting of the Boulby Potash resulted from the growth of a salt dome or pillow to the north-east of the Mine. As the salt dome/pillow developed salt beds in the adjoining areas would have migrated towards its base (i.e. from the Mine north-eastwards) to take the place of the beds which had already risen due to their own buoyancy. Only when the salt dome/pillow ceased rising under its own buoyancy (i.e. it had achieved gravitational equilibrium) would the salt beds observed in the Mine have ceased migrating on a large scale.

After the above movement ceased the denser Boulby Shale sank into the Boulby Potash which migrated locally into small swells (axes orientated $024^{\circ} \pm 10^{\circ}$). In areas of major local gravitational disequilibrium the potash bed flowed laterally into small scale salt domes, some of which became detached from their roots and rose up through the Boulby Shale to accumulate beneath the Rotten Marl (Talbot, 1977). These movements, which have considerably modified the pre-existing overfolds and overthrusts, continued until local gravitational equilibrium was attained.

The final episode of movement caused monoclines to develop at the base of the Boulby Potash in response to overthrusting in the Upper Magnesian Limestone and Billingham Main Anhydrite. Similar monoclinal and flexural structures have been described in the Billingham Main Anhydrite at the Billingham Mine by Raymond (1960),

who regarded them as being Tertiary in age. Therefore, by comparison with Billingham Mine, it seems likely that the overthrust in the above units in the Boulby Mine represents a minor adjustment possibly associated with strong Alpine movements on the Continent.

Uplift and erosion have taken place since some time in the Tertiary and the small swells and basins in the top of the Boulby Potash and the overthrusting in the Upper Magnesian Limestone may have occurred in this period of time.

CHAPTER 11COMPARATIVE STUDIES

I Comparison of the geology of the sequence examined at
Boulby and other boreholes in north-east England

General petrographic descriptions of the Boulby Halite, Boulby Potash and Boulby Shale, or its equivalent rock type, have been given by Armstrong et al. (1951) and Raymond (1953) for boreholes E3, 4 and 6 and E2 to 7 respectively. Stewart (1951a, 1956) has presented detailed petrological descriptions of these rocks in the E2 borehole and of the Boulby Potash in the F boreholes.

(1) Brief description of the rocks from the upper part of
the Boulby Halite to the base of the Rotten Marl in the E
and F boreholes

(a) The upper part of the Boulby Halite

These rocks are of fairly uniform character and are principally composed of granular halite which is very coarse grained in places. Small quantities of disrupted anhydritic shale occur in interstitial areas. The halite crystals enclose small amounts of carnallite and sylvite. Anhydrite, magnesite and quartz occur in small quantities in the rock; frequently being associated with shale laminae.

(b) The Boulby Potash

Table 11.1 gives the thickness and percentages of KCl in the unit, which is generally composed of sylvite, halite, magnesite and quartz \pm carnallite \pm rinneite \pm boracite (Table 11.2).

In boreholes E2 to 7 the bed is usually a physical mixture of granular, sometimes equidimensional, sylvite and halite crystals, the majority of which are 1 to 3 cm. in maximum dimension. However Stewart (1951a) has observed sylvite and halite crystals up to 5 cm. in width in the E2 borehole. The sylvite crystals vary in colour from milky-white to yellow to red, whilst the halite crystals are colourless to dark grey-black. Minor carnallite usually forms small rounded crystals enclosed in halite. Rinneite, quartz and magnesite are all fine grained accessories generally associated with clays. Anhydrite occurs as euhedral crystals and is sometimes associated with clays which are usually interstitial to sylvite and halite.

The Boulby Potash of E4 is exceptional in that it is composed of alternating sylvite rich and halite rich layers (Armstrong et al., 1951; p 680); the latter of which contain 5% carnallite. The sylvite crystals lack coloration in contrast to those from the other E boreholes. Boreholes E6 and 7 contain greater quantities of clays than the other E boreholes.

Table 11.1

Comparison of the thickness and percentage of KCl in the Boulby Potash of

boreholes E2 - 7 and F1 - 4

S-20	E2	(Aislaby)	3.3	15.3	10.33	11.00	3.67	4.0	4.7	F1	(Robin Hood's Bay)	~10	~20
	E3	(Sleights)								E7	(Rockhead)		
	E4	(Sneaton)								E6	(Upgang)		
	E5	(Eskdalegate)								E7	(Rockhead)		
	E2	(Aislaby)								E6	(Upgang)		
	E3	(Sleights)								E5	(Eskdalegate)		
	E4	(Sneaton)								E4	(Staintondale)	~4	~8
	E5	(Eskdalegate)								F3	(Little Beck)	~11	~24
	E6	(Upgang)								F4	(Hawsker)	~7	~24
	E7	(Rockhead)											
	F1	(Robin Hood's Bay)											
	F2	(Staintondale)											
	F3	(Little Beck)											
	F4	(Hawsker)											

Thickness
(in metres)

% KCl

Table 11.2 Comparison of the mineralogy of the upper part of the Boulby Halite and the potassium mineral bearing zone of Z3¹ in the C.P.L. concession area and other boreholes in north-east England²

C.P.L. concession area		E2	E3	E4	E5	E6	E7	F1	F2	F3	F4
<u>The potassium mineral bearing zone³</u>											
Halite	x	x	x	x	x	x	x	x	x	x	x
Sylvite	x	x	x	x	x	x	x	x	x	x	x
Carnallite	-	x	-	x	x	-	x	x	x	x	x
Rinneite	-	-	-	-	x	x	x	x	x	x	x
Anhydrite	x	x	x	x	x	x	x	x	x	x	x
Magnesite	x	x	x	x	x	x	x	x	x	x	x
Quartz	x	x	x	x	x	x	x	x	x	x	x
Hematite	x	x	x	x	x	x	x	x	x	x	x
Clays	x	x	x	x	x	x	x	x	x	x	x
Pyrite	x	x	x	-	-	-	-	x	x	x	x
Boracite	-	x	-	-	-	-	-	-	-	-	-
Iron-boracite	x	-	-	-	-	-	-	-	-	-	-
Ericaite	x	-	-	-	-	-	-	-	-	-	-
Parahilgardite	x	-	-	-	-	-	-	-	-	-	-

Table 11.2 (cont.)

C.P.L.
concession
area

The upper part of the Boulby Halite

	E2	E3	E4	E5	E6	E7	F1	F2	F3	F4
Halite	x	x	x	x	x	x	n.d	n.d	n.d	n.d
Sylvite	x	x	x	x	x	x	n.d	n.d	n.d	n.d
Carnallite	x	x	x	x	x	x	n.d	n.d	n.d	n.d
Anhydrite	x	x	x	x	x	x	n.d	n.d	n.d	n.d
Magnesite	x	x	x	x	x	x	n.d	n.d	n.d	n.d
Quartz	x	x	x	x	x	x	n.d	n.d	n.d	n.d
Clays	x	x	x	x	x	x	n.d	n.d	n.d	n.d
Hematite	x	x	x	x	x	x	n.d	n.d	n.d	n.d
Kieserite	-	-	-	-	-	-	-	-	x	-

1. Z3 = 3rd Zechstein evaporite cycle.

2. Sources of data on the E and F boreholes:- Armstrong et al. (1951), Stewart (1951a, 1956), Raymond (1953).

3. x = mineral present; - = mineral absent; n.d = no data.

Table 11.3

Evidence for movement in the rocks from the upper part of
the Boulby Halite to the Rotten Marl in the
E and F boreholes

1. Shale laminae are contorted in the Boulby Halite of the E boreholes.
2. In E3 (Sleights) there is strong contortion of the Boulby Potash over the depth range 1279.5-1280.3 metres and some lineation in the chlorides due to flow (Raymond, 1953).
3. In E4 (Sneaton), over the depth range 1405-1407.8 metres, yellow tinged crystals of sylvite are streaked out parallel to the bedding plane of a granular halite rock in the Boulby Potash (Raymond, 1953).
4. The Rotten Marl contains a complex network of minor faults and movement planes which contain halite, sylvine, carnallite and rinneite in some of these boreholes (Smith, 1974).

Table 11.4

Comparison of the replacement and recrystallization
processes in the Boulby Halite and the overlying potassium
mineral bearing zone at Boulby¹ and in the E2 and F
boreholes

<u>Recrystalli-</u> <u>zation and</u> <u>replacement</u> <u>processes</u>	Boulby		E2 borehole ²		F boreholes ³	
	<u>Occurs</u>	<u>Scale</u>	<u>Occurs</u>	<u>Scale</u>	<u>Occurs</u>	<u>Scale</u>
<u>The potassium mineral bearing zone</u>						
c → n ⁶	X ⁴	I ⁵	?	?	X	Maj
c → sy	X	I → Maj	?	?	X	?Maj
n → c	-	-	-	-	X	S
sy → n	X	S → Maj	-	-	X	?Maj
n → sy	-	-	-	-	X	I
Recryst. of sy	X	Maj	X	?Maj	-	-
Recryst. of n	X	Maj	X	Maj	-	-
Recryst. of a	X	S	X	S	-	-
cl → h+m+q	X	S	X	S	X	S
r → n	-	-	-	-	X	S
n → r	-	-	-	-	X	S
a → r	-	-	-	-	X	S
?r → sy+n+a	-	-	-	-	X	S
Recryst. of p	X	Maj	-	-	-	-
p → sy	X	S → I	-	-	-	-
p → n	X	S	-	-	-	-
p → a	X	S	-	-	-	-
p → q	X	S	-	-	-	-
I.B → n	X	S → Maj	-	-	-	-
I.B → sy	X	S → Maj	-	-	-	-
I.B → q	X	S	-	-	-	-
Er → I.B	X	?Maj	-	-	-	-

Table 11.4 (cont.)

Recrystallization and replacement processes	Boulby		E2 borehole ²		F boreholes ³	
	<u>Occurs</u>	<u>Scale</u>	<u>Occurs</u>	<u>Scale</u>	<u>Occurs</u>	<u>Scale</u>

The potassium mineral bearing zone (cont.)

Er → sy	X	S	-	-	-	-
Er → n	X	S	-	-	-	-
m → sy	X	S → Maj	-	-	-	-
m → n	X	S → Maj	-	-	-	-
?m → t	X	S	-	-	-	-
t → n	X	S	-	-	-	-
cl → a	X	S	-	-	-	-
cl → n	X	S → Maj	-	-	-	-

The upper part of the Boulby Halite

Recryst. of n	X	Maj	X	Maj	n.d	-
Recryst. of a	X	S	X	S	n.d	-
cl → m+q+h	X	S	X	S	n.d	

1. For the purposes of this comparison the potassium mineral bearing zone at Boulby includes the sylvinite and beds B.S.1, 3 and the lower part of 4.
2. After Stewart (1951a).
3. After Stewart (1956).
4. X = reaction has occurred; - = no evidence for reaction; ? = inconclusive evidence for reaction or scale of a reaction; n.d = no data.
5. Maj = reaction occurred on a large scale; I = reaction occurred on an intermediate scale; S = reaction occurred on a small scale.
6. c = carnallite; sy = sylvite; n = halite; a = anhydrite; cl = clays; h = hematite; m = magnesite; q = quartz; r = rinneite; p = parahilgardite; I.B = iron-boracite; Er = ericaite; t = talc.

Table 11.5

Differences in the character of the upper part of the
Boulby Halite in the E and F boreholes and the C.P.L.
concession area

1. Carnallite in the E2 boring (Stewart, 1951a) is only observed in contact with halite, whereas in the Mine it is associated with hematite and clays.
2. Blood red halite found in small quantities in the E2 borehole (Stewart, 1951a) is absent at Boulby.
3. Minor amounts of kieserite lying immediately beneath the Boulby Potash in the F3 borehole (F.H. Stewart; pers. comm.) is absent at Boulby.

In the F boreholes this unit has been extensively modified by numerous complicated replacement and recrystallization reactions (Stewart, 1956). Where least modified it is medium grained and contains variable proportions of dark grey-black clay and halite, with subsidiary anhydrite, magnesite and quartz and minor carnallite and sylvite. Stewart (1956) showed that the unit was originally composed of halite rich and carnallite rich layers, but that the carnallite has since been replaced by halite.

(c) The Upper Halite

This unit is generally composed of granular, colourless to pink, halite (up to 1 cm. in grainsize). Small quantities of sylvite, anhydrite and magnesite are also present.

(2) Comparisons and discussion

The principal difference between the stratigraphy of the sequence examined at Boulby and the E boreholes is that in the former area the potash bed is directly overlain by a series of shales, whilst in the latter it is capped by a halite bed. It seems likely that this reflects a primary lateral facies variation.

Table 11.3 presents the evidence for movement of these rocks in the E and F boreholes. The marked

schistosity and overfolding of the Boulby Potash in the Mine indicates that movement appears to have occurred on a much larger scale in the C.P.L. concession area than in the rocks around Whitby. If the overfolds at Boulby result from the bed migrating towards a salt dome to the north-east, then the boundary of the "zone of halokinesis"¹ in the southern North Sea shown by Brunstrom and Walmsley (1969) must be extended onshore.

The general character and mineralogy of bed B.H.1 at Boulby closely resembles that of the upper part of the Boulby Halite in boreholes E2 to 7 (see Table 11.2). Table 11.4 shows that the replacement and recrystallization reactions at Boulby and in the E2 boring (Stewart, 1951a) are also very similar. Throughout north-east England the major change has been the repeated recrystallization of halite. Table 11.5 indicates that there are slight differences in the character of this unit in different areas and these presumably reflect localized conditions during diagenesis and burial.

There is considerable variation in the character of the potassium mineral bearing rocks² throughout the

1. Trusheim (1960) defined "halokinesis" as "... a collective term for all processes connected with the autonomous isostatic movement of salt".

2. see next page.

area from Boulby to Robin Hood's Bay, south of Whitby. The KCl contents and thicknesses of these rocks vary enormously (see Table 11.1); at Boulby the latter is the result of tectonic activity, but this does not appear to be the case further south. In part these differences probably reflect lateral facies variation at the time of deposition, but Stewart (1956) also showed that the present distribution of potassium bearing minerals in the F boreholes is different from the original, in both vertical and lateral senses, because of subsequent modification by brines. This is also true at Boulby.

Table 11.2 shows that the mineralogy of the potash zone is fairly uniform. Carnallite is absent at Boulby, but present (often only in small quantities) in most other boreholes. Rinneite ($K_3NaFeCl_6$) occurs in many of the boreholes around Whitby, but not at Boulby which is characterized by a suite of borate minerals absent elsewhere. The iron-bearing minerals in the C.P.L.

2. The Boulby Potash in the E and F boreholes refers to all rocks containing appreciable quantities of potassium bearing minerals. Therefore, in this comparison, the sylvinite and basal rocks of the Boulby Shale in the Mine are regarded as the "Boulby Potash" although this is not in accord with the stratigraphical meaning of the term in the C.P.L. concession area.

concession area are iron-boracite and ericaite.

There is an enormous variation in the clay content of these rocks. Clays are (or were) the matrix minerals in the F boreholes (Stewart, 1956) but are only minor constituents in the majority of the E boreholes (Raymond, 1953). At Boulby they are a minor constituent in the sylvinite, but occur in major proportions in the basal rocks of the Boulby Shale. These differences presumably reflect lateral facies variation at the time of deposition.

Table 11.4 indicates that a large number of replacement and recrystallization reactions have occurred in these rocks. There is considerable variation in the nature and scale of the reactions between different areas; with all those involving borates occurring at Boulby and those involving rinneite in the boreholes around Whitby. It is surprising that secondary rinneite has not formed in the basal rocks of the Boulby Shale in the Mine, bearing in mind the iron content of iron-boracite (15-25% FeO) and the abundance of NaCl and KCl in the vicinity.

There are only a limited number of major reactions which appear to have occurred over much of the area; these involve the recrystallization of sylvite and halite and possibly the breakdown of carnallite. The former carnallite in the Boulby Shale in the Mine appears to have been replaced by halite from a brine saturated in this mineral; the sylvite released by this reaction now forms

large porphyroblasts. The original carnallite in the F boreholes also seems to have broken down in this manner (Stewart, 1956). Stewart (1951a) has suggested that red sylvite crystals in the Boulby Potash of the E2 boring may have formed by the breakdown of carnallite. This being the case, then carnallite was probably a major primary constituent of all this potash zone in north-east England. However, comparison of the third Zechstein evaporite cycle as a whole with phase equilibria data for MgSO_4 and/or SO_4 depleted systems suggests that primary sylvite-halite rocks may also occur underlying carnallite bearing rocks, as may be the case at Boulby.

The upper beds of the Boulby Shale in the C.P.L. concession area contain much larger quantities of clays than the Upper Halite of the E boreholes.

II Comparison of MgSO_4 depleted and/or CaCl_2 enriched evaporite deposits

MgSO_4 -free salt sequences are characterized by the absence of primary kainite and magnesium sulphate minerals both below and within the potash seams. Important deposits of this type include Oberrhein (Tertiary of Alsace), West Ural (Permian in Russia), Pripjat Senke (Upper Devonian in Russia), Saskatchewan (Middle Devonian in Canada) and the southern margins of the Stassfurt cycle in Germany. These deposits have become depleted in

MgSO₄ minerals as a result of bacterial reduction of (SO₄²⁻) anions, influxes of terrestrial waters, dolomitization, or a combination of these (Valyashko, 1956; Hermann, 1977).

Calcium chloride enriched evaporite cycles are very rare. Primary tachyhydrite occurs in basins in the Aptian evaporites of Sergipe in Brazil (Wardlaw, 1972) and in similar rocks in the Congo (Brazzaville; Belmonte et al., 1965). Tachyhydrite of secondary origin forms nests in the Stassfurt potash seam in Germany (Kühn, 1969).

Comparison of Boulby with the Stassfurt cycle of Germany and calcium chloride rich deposits reveals certain interesting features in the former deposit.

(1) Brief description of the Stassfurt cycle of the German Zechstein

The Stassfurt series forms the second Zechstein evaporite cycle in north Germany. According to Richter-Bernburg (1957), these beds were deposited in a basin with its southern margin near Reyerhausen and Königshall-Hindenberg and centre in the area of Hannover. The strata thicken towards the centre of the basin (see Table 11.6).

Over much of this area these rocks have been extensively modified by secondary processes (Kühn, 1962) and tectonic activity (Trusheim, 1960). However in many

Table 11.6

Comparison of the thicknesses of the beds in the
Stassfurt Series, Germany

<u>Stratigraphical Unit</u>	<u>Centre of the basin around Stassfurt¹</u>	<u>Southern edge of the basin around Reyerhausen and the Königshall-Hindenberg Mine²</u>
Covering rock salt and anhydrite	1.5-4.0 m.	2.0 m.
Stassfurt seam	10.0-30.0 m.	12.0-25.0 m.
Stassfurt rock salt	100-600 m.	50.0-70.0 m.
Basal Anhydrite	1.5-2.5 m.	15.0 m.
Basal carbonate layer ³	4.0-10.0 m.	40.0 m.

1. After Braitsch (1972).

2. After Hentschel (1961).

3. At the margins of the basin this unit is referred to as the Hauptdolomit, whereas in the centre it is called the Stinkschiefer.

Table 11.7

Comparison of mineralogical sequences in the
Stassfurt rock salt and Stassfurt seam, Germany

<u>Stratigraphical unit</u>	<u>Centre of the basin around Stassfurt¹</u>	<u>Southern edge of the basin in the Königshall-Hindenberg Mine²</u>
Stassfurt seam	ks ³ , n, c	c, n, a ? sy, n, a
Stassfurt rock salt	ks, n p, n a, n	n, a

1. Section from the Stassfurt anticline, beneath the major overthrust, after Braitsch (1972).
2. Only the upper section of the Stassfurt rock salt has been opened up in the Königshall-Hindenberg Mine, but boreholes into the lower rocks in surrounding regions indicate a complete absence of MgSO_4 minerals.
3. ks = kieserite; n = halite; c = carnallite;
p = polyhalite; a = anhydrite; sy = sylvite.

cases the German geologists have been able to elucidate the original sequence and nature of the strata.

Tables 11.6 and 11.7 show that at the margins of the basin the basal carbonate layer is thick and the halite and potash beds are completely depleted in MgSO_4 minerals. It is also uncertain whether a primary sylvinite layer was ever deposited; suggesting that the composition of the brine may have lain in the carnallite composition field in the CaCl_2 rich system (Figure 7.3) at the end of precipitation of the halite layer (Braitsch, 1972). However no primary calcium chloride rich minerals have been discovered.

The most complete primary sequence at the centre of the basin occurs in the Stassfurt anticline; beneath the major overthrust (Braitsch, 1972). There the basal carbonates are very thin and MgSO_4 minerals occur in the overlying salt beds (see Tables 11.6 and 11.7). However Table 11.7 shows that kainite is conspicuously absent. Braitsch (1972) believes that the strata are so similar to the theoretical sequence (see Table 7.1) that kainite has been removed by reaction at the time of deposition or by subsequent thermal metamorphism.

Nests of Tachyhydrite, associated and intergrown with kieserite, occur in carnallite rocks of the Stassfurt seam in the centre of the basin (Kühn, 1969). This must be a secondary mineral assemblage, as kieserite and tachyhydrite cannot precipitate together from primary

brines (see Figures 7.1 and 7.3). If there had been a large scale influx of CaCl_2 brines into these rocks during diagenesis or burial, then CaSO_4 reaction products would have formed. The absence of these reaction products indicates that the formation of tachyhydrite must have been a localized process, produced by the sudden influx of CaCl_2 rich hydrothermal solutions or the infiltration of dolomitizing solutions from the Grauer Salztun (Kühn, 1962; 1969).

(2) Brief description of primary tachyhydrite in Brazil and the Congo

Tachyhydrite occurs in units of over 100 metres in thickness interbedded with carnallite layers in the Aptian evaporites of these localities. At Sergipe, in Brazil, these evaporites appear to have formed in fault bounded troughs. The brines which produced these deposits must have been enormously enriched in CaCl_2 and depleted in SO_4 . Brines of these characteristics occur in the Red Sea and Dead Sea today, where the structural setting, in fault bounded troughs with large relief, may have resulted in modification of marine brines by discharge of CaCl_2 rich groundwaters. If South America and Africa began to drift apart in the Jurassic, then these Aptian evaporites of the east coast of Brazil and west Africa could have formed in a similar structural setting to the present day Red Sea.

In Brazil and west Africa these sequences lack basal sulphate deposits. Wardlaw (1972) regards the brines which deposited tachyhydrite at Sergipe as having already precipitated Ca , CO_3 and SO_4 elsewhere.

Bromine analyses of tachyhydrite, carnallite, sylvite and halite from Sergipe indicate that these minerals are of marine origin. The regular upward increase of bromine and the constancy of Sr through the upper zones of tachyhydrite suggest that crystallization was uninterrupted by sudden influxes of more dilute brines. Wardlaw (1972) postulates that at this stage of deposition the basin was probably closed to marine influxes, and 100 m. of tachyhydrite crystallized from little more than 200 metres of brine saturated in this mineral. As tachyhydrite breaks down on exposure to air there must always have been a covering of brine and the "dry lake" stage of Valyashko (1956) cannot have been reached.

(3) Comparison and discussion

The thicknesses of the beds from the basal carbonate layer to the Stassfurt rock salt at Königshall-Hindenberg are very similar to their equivalent beds at Boulby. However the Stassfurt potash seam is much thicker than the Boulby Potash. As at Boulby, Braitsch (1972) believes that the evaporite beds at Königshall-Hindenberg are depleted in MgSO_4 minerals either because of dolomitization of the thick basal carbonate layer or

because of influxes of calcium bicarbonate in terrestrial waters. If the former hypothesis is true, the MgSO_4 minerals exist in the central basin in north Germany, because the Stinkschiefer is so thin dolomitization has only occurred on a small scale. If the latter case applies, then the MgSO_4 minerals in the central basin are due to continuous influxes of fresh seawater (Braitsch, 1972) into that area of the basin. Anhydrite is a minor mineral in the halite and potash rocks at Boulby and Königshall-Hindenberg. Small influxes of fresh seawater and/or terrestrial waters must have occurred during the formation of these beds to account for this anhydrite.

If dolomitization of the Upper Magnesian Limestone played an important rôle in depleting the overlying brines in MgSO_4 minerals, then, by comparison with the Stassfurt Series, one might expect these minerals to occur in halite and potash rocks in areas where this limestone is thinner (possibly far offshore) or where dolomitization has been less complete.

Boulby bears no resemblance to the calcium chloride mineral occurrences in Brazil, the Congo or in the central part of the Stassfurt basin. Boulby appears to be the only recorded locality in the world where primary CaCl_2 minerals have developed in an evaporite deposit displaying a complete sequence of beds from basal carbonates to an upper potash bed.

In view of the number of deposits which display

complete depletion in MgSO_4 minerals, it is surprising that primary CaCl_2 minerals are so rare. For example it seems certain that the upper beds at K nigshall-Hindenberg formed by the crystallization of brines in the CaCl_2 rich system; yet primary CaCl_2 minerals are absent. The most likely explanation seems to be that either they did form but were subsequently redissolved by the influx of fresh brines during the regressive phase or that these fresh brines incurred prior to precipitation of the CaCl_2 minerals. The same reasoning probably applies to many of the other deposits. The relative insolubility of parahilgardite led to it being preserved at Boulby.

III Comparison of the principal marine borate deposits of the world

(1) General

Most of the world's borate deposits (e.g. Turkey, S. America and in California) are of non-marine origin and in areas of recent volcanic activity. Much of the boron in these deposits is derived from hydrothermal solutions which percolated into the rocks at the time of their formation (Schaller, 1937).

Significant concentrations of borates of marine origin are rare, as the boron in marine evaporites is

generally contained as a trace element in sulphates or clays or remains in solution. The principal marine borate deposits of the world are the Zechstein of Germany; the Lower Permian rocks of the Inder region of Russia; the Middle and Upper Permian rocks of Oklahoma and in the Upper Mississippian Windsor series of Nova Scotia and New Brunswick. To them must now be added the Boulby deposit in bed B.S.3.

Minor amounts of marine borate minerals are found in the Permian of Texas and New Mexico; in the Pennsylvanian of the Paradox basin of south-east Utah; in the Louisiana salt domes and the Aptian potash deposits of the Congo.

(2) Brief description of marine borate deposits

(a) Inder district, Russia

This district is situated 160 kms. north of the Caspian Sea and is the largest known marine borate deposit in the world. The evaporites have a domal structure, covering 250 square kilometres, with a core of halite, potassium-bearing minerals and anhydrite (1000 metres thick), covered by an outcropping cap of gypsum 50 metres thick. A karst topography has been developed in the gypsum rocks and it is these gypsum rocks which contain the borate minerals of commercial value.

The principal borate minerals are β ascherite and hydroboracite with subsidiary priceite, inyoite and colemanite (Godlevsky, 1937; Yarzhemsky, 1945; see Table 11.8). These minerals occur in nodules, beds and lenses, within a sequence of grey argillaceous rocks which are interbedded with clays in the gypsum series. They occur in beds of clay, where they have replaced the clay, but some have formed replacement lenses in the gypsum rocks. β ascherite and hydroboracite are the earliest formed minerals and they have been replaced, sometimes successively, by colemanite, inyoite and ulexite.

However primary kaliborite is occasionally found in association with sylvite, kainite, polyhalite and carnallite in the potash rocks least affected by leaching (Yarzhemsky, 1945). At the edge of the potash rocks kaliborite has often been replaced by β ascherite.

Godlevsky (1937) and Yarzhemsky (1945) interpret kaliborite as having formed by the evaporation of seawater. The boron was then transported from the potash salts, by the breakdown of kaliborite, into the overlying gypsum rocks and deposited there as hydroboracite or β ascherite during leaching at the time of formation of the karst topography. These minerals were subsequently replaced by the other minerals. The ability of clay minerals to absorb boron (Porrenga, 1967) probably resulted in the boron minerals being concentrated in clay horizons. No hydrothermal springs or igneous rocks occur in the

Table 11.8

Principal occurrences of borate minerals
in marine evaporites

Permian of the Inder district, Russia

β -ascherite (szaibelyite) ^{1,2}	MgHBO_3
Colemanite ^{1,2}	$\text{Ca}_2\text{B}_6\text{O}_{11} \cdot 5\text{H}_2\text{O}$
Hilgardite ²	$\text{Ca}_2[\text{B}_5\text{O}_8(\text{OH})_2]\text{Cl}$
Hydroboracite ^{1,2}	$\text{CaMgB}_6\text{O}_{11} \cdot 6\text{H}_2\text{O}$
Inderite ^{1,2}	$\text{Mg}_2\text{B}_6\text{O}_{11} \cdot 15\text{H}_2\text{O}$
Inderborite ³	$\text{CaMgB}_6\text{O}_{11} \cdot 11\text{H}_2\text{O}$
Inyoite	$\text{Ca}_2\text{B}_6\text{O}_{11} \cdot 13\text{H}_2\text{O}$
Kaliborite ²	$\text{KMg}_2\text{B}_{11}\text{O}_{19} \cdot 9\text{H}_2\text{O}$
Kurgantaite ³	$(\text{Sr}, \text{Ca})_2\text{B}_4\text{O}_8 \cdot \text{H}_2\text{O}$
Kurnakovite ⁴	$\text{Mg}_2\text{B}_6\text{O}_{11} \cdot 13\text{H}_2\text{O}$
Preobrashenskite ³	$\text{Mg}_3\text{B}_{11}\text{O}_{15}(\text{OH})_9$
Priceite (pandermite) ^{1,2}	$\text{Ca}_2\text{B}_{12}\text{O}_{23} \cdot 8\frac{1}{2}\text{H}_2\text{O}$
Strontioginorite (volkovite) ³	$(\text{Sr}, \text{Ca})\text{B}_{14}\text{O}_{23} \cdot 8\text{H}_2\text{O}$
Ulexite ^{1,2}	$\text{NaCaB}_5\text{O}_9 \cdot 8\text{H}_2\text{O}$

German Zechstein

Ascherite ⁵	MgHBO_3
Boracite ³	$\text{Mg}_3\text{B}_7\text{O}_{13}\text{Cl}$
Congolite ³	$\text{Fe}_3\text{B}_7\text{O}_{13}\text{Cl}$
Danburite ³	$\text{CaB}_2\text{Si}_2\text{O}_8$
Ericaite ³	$(\text{Fe}, \text{Mg}, \text{Mn})_3\text{B}_7\text{O}_{13}\text{Cl}$
Fabianite ⁶	$\text{CaB}_3\text{O}_5(\text{OH})$
Heidornite ³	$\text{Na}_2\text{Ca}_3\text{Cl}(\text{SO}_4)_2\text{B}_5\text{O}_8(\text{OH})_2$
Howlith ³	$\text{Ca}_2(\text{BOOH})_5\text{SiO}_4$

Table 11.8 (cont.)

German Zechstein (cont.)

Hydroascherite ³	$\text{Mg}_{1.95}\text{B}_{1.7}\text{H}_{2.6}\text{O}_{5.8}$
Hydroboracite ³	$\text{CaMgB}_6\text{O}_{11}\cdot 6\text{H}_2\text{O}$
Iron-boracite ³	$(\text{Fe}, \text{Mg}, \text{Mn})_3\text{B}_7\text{O}_{13}\text{Cl}$
Lüneburgite ³	$\text{Mg}_3\text{B}_2(\text{OH})_6(\text{PO}_4)_2\cdot 6\text{H}_2\text{O}$
Pinnoite ³	$\text{Mg}(\text{BO}_2)_2\cdot 3\text{H}_2\text{O}$
Strontiohilgardite ³	$(\text{Ca}, \text{Sr})_2[\text{B}_5\text{O}_8(\text{OH})_2]\text{Cl}$
Sulphoborite ³	$\text{Mg}_6\text{H}_4(\text{BO}_3)_4(\text{SO}_2)_2\cdot 7\text{H}_2\text{O}$
Ulexite ³	$\text{NaCaB}_5\text{O}_6(\text{OH})_6\cdot 5\text{H}_2\text{O}$
p-Veachite ³	$4(\text{Sr}, \text{Ca})\text{O}\cdot 11\text{B}_2\text{O}_3\cdot 7\text{H}_2\text{O}$
Strontioginiorite ³	$(\text{Sr}, \text{Ca})_2\text{B}_{14}\text{O}_{23}\cdot 8\text{H}_2\text{O}$

English Zechstein

Boracite ^{7,8}	$\text{Mg}_3\text{B}_7\text{O}_{13}\text{Cl}$
Ericaite ⁹	$(\text{Fe}, \text{Mg}, \text{Mn})_3\text{B}_7\text{O}_{13}\text{Cl}$
Iron-boracite ^{9,10}	"
Parahilgardite ⁹	$\text{Ca}_2[\text{B}_5\text{O}_8(\text{OH})_2]\text{Cl}$
p-Veachite ^{11,12}	$4(\text{Sr}, \text{Ca})\text{O}\cdot 11\text{B}_2\text{O}_3\cdot 7\text{H}_2\text{O}$
Sulphoborite ¹³	$\text{Mg}_6\text{H}_4(\text{BO}_3)_4(\text{SO}_2)_2\cdot 7\text{H}_2\text{O}$

Texas, New Mexico and Louisiana (U.S.A.)

Boracite ¹⁴	$\text{Mg}_3\text{B}_7\text{O}_{13}\text{Cl}$
Danburite ¹⁴	$\text{CaB}_2\text{Si}_2\text{O}_8$
Hilgardite ¹⁴	$\text{Ca}_2[\text{B}_5\text{O}_8(\text{OH})_2]\text{Cl}$
Lüneburgite ¹⁵	$\text{Mg}_3\text{B}_2(\text{OH})_6(\text{PO}_4)_2\cdot 6\text{H}_2\text{O}$
Parahilgardite ¹⁴	$\text{Ca}_2[\text{B}_5\text{O}_8(\text{OH})_2]\text{Cl}$

Table 11.8 (cont.)

Utah (U.S.A.)

Braitschite¹⁶ $7(\text{Ca}, \text{Na}_2)\text{O} \cdot \text{RE}_2\text{O}_3 \cdot 11\text{B}_2\text{O}_3 \cdot 7\text{H}_2\text{O}$

Oklahoma (U.S.A.)

Priceite¹⁷ $\text{Ca}_4\text{B}_{10}\text{O}_{19} \cdot 7\text{H}_2\text{O}$
 Probertite¹⁷ $\text{NaCaB}_5\text{O}_9 \cdot 5\text{H}_2\text{O}$
 Ulexite¹⁷ $\text{NaCaB}_5\text{O}_9 \cdot 8\text{H}_2\text{O}$

Nova Scotia and New Brunswick, Canada

Danburite^{17,18} $\text{CaB}_2(\text{SiO}_4)_2$
 Ginorite¹⁷ $\text{Ca}_2\text{B}_{14}\text{O}_{23} \cdot 8\text{H}_2\text{O}$
 Howlite^{17,18} $\text{Ca}_2\text{SiB}_5\text{O}_9(\text{OH})_5$
 Hydroboracite¹⁸ $\text{CaMgB}_6\text{O}_{11} \cdot 6\text{H}_2\text{O}$
 Inyoite¹⁷ $\text{Ca}_2\text{B}_6\text{O}_{11} \cdot 13\text{H}_2\text{O}$
 Ulexite¹⁷ $\text{NaCaB}_5\text{O}_9 \cdot 8\text{H}_2\text{O}$
 ?¹⁸ $\text{KCaB}_{23}\text{O}_{40} \cdot 8\text{H}_2\text{O}$

Congo (Africa)

Congolite¹⁹ $\text{Fe}_3\text{B}_7\text{O}_{13}\text{Cl}$

1. Godlevsky, 1937.
2. Yarzhemsky, 1945.
3. Kühn, 1972.
4. Palache, Berman and Frondel, 1951.
5. Braitsch, 1972.
6. Kühn et al., 1962.
7. Guppy, 1944.
8. Stewart, 1951a.
9. This study.
10. Milne et al., 1977
11. Stewart et al., 1954.
12. Beevers and Stewart, 1960.
13. Stewart, 1963a.
14. Hurlbut and Taylor, 1938.
15. Schaller and Henderson, 1932.
16. Raup et al., 1968.
17. Ham et al., 1961.
18. B. Roulston (pers. comm.).
19. Wendling et al., 1972.

Inder district.

(b) The German Zechstein

Borate minerals occur at many different localities in the German Zechstein but are chiefly confined to halite and potash beds. These minerals (Table 11.8) usually occur as discrete grains which are rather irregularly distributed and seldom form beds or lenselike deposits.

Boracite is the principal borate mineral with microscopic sized crystals (0.1 mm.) being widely distributed, particularly in the Stassfurt Series. Larger crystals (2 mm.) are associated with fractures in the Königshall-Hindenberg, Reyerhausen and other mines, and these are believed to have formed from infiltrating hydrothermal solutions (Kühn, 1962).

Boracite also occurs in nodules (Stassfurtite) in the Stassfurt seam and overlying Decksteinsalz. The stassfurtite nodules are roundish lumps, generally a few tens of centimetres in diameter, composed almost entirely of submicroscopic aggregated boracite crystals (see Figures 11.2 and 3). They are irregularly distributed and locally concentrated, particularly in the Hannover region. The origin of these nodules is uncertain. Braitsch (1972) regards them as being secondary but not post-diagenetic, as otherwise they could not be preserved in carnallite rocks which would be unstable in subsequent

infiltrating solutions. However according to Kühn (1962) the fact that these nodules sometimes enclose tachyhydrite and are occasionally found in paragenesis with blue halite indicates that they are secondary and most probably formed by the crystallization of epigenetic semi-saline boron containing solutions, which percolated into the Stassfurt potash seam along fractures, bedding planes and kieserite bands. The amount of this solution must have been rather small, otherwise the surrounding carnallite would have been redissolved (Kühn, 1962).

Ascherite is the other principal borate mineral of the German Zechstein. In the Stassfurt seam it occurs as small evenly distributed crystals and nodules. Braitsch (1972) regards the ascherite nodules as being early diagenetic, whilst D'Ans and Behrendt (1957) interpret them as having formed from infiltrating epigenetic semisaline solutions.

(c) The English Zechstein

The relations of the borate minerals, besides those at Boulby, are given in Table 5.4.

(d) Texas, New Mexico and Louisiana (U.S.A.)

Lüneburgite occurs at many localities in the potash beds near Carlsbad, New Mexico. According to Schaller and Henderson (1932) it forms small white blebs in halite

and clays associated with sylvite.

Hilgardite, parahilgardite, boracite and danburite occur in insoluble residues from Jurassic and Cretaceous halite rocks, with subordinate potash beds, from Choctaw salt dome, Louisiana (Hurlbut and Taylor, 1937, 1938; Taylor, 1938). It is not possible to tell if these minerals occur disseminated within the halite and potash beds or whether they form discrete horizons.

(e) Utah (U.S.A.)

The rare earth borate braitschite occurs in small nodules in a bed at the base of an anhydrite rock immediately overlying a potash bed of the Paradox Member, Hermosa Formation, in the Paradox basin of south-east Utah, near Moab (Raup et al., 1967, 1968; Raup, 1972). The nodules are composed of 65% braitschite and 35% of quartz, anhydrite, dolomite, halite and minor hematite and chalcopryrite. According to Raup et al. (1968) the origin of these nodules is as follows:- rare earth elements, boron, calcium, iron and copper were concentrated in brines; the rare earths and copper being derived from groundwaters from the neighbouring landmasses. The brine could have occupied the interstitial space in the crystal "mush" of sylvite and halite at the top of the salt bed. During lithification the brine was probably expelled against the overlying anhydrite to react

with it, to form braitschite nodules.

(f) Oklahoma (U.S.A.)

Probertite, priceite and ulexite occur in nodules in massive gypsum beds of the Blaine Formation (Middle Permian) and the Cloud Chief Formation (Late Permian) in three districts of Custer and Blaine Counties in West Central Oklahoma. They occur in an area of at least 20,000 square miles (Ham et al., 1961). Probertite is the principal or only borate mineral at many localities, whereas ulexite and priceite are rare occurrences. These minerals occur in nodules up to 12.5 cm. in maximum dimension. They always occur in gypsum adjacent to boron containing anhydrite rocks. The gypsum has formed by the hydration of anhydrite in recent weathering cycles. According to Ham et al. (1961) the transformation of anhydrite to gypsum resulted in the release of boron into solutions which precipitated the borate minerals by reaction with gypsum.

(g) Nova Scotia and New Brunswick, Canada

The Windsor series of late Mississippian age in these areas contains borate minerals associated with, locally steeply dipping, massive gypsum and anhydrite (Ham et al., 1961) and potash beds (B. Roulston; pers. comm.). Inyoite, ginorite, howlite, ulexite and danburite occur

as replacement nodules or cavity encrustations in massive beds of gypsum and anhydrite which are interbedded with fossiliferous limestone and brick red argillaceous shale. Hydroboracite, howlite, danburite and an unidentified borate mineral ($\text{KCaB}_{23}\text{O}_{40} \cdot 8\text{H}_2\text{O}$) have been found as scattered crystals and blebs in a 10 metres thick zone associated with potassium bearing minerals near the top of a thick evaporite sequence (B. Roulston; pers. comm.). According to Ham et al. (1961) the borate minerals in the gypsum and anhydrite rocks have formed by the same process as the borate minerals in Oklahoma. It is probable that the borate minerals associated with the potash beds may be primary or early diagenetic in origin. There are no extrusive volcanic rocks associated with these beds, but occasionally they are invaded by thin veins containing fluorite. The borate minerals, however, are not closely associated with these veins.

(h) Congo (Africa)

Congolite, the trigonal iron-boracite mineral, has been reported from the Aptian potash beds of the Congo by Wendling et al. (1972), but they did not document its distribution.

(3) Comparisons and discussion

The rocks of the English and German Zechstein, the Inder region of Russia, Texas and New Mexico are characterized by magnesium borates which usually occur associated with sodium and potassium salts. The majority of the Inder borates have been derived from these salts. In all these cases the association of magnesium borates with minerals which formed in the late stages of evaporation is in agreement with the theoretical predictions of Van't Hoff (1909) and Jänecke (1915) and the Russian experimental data (Valyashko, 1972b).

There is considerable variation in the mode of occurrence and time of formation of borates in halite and potash deposits. The evenly distributed boracite crystals of the German Zechstein, those of the English Zechstein (Guppy, 1944), the disseminated kaliboraite of the Inder deposit and the lüneburgite of Texas and New Mexico appear to be primary. However the iron-boracite and parahilgardite at Boulby and the braitschite at Moab, in Utah, occur in nodules in distinct beds and are of diagenetic origin. In contrast the stassfurtite and ascherite nodules of the Stassfurt seam in Germany, which may be of diagenetic origin, are randomly distributed both laterally and vertically. The differences in the mode of occurrence of these minerals in rocks, which were all deposited during the final stages of evaporation of seawater, coupled with the difficulty in precipitating

boracite from natural eutonic brines theoretically saturated with respect to the mineral from the beginning of halite precipitation (Nikolaev and Chelishcheva, 1940a; Braitsch, 1972) suggest that local chemical conditions, apart from composition, are also important in governing whether these minerals are precipitated. Complexing of boron by other elements may prevent it from precipitating.

Calcium borates normally characterize anhydrite-gypsum deposits (i.e. Oklahoma, Nova Scotia; see Table 11.8). Boulby is the only known locality in the world where a primary or early diagenetic calcium borate (parahilgardite) is known to be extensively developed in potassium bearing salts; its presence being directly related to the chemical evolution of the primary brines. Hermann and Hoffmann (1961) showed that the small quantities of calcium borates in the German potash deposits formed by the reaction of boron rich oilfield brines with minor anhydrite and gypsum at depth. The hilgardite and parahilgardite from Choctaw salt dome in Louisiana, which is closely associated with oil bearing strata, may also have formed in this manner.

The borate minerals of gypsum-anhydrite rocks contrast sharply with those of halite and potash deposits in that they contain abundant calcium and have formed by secondary processes in recent times. The nature of these reactions is, however, variable. In the

gypsum-anhydrite rocks of Oklahoma and Nova Scotia the borate minerals formed from boron released from the anhydrite structures as the mineral became hydrated to gypsum on exposure to groundwater. The boron was derived from an internal source. However in the Inder deposit in Russia the gypsum beds provide calcium cations for the borate minerals but the boron has been derived from an external source (solution of borate in the potash beds).

There is little difficulty in appealing to seawater as the ultimate origin of the boron in these deposits (excluding boron known to be derived from oilfield brines). The boron content of the sequence examined at Boulby is not in excess of the theoretical value for evaporated seawater during halite precipitation. Both Harder (1959) and Braitsch (1960) have shown that the boron present in the German Zechstein could have been derived by the evaporation of seawater. Table 11.9 indicates that the boron content of the Boulby Potash is approximately comparable with that of the Stassfurt potash seam in the Hildesia Mine of north Germany. However it is interesting that the boron in the Stassfurt seam is present in boracite, whilst that of the Boulby Potash is contained in anhydrite and clays. The absorption of boron by anhydrite and clays probably prevented the crystallization of boracite in the latter bed. The Boulby Halite, however, contains more of this element than the Stassfurt

Table 11.9

Comparison of the boron contents of rocks and insoluble residues from the Zechstein
Evaporites of north Germany and England

Locality	Material	No. of samples	ppm B ₂ O ₃		Source of data
			Range	Average	
Wintershall Mine, Werra- Fulda region, N. Germany	Unteres Werra Steinsalz (NaIα) 8m. below the Thuringen Potash Bed	1	0	-	Harder (1959)
"	Hartsalz from the lower part of the Thuringen Potash Bed	1	0	-	"
"	Carnallite (KITH), upper part of the Thuringen Potash Bed	1	0	-	"
"	Mittleres Werra Steinsalz (NaIβ)	1	0	-	"
"	Hartsalz (KIH) of the Hessen Potash Bed	1	0	-	"
"	Oberes Werra Steinsalz 20m. below the Braun- roter Salzton	1	0	-	"
"	Braunroter Salzton	1	2157.5	-	"

Table 11.9 (cont.)

Locality	Material	No. of samples	ppm B ₂ O ₃		Source of data
			Range	Average	
Reyerhausen, North Germany	Ältestes Steinsalz (Na1)	1	0	-	Harder (1959)
"	Älteres Steinsalz (Na2)	1	161	-	"
"	Älteres Kalilager (K2)	1	32.20	-	"
"	Clay band in carnallite (without anhydrite)	-	1610-2898	-	"
"	Grauer Salzton (T3)	1	6440	-	"
"	Jüngeres Steinsalz (Na3)	1	9.66	-	"
"	Roter Salzton (T4)	1	1610	-	"
Stassfurt Mine, North Germany	Stassfurt Seam (K2)	31	0-490	257.6	Biltz & Marcus (1911)
Vienenburg Mine, North Germany	Stassfurt Seam (K2)	20	0-630	145	"
Königshall- Hindenberg Mine, North Germany	Middle of the Stassfurt rock salt	n.d.*	n.d.	32	Braitsch (1972)

Table 11.9 (cont.)

Locality	Material	No. of samples	ppm B ₂ O ₃		Source of data
			Range	Average	
Königshall-Hindenberg Mine, North Germany	Upper part of the Stassfurt rock salt	n.d.	n.d.	225	Braitsch (1972)
"	Stassfurt Seam (K2) (anhydritic sylvite-halite)	n.d.	n.d.	64	"
"	Stassfurt Seam (impoverished in K)	n.d.	n.d.	193	"
Hildesia Mine, North Germany	Stassfurt Seam	100	322-6440	1288	Kokorsch (1960)
Hannover Potash District, North Germany	Stassfurt Seam (K2) - grey sylvite-kieserite-halite rock	n.d.	n.d.	1932	Kuhn (1955)
E3 boring, Sleights, Yorkshire	Insoluble residues from the Boulby Potash at 1345.3 m.	n.d.	322-1610	n.d.	Armstrong et al. (1951)
"	Insoluble residues from the Boulby Potash at 1348.7 m.	n.d.	tr	n.d.	"
"	Insoluble residues from the Boulby Potash at 1363.3 m.	n.d.	1610-3220	n.d.	"

Table 11.9 (cont.)

Locality	Material	No. of samples	ppm B ₂ O ₃		Source of data
			Range	Average	
E3 boring, Sleights, Yorkshire	Insoluble residues from the Boulby Potash at 1370.0 m.	n.d.	322-1610	n.d.	Armstrong et al. (1951)
"	Insoluble residues from the Boulby Potash at 1377.0 m.	n.d.	322-1610	n.d.	"
"	Insoluble residues. Average sample of 6m. of sylvite-halite rock of the Boulby Potash	n.d.	n.d.	50	Stewart (1963b)
"	Insoluble residues. Average sample of 6m. of sylvite-halite rock of the Upper Potash	n.d.	n.d.	tr	"
E4 boring, Smeaton, Yorkshire	Average of 13m. of salt clay containing 10% camallite and 17% halite from the Carnallite Marl	n.d.	n.d.	1000	"
Boulby Mine	Boulby Potash	18	70-2600	954	This study
"	Boulby Halite	8	270-1000	584	"

* n.d. = no data

rock salt and other halite rocks of the German Zechstein as it contains larger quantities of clay and anhydrite. In addition Ham et al. (1961) showed that the boron content of the anhydrite rock in Oklahoma is comparable with that which is recorded in pools of evaporated seawater, which are precipitating gypsum and halite, adjoining the Gulf of Mexico and Gulf of California.

One would have expected borate minerals to be more abundant in halite and potash deposits as they are saturated with respect to boracite during halite precipitation and even at Boulby the rocks do not contain excess boron. Absorption of boron by clays and anhydrite or the difficulty borates have in attaining equilibrium may have prevented crystallization of these minerals in other deposits. In addition, if boron became concentrated in the residual brines, as has occurred at Boulby, dilution of these brines by more dilute seawater, groundwater or a rainstorm would be sufficient to prevent precipitation of borate minerals.

Marine borate deposits are unlikely to be of any commercial value unless the minerals occur concentrated in a specific bed as at Boulby or have accumulated in the manner of the Inder deposit. In the latter case where the borates occur at the surface, ease of access makes exploitation of the deposit a viable proposition. Where the borate minerals occur in a specific bed associated with potassium bearing salts, they are likely

to be buried at depth. Under these conditions they may be of commercial value as a by-product of potash extraction. The brecciation of bed B.S.3 precludes this possibility at Boulby under normal conditions. However they might provide a useful indigenous source of boron should the U.K. find itself unable to import large quantities of borate minerals from elsewhere.

PART II

EXPERIMENTAL STUDIES

CHAPTER 12AN EXPERIMENTAL STUDY OF THE SYSTEM $\text{NaCl-H}_2\text{O}$ AT 25°C AND
AT PRESSURES UP TO 2.5 KILOBARSI Introduction

The General Introduction at the beginning of the thesis explained that the initial aim of the research project was to study the effects of pressure (up to 2.5 kilobars) and temperature (up to 200°C) on phase equilibria in multicomponent salt systems. It was hoped that this would help to elucidate processes related to diagenesis during burial of evaporite deposits, and the transportation of base metal cations in solutions and brines. This general investigation was, however, discontinued after 7 months in favour of a study of the Boulby Mine material.

The temperature and pressure limits of this study were designed to cover the range found in evaporite deposits and shallow hydrothermal associations. Sylvite-halite rocks may be buried to a depth of 5000 m. which would give rise to a pressure of 1.5 kilobars and temperatures around 90°C assuming a temperature gradient of 15°C/km. Temperatures up to 200°C may be found in hydrothermal environments.

Adams (1931), MacDonald (1953) and Braitsch (1972)

all commented on the paucity of experimental data related to the effects of pressure on multicomponent salt systems even though pressure might be relevant to the study of evaporite diagenesis and saline hydrothermal solutions (Dunham, 1966). Adams (1931) and Sourirajan and Kennedy (1962) investigated the system $\text{NaCl-H}_2\text{O}$ under pressure whilst MacDonald (1953) discussed a theoretical study of the system $\text{CaSO}_4\text{-H}_2\text{O}$ under similar conditions. Rawitsch (1958) evaluated water-salt equilibria at temperatures of 600-650°C and 300-350 kg/cm² but had problems related to the quenching of solutions co-existing with crystalline phases.

Adams (1931) studied the system $\text{NaCl-H}_2\text{O}$ at 25°C and at pressures up to 16 kilobars (Figure 12.1). It was found that the solubility of NaCl rose from 26.42 weight percent to 27.60 weight percent over the pressure range from 0 to 4 kilobars. A further increase of pressure caused the solubility of NaCl to diminish steadily. At pressures between 8 and 11.8 kilobars $\text{NaCl}\cdot 2\text{H}_2\text{O}$ was found to be the stable crystalline phase in equilibrium with the liquid. Above 11.8 kilobars NaCl is in equilibrium with solution or ice.

Sourirajan and Kennedy (1962) investigated critical phenomena in the system $\text{NaCl-H}_2\text{O}$, at temperatures up to 800°C and pressures up to 400 bars, and showed that the supercritical fluids associated with shallow igneous intrusions could carry up to 3% dissolved NaCl and give

rise to saline hot springs.

MacDonald (1953) calculated the effect of pressure on the gypsum-anhydrite transition point. It was found that under conditions of hydrostatic pressure the transition point was raised by 12°C /kilobar pressure increase, whilst under differential pressure it was reduced 1°C per 40 atmospheres pressure increase.

Critical phenomena occur at temperatures too high to be important in evaporite deposits, except next to the intrusion of igneous bodies as the critical temperature of water (374°C) is raised by the presence of dissolved involatile solute (Ölander and Liander (1950)). Benedict (1939), Keevil (1942), Rawitsch (1958) and Sourirajan and Kennedy (1962) all showed that saturated solutions of highly soluble salts such as NaCl do not exhibit critical phenomena, whilst those of more insoluble salts such as Na_2SO_4 and Na_2CO_3 do so at temperatures very close to the critical temperature of water. Na_2SO_4 (thenardite) and Na_2CO_3 are only rarely found in marine evaporite sequences and hydrothermal environments.

From the above it may be seen that little effort has been directed towards examining systems of more than 2 components even though pressure and temperature effects may be relevant in considering the migration of solutions through fissures in buried salt deposits. These may cause changes in mineral solubilities with respect to

water and brines. It is very unlikely that such migrating salt solutions would be composed of only two components, i.e. H_2O and a single salt component.

It was thought initially advisable to study a simple system such as $\text{NaCl-H}_2\text{O}$ in order to develop and test experimental equipment suitable for the subsequent investigations. An emulation of Adams' (1931) result would indicate the apparatus was in working order.

II Experimental Equipment

It is not yet possible to use the quench technique for experiments with salt solutions as a drop in temperature will cause a saturated salt solution to crystallize. Zen (1965), whilst analysing the system $\text{NaCl-CaSO}_4\text{-H}_2\text{O}$ at 35°C , 50°C and 70°C noted that if the liquid was not sampled at the temperature of formation, then it crystallized on cooling, and it was impossible to tell the difference between primary halite and secondary halite formed on cooling. Thus any equipment designed to study salt systems at varying pressure and temperature requires to have a liquid sampling mechanism.

It is instructive to briefly examine the equipment used by Adams (1931), Sourirajan and Kennedy (1962) and Dickson et al. (1963), all of which had liquid sampling mechanisms, but none of which could be used in the study of multicomponent systems for various technical reasons.

(1) Hydrothermal Equipment Review

Adams (1931) used a method of liquid sampling to study the system $\text{NaCl-H}_2\text{O}$ under pressure. The apparatus (Figure 12.2) measured the volume changes of the system at different pressures at constant temperature, enabling an equilibrium diagram to be constructed. The piezometer illustrated in Figure 12.2 was used. It consisted of a bulb of pyrex glass, with a ground glass stopper surrounded by a mercury seal and at the bottom a re-entrant capillary tube drawn down at its tip. The bulb was housed in a thin-walled cylindrical capsule of stainless steel, containing up to 3 cm^3 of mercury. As the piezometer was subjected to pressure the liquid within the bulb contracted and mercury flowed down the capillary. On releasing the pressure the solution expanded and some of it passed down the capillary out of the bulb. The solution within the piezometer was then separated from the mercury and analysed. The weight of mercury in the bulb was a measure of the amount of compression of the solution at the highest pressure to which it was subjected.

The equipment is not suitable for the study of multi-component systems as (a) with more than 2 components present it is difficult to evaluate volume changes and (b) it is not possible to examine the crystal phases present without inducing crystallization of the liquid.

Sourirajan and Kennedy (1962) used equipment of the type illustrated in Figure 12.3 with the pressure vessel

heated in an oven. The method depends on slightly reducing the pressure in either the gas or liquid lines, thus drawing off a sample of the gas or liquid phase. If a sample of gas was drawn off the pressure dropped by no more than 2 bars and the temperature by a maximum of 0.5°C . A small volume of water was then added to compensate for this gas. Prior to sampling, the pressure and temperature of the pressure vessel were accurately recorded. The sample was drawn into a weighed standard volumetric flask half-filled with distilled water. The difference between the initial and final weight of the volumetric flask gave the exact weight of the sample. There are 2 difficulties with the study of saturated solutions, (i) the crystal present in a multicomponent system cannot be seen without opening the pressure vessel and (ii) crystals tend to block the sampling lines.

Dickson et al. (1963) used a pressure vessel of the type shown in Figure 12.4. The equipment consisted of a variable volume teflon sample cell suspended in a stainless steel pressure vessel. Pressure was applied by pumping fluid into the space between the cell and the stainless steel bomb. Samples of the solution were taken by opening the sampling line and drawing liquid from the cell into a cooled glass container. Simultaneously, fluid was pumped into the steel pressure vessel at the same rate as liquid was removed from the sample cell, thus keeping the pressure constant to ± 5 bars. The

disadvantage of this equipment is that for a system of more than 2 components, one cannot examine the crystal phases without opening the cell.

(2) Experimental Equipment used in this study

It is evident that this equipment must allow rapid liquid sampling and fast easy access to the crystalline phase. The pressure vessel and pressure circuit used in this study are shown in Figures 12.5 and 12.6. The principle of this pressure vessel is that when equilibrium is attained the liquid is rapidly pushed out through a filter at one end of the pressure vessel. The crystalline phases are caught on the filter and they may be quickly removed from the pressure vessel for microscopic examination. This method allows fast extraction of the liquid, whilst the equilibrium crystalline assemblage and the solution composition are preserved.

The pressure vessel is 22.86 cm long and the solution chamber has a capacity of 10 cm^3 . It has an internal diameter (ID) of 1.40 cm, an outer diameter (OD) of 4.19 cm and a radius ratio (OD/ID) of 3. The end nuts have 2.86 cm U.N.F. threads and a 0.32 cm bore tube along their length. Oil applies pressure to the solution via a teflon plunger. At the opposite end of the pressure vessel a glass filter is housed in a teflon holder. The pressure vessel is designed to withstand pressures of 2.5 kilobars and the threading of the end nuts have a

safety factor of 5 whilst the brackets have a safety factor of 10. The calculations made to determine these parameters are given in Appendix 7.

The pressure vessel is constructed from chromium-nickel austenitic stainless steel which contains 0.08% C, 2.00% Mn, 0.045% P, 0.03% S, 1.00% Si, 16.00-18.00% Cr, 10.00-14.00% Ni and 2.00-3.00% Mo. This type of austenitic stainless steel is particularly resistant to oxidation at high temperatures and thus the likelihood of corrosion is much reduced. As teflon is stable at temperatures below 300°C (Graf, 1974), and it is not attacked by salts, it is a suitable material for the plunger and filter holder. Scinta glass filters proved effective in trapping crystals which were in equilibrium with the solutions. The pressure tubing is of the 60,000 psi flexible variety and the sampling line leads to valves of the 60,000 psi Aminco type.

The temperature of the pressure vessel was maintained by placing it in a waterbath (Figure 12.6). The water temperature, and hence that of the pressure vessel was measured by an accurate thermometer to within 0.2°C. A Budenberg bourdon tube gauge recorded the pressure within the pressure vessel. In order to promote mixing of the sample solutions in the pressure vessel it was rocked on a platform in the waterbath during experiments. This was found to shorten the time it took for solutions to reach equilibrium. The sample extraction lines did

not require to be heated to prevent crystallization of the solution as the room temperature was almost 25°C when samples were taken.

Prior to conducting the experiments it was necessary to calibrate the pressure vessel and equipment. It was important to determine:- how constant the temperature was within the pressure vessel for long periods of time; the temperature within the pressure vessel relative to the thermometer in the waterbath; the rate of extraction of the liquid from the pressure vessel; the contamination of the extracted solutions and the time required for a solution to come to equilibrium. The calibration experiments and their results are described in Appendix 8. These experiments demonstrated that the pressure vessel temperature was constant over prolonged periods of time and corresponded to that of the waterbath to within 0.2°C. Initial solutions were found to leach iron from the sidewalls of the solution chamber but after five experiments analyses showed negligible iron, manganese, chromium and nickel in the extracted liquid. 10 mls. of solution could be extracted in approximately half a minute. Figure 12.7 shows that, at 25°C, equilibrium between NaCl crystals and a solution of constant composition is established in 15 hours.

(3) Experimental Method and Operation of Equipment

Each experiment on the system $\text{NaCl-H}_2\text{O}$, at 25°C , and up to pressures of 2.5 kilobars was conducted in the following manner. A solution of known composition was made up from recrystallized Analar NaCl and distilled water at 25°C . The teflon plunger was inserted at the end of the pressure vessel to be connected to the oil pressure line and the end nut was screwed tightly in place. The chamber of the pressure vessel was filled almost to the brim with the solution and then the filter holder, containing the filter, was emplaced. Any air present in the solution escaped through the filter at this point. The nut, connected to the clean sampling line, was then tightened. The pressure vessel was placed on the rocking platform in the waterbath and connected to the pressure line and the sampling valve. After half an hour the pressure vessel reached the temperature of the waterbath and pressure was applied. The rocking mechanism was set in motion and the experiment was left for 24 hours.

To extract the solution the sampling valve was quickly opened and slight pressure applied to the plunger. The first 2 mls. to pass through the sampling line were discarded. The remainder of the solution was collected in six weighed volumetric test-tubes and the mass of the liquid in each was later determined by difference. The pressure vessel was then opened and the crystals on the filter examined. The six aliquots were analysed to

determine their NaCl content.

III Method of Chemical Analysis

An EEL flame photometer was used to determine the NaCl content of the solutions by comparing the samples with known standards. Six aliquots of each solution were analysed to evaluate the precision (reproducibility) of the analyses. Table 12.1 shows that the relative standard deviation (coefficient of variation), which is a measure of precision, of all the solutions is less than 0.5%. The results are thus highly reproducible. Appendix 9 outlines the calculation of the relative standard deviation.

The accuracy (i.e. the correctness of the measurements in the analyses) of the results is thought to be good. A few duplicate experiments in which the solutions were analysed using both the flame photometer and a weighing and evaporation technique produced similar results. The NaCl contents of the standards with which the solutions were compared were known very accurately.

IV Results and Conclusions

The results of the study of the system NaCl-H₂O, at 25°C, and pressures up to 2.5 kilobars are shown in Table 12.1 and Figure 12.8. The equilibrium solution

Table 12.1 Equilibrium Data for the System NaCl-H₂O, at 25°C, and up to 2 kilobars
Pressure

Temperature	Pressure (bars)	Comp. of initial solution in wt% NaCl	Comp. of final solution in wt% NaCl	Relative Standard Deviation	NaCl crystals present or absent on filter
25°C	Atmos.	26.36	26.36±0.05	0.19	Absent
"	"	26.42	26.42±0.08	0.30	Present
"	"	28.00	26.43±0.07	0.26	Present
"	717.8	26.42	26.42±0.04	0.15	Absent
"	1142.0	26.90	26.76±0.12	0.45	Present
"	1570.3	26.80	26.80±0.06	0.22	Absent
"	2141.3	27.00	27.00±0.03	0.11	Absent
"	2426.8	28.00	27.11±0.07	0.26	Present
"	2498.2	28.00	27.23±0.09	0.33	Present

curve was approached from the undersaturated and oversaturated directions. The solubility curve passes between points A and B as their standard deviations overlap representing experimental error. In theory they should both lie on the curve.

The solubility of NaCl at atmospheric pressure was found to be 26.42 weight percent rising to 27.23 weight percent at 2.5 kilobars pressure.

These results confirm observations which were obtained using a different experimental technique. The NaCl saturation value at atmospheric pressure is also in agreement with the recently published value of Potter II et al. (1975). The fact that these results agree with those of Adams (1931) and Potter II et al. (1975) strongly suggests that the experimental equipment used in these studies is a valid method of examining phase equilibria. There is every reason to suggest that the equipment could operate successfully in studying multi-component systems.

The experimental data indicate that water percolating down through the fissures in an evaporite deposit would be capable of dissolving slightly more NaCl out of the host rock than at the surface. The change in solubility of NaCl with pressure does not have a major effect on evaporite diagenesis at 25°C.

CHAPTER 13SUMMARY AND CONCLUSIONS

This thesis is divided into two parts: the first part describes the results of a petrological and geochemical examination of the upper part of the Boulby Halite, the Boulby Potash and the Boulby Shale in the C.P.L. concession area aimed at contributing to our knowledge of the geological history of these rocks; Part II presents the results of an experimental study of the system $\text{NaCl-H}_2\text{O}$ at 25°C and at pressures up to 2.5 kilobars. The conclusions of these studies are given separately.

I Part I

The beds of the third Zechstein evaporite cycle at Boulby may have accumulated in a basin/lagoon (as defined in Chapter 8), supratidal, or possibly both of these types of environments. However the chemical characteristics of the strata favour the first hypothesis.

In a basinal/lagoonal environment these beds would have been deposited in a large rapidly subsiding lagoon which evolved on the Upper Magnesian Limestone shelf. The bar, which may have been a topographic high or carbonate reef, presumably lay somewhere in the middle

of the present southern North Sea. The lagoon was not completely isolated from the sea and consequently inflowing water gradually became more concentrated as it migrated towards the distal areas because of evaporation and mixing with more concentrated brines. The evaporite minerals, therefore, precipitated in the distal regions first; initially as calcium carbonate minerals, followed by calcium sulphates and then halite. That the brines were, in part, refluxed back to the sea is indicated by the relative thinness of the Boulby Halite when compared with the sulphates and carbonates of this cycle. The brines became depleted in MgSO_4 and enriched in CaCl_2 over a prolonged period of time because of influxes of calcium bicarbonate rich terrestrial waters or calcium cations released as a result of dolomitization of the Upper Magnesian Limestone by evaporite brines. In the final stages of halite precipitation the lagoon was very shallow and the halite probably became emergent. Gentle irregular subsidence caused the potassium and magnesium rich brines to migrate laterally into depressions, forming lakes with halite shores, where they precipitated potassium bearing minerals. Towards the end of desiccation the CaCl_2 brines migrated into small depressions because of further differential subsidence or an earth movement of some sort.

If the Boulby Halite and associated potassium bearing minerals are of supratidal origin, then the environment at the end of precipitation of the Billingham Main

Anhydrite, which is largely of subaqueous origin, probably resembled that of the salt flats in Baja California at the present day. Repeated influxes of normal seawater onto the gently subsiding landsurface resulted in the precipitation of layers of halite and concentration of the remaining brines as they migrated inland into shallow depressions. These brines gradually became enriched in potassium and magnesium ions due to evaporation and recurrent flooding over a long period of time. Halite precipitation exceeded subsidence and the salt flats advanced seaward. After prolonged topographical stability, accompanied by gentle subsidence, large quantities of potassium and magnesium brines and minerals would have lain on or beneath the halite surface. Evaporation of lakes of these brines, enriched in CaCl_2 , which lay on the surface of the halite, accompanied by differential subsidence similar to that of the former hypothesis, would have caused the present sequence and distribution of rock types at Boulby. However there is no identifiable source of CaCl_2 in this hypothesis.

During the final stages of desiccation detrital material of fluvial or windblown origin was deposited on the halite plain. The fine grainsize of the clays suggests that, if they are of fluvial origin, they were deposited on the distal portions of a flood plain. A pronounced dilution of the brines occurred after deposition of the lower parts of bed B.S.4; possibly

reflecting reworking of the halite beds by continental waters carrying detrital material and probably accompanied by occasional marine incursions. Equally a rapid transgression of seawater, which had deposited its carbonate component elsewhere, accompanied by influxes of terrestrial material from the adjacent landmass, would account for these beds.

Numerous diagenetic reactions occurred in the rocks of the sequence examined; particularly the lower beds of the Boulby Shale. These may have taken place as the upper beds of the cycle were still being deposited.

Carnallite, which was an original mineral in many of the rocks of beds B.S.1 - 4, was replaced by halite during early diagenesis, by reaction with brines saturated in NaCl. Sylvite, released by this reaction, is observed over approximately the same depth range as the halite pseudomorphs after carnallite, but is irregularly distributed in the lateral and vertical senses; suggesting there may have been much redistribution of secondary KCl rich brines. If the Boulby Potash was a primary carnallite-halite rock, then it is likely that the carnallite also broke down at this time.

In the area of iron-boracite nodules in bed B.S.3 an original metastable iron-boracite polymorph (see Table 5.10) grew by the reaction of boron containing brines enriched in MgCl_2 , partly released by the breakdown of carnallite and possibly bischofite, with iron-containing

clays during diagenesis. These crystals formed aggregates which often combined with sylvite (secondary after carnallite) and magnesite to form nodules. The proportions of these minerals in the nodules is very variable. Since diagenesis the metastable iron-boracite polymorph has been attaining equilibrium by inverting to other polymorphs and sylvite has replaced the other minerals to varying degrees (see Table 5.24).

In the area of parahilgardite nodules in bed B.S.3 small, possibly metastable, parahilgardite crystals grew from CaCl_2 rich brines which may themselves have resulted from the breakdown of pre-existing calcium chloride minerals. These small crystals grew in rosettes which displaced the host clays. After a time, perhaps during late diagenesis, many of the small parahilgardite crystals recrystallized into much larger ones which also formed rosettes. The aggregates of larger rosettes constitute the present nodules. The small quantities of sylvite in these nodules and their host rock suggests that carnallite was originally much less abundant than in the area of iron-boracite nodules; this is in accordance with phase equilibria data.

Chemical analyses of bulk rock samples and insoluble residues show that the boron necessary for the formation of iron-boracite and parahilgardite was derived by the evaporation of seawater without large additions from extraneous sources.

The clays have been extensively displaced or replaced by anhydrite in the upper parts of bed B.S.4 in the East Spearhead. The irregular lateral distribution of this reaction suggests it may be due to more dilute brines migrating downwards during diagenesis. The occurrence of authigenic quartz, magnesite and hematite along the contacts between clays and chloride minerals in the Boulby Shale is evidence of the interaction of the clays with concentrated brines.

At an unknown depth stress induced fissures developed in the rocks from the base of the Boulby Shale to the Upper Anhydrite of the Staintondale Group. As the fissures dilated, KCl-NaCl solutions from the Boulby Potash migrated upwards and sylvite and minor quantities of halite crystallized. Crystal growth was in the direction of least stress, resulting in the formation of fibrous crystals. With each successive dilation new mineral fibres formed and the pre-existing fibres grew longer.

There is much lateral variation in the intensity of fissure development, suggesting that the stress field may have been inhomogeneous or that there may have been considerable lateral variation in the mechanical properties of the rocks at that time. The mineral fibres in some of the veins are curved, indicating that the stress field changed with time.

After formation of the fibrous sylvinite veins, but

probably prior to the overfolding of the Boulby Potash, a solution saturated in NaCl migrated down into the rocks of the Boulby Shale. It has changed the character of these beds, to varying degrees, over much of the C.P.L. concession area. In the area of the Mine enclosed by roadways 2E, 2S, 5W and 3N colourless halite has almost completely replaced all the minerals of beds B.S.3 - 5 and the majority of the sylvinite veins. However in many of the boreholes and in the East Spearhead of the Mine it has replaced the minerals of these beds on a much more limited scale. The brine may have been generated by the dissolution of a halite bed in the upper part of the Boulby Shale or by the dehydration of the Rotten Marl.

Trusheim (1960) has observed that in north Germany large scale lateral migration of salt beds has only occurred when they have been buried to depths in excess of 1000 metres. Such depths would have been reached during the Jurassic at Boulby. However it seems likely that the overfolding and overthrusting of the beds of the sequence examined occurred when they were buried at greatest depth (2200 - 3200 metres) towards the end of the Cretaceous and in the early Tertiary. This is substantiated by Brunstrom and Walmsley (1969) who noted that the majority of halokinesis in the British sector of the North Sea, north of latitude 54N (approximately Scarborough), took place in the Tertiary.

The critical boundary between the elastic and plastic

conditions is lower for potassium salts than rock salt (Trusheim, 1960); suggesting the Boulby Potash was probably the first bed to flow. This phase of movement is the principal cause of bed attenuation in the C.P.L. concession area.

The overfolds and overthrusts in the Boulby Potash may result from the growth of a salt dome or pillow to the north-east of the Mine (Talbot, 1977). As the salt dome/pillow grew, salt beds in the adjacent regions would have migrated towards its base (i.e. from the Mine north-eastwards) to replace the beds which had already risen due to their own buoyancy. The salt beds in the Mine would have ceased large scale lateral migration when the salt dome/pillow attained gravitational equilibrium.

On cessation of the above movement the denser Boulby Shale sank into the Boulby Potash, which migrated locally into small swells (axes orientated $024^{\circ} \pm 10^{\circ}$). In areas of major local gravitational disequilibrium the potash bed flowed laterally into small scale salt domes, some of which became detached from their roots and rose up through the Boulby Shale to accumulate beneath the Rotten Marl (Talbot, 1977). These movements have considerably modified the pre-existing overfolds and overthrusts.

In the final phase of movement monoclines developed at the base of the Boulby Potash in response to overthrusting in the Upper Magnesian Limestone and the Billingham Main Anhydrite. Raymond (1960) has described

similar structures in the Billingham Main Anhydrite at the Billingham Mine and he regards them as being Tertiary in age. Therefore, by comparison with Raymond's (1960) data, it seems likely that the overthrust in the above units at the Boulby Mine represents a minor adjustment possibly associated with Alpine movements on the Continent.

Uplift and erosion has occurred since some time in the Tertiary and the small swells and depressions in the top of the Boulby Potash and the overthrust in the Upper Magnesian Limestone may have formed in this time interval.

Comparison of the third Zechstein evaporite cycle at Boulby with other evaporite sequences in north-east England and the rest of the world shows that:-

(i) The halite and potash beds at Boulby appear to be extensively deformed relative to those of this cycle in the vicinity of Whitby. If these beds at Boulby have migrated towards a salt dome/pillow to the north-east of the Mine, then the "zone of halokinesis" in the southern North Sea (Brunstrom and Walmsley, 1969) must be extended onshore.

(ii) Shaly strata are more abundant in the rocks overlying the potassium mineral bearing zone of this cycle at Boulby than in those around Whitby.

(iii) The halite and potash beds of this cycle throughout north-east England are characterized by almost complete depletion in MgSO_4 minerals, and the beds representing the final stages of desiccation at Boulby are enriched

in a CaCl_2 mineral (parahilgardite) and borate minerals (iron-boracite, ericaite, parahilgardite) relative to those of the E and F boreholes.

(iv) Outside north-east England the sequence of strata at Boulby most closely resembles the unaltered sequence of beds of the Stassfurt Series in the Königshall-Hindenberg Mine, north Germany; although no primary or early diagenetic CaCl_2 rich minerals have been observed in the latter case.

(v) Boulby appears to be the only locality in the world where a full sequence of evaporite beds occurs in association with a primary or early diagenetic CaCl_2 rich mineral.

(vi) Boulby is the largest known occurrence of early diagenetic iron-boracite and parahilgardite in the world.

(vii) The great variation in the mode of occurrence of borate minerals in rocks representing the final stages of desiccation of evaporite cycles suggests that local conditions are critical in determining whether or not these minerals will precipitate.

II Part II

Experimental equipment was designed to study the system $\text{NaCl-H}_2\text{O}$ at 25°C and pressures up to 2.5 kilobars. The equilibrium solution curve was approached from the undersaturated and oversaturated directions. The

solubility of NaCl in water increases from 26.42 weight percent at atmospheric pressure to 27.23 weight percent at 2.5 kilobars. This result is in agreement with those of Adams (1931) and Potter II et al. (1975), both of whom used different experimental techniques from the writer. Therefore, at 25°C, water percolating down through fissures in an evaporite deposit would be capable of dissolving more halite out of the host rock than at the surface.

Acknowledgements

I would like to thank:-

- Sir Frederick Stewart, Professor M.J. O'Hara, and Dr. C.E. Ford for acting as my supervisors and introducing me to the geology of saline deposits.
- the Management of Cleveland Potash Ltd., especially Mr. P.J.E. Woods and the members of the Geology Dept., for granting me access to the Boulby Mine and much borehole data.
- M.J. Saunders and Dr. P. Hill for discussing and helping me with wet chemical and electron microprobe analytical techniques.
- Drs. F. Glasser and M. Barrow of the Chemistry Departments of Aberdeen and Edinburgh Universities, respectively, for allowing me the use of X-ray facilities.
- Professor G. Richter-Bernburg for arranging my field excursion to the salt mines of north Germany.
- Drs. H. Roth, E. Schachl, and C. Käding of Kali und Salz A.G. and Dr. W. Herde of Kalichemie A.G. for numerous discussions about the genesis of salt deposits and guiding me around the salt mines of north Germany.
- Dr. R. Kühn, of the Kaliforschung Institut, in Hannover, for numerous discussions on the origin of marine borate deposits.
- Dr. D.J. Shearman, of Imperial College, London, for showing me the carbonate and sulphate rocks of the Trucial

.Coast and discussions related to the genesis of evaporite deposits.

- Mrs. P. Scrutton for typing the thesis.
- the Natural Environment Research Council for providing financial support for this study.

Appendix 1Well-log data used to compile Plate I

This appendix contains the well-logs of the upper part of the Boulby Halite, the Boulby Potash and the Boulby Shale compiled by the writer from the boreholes in the C.P.L. concession area. The logs for each borehole start from the top of the Boulby Shale and work downwards.

Borehole A1117.67 - 1119.42 m.

Fine grained red-brown marl with a few rounded and elongate pockets of halite and anhydrite up to 1 cm. in width. The lower contact is sharp but irregular.

1119.42 - 1121.55 m.

Halite rock. The upper metre is composed of coarse grained (3 cm.) granular, shaly, white - pale brown halite with a few patches of hematite (3 mm.). This rock grades into colourless granular halite with crystals up to 1 cm. in width. The lowermost 0.67 m. is granular-gneissoze halite with crystals up to 1 cm. in maximum dimension. The lower boundary is sharp.

1121.55 - 1123.50 m.

Gneissoze, red-grey sylvinite containing black-grey anhydritic shale inclusions. Crystals generally less than 1 cm. in width. In the lower 0.67 m. colourless recrystallized halite crystals, up to 2 cm. in width, cross-cut the gneissosity. Rounded black-grey anhydritic shale inclusions (3 cm. in maximum dimension) increase in numbers towards the base. The lower contact is diffuse over 10 cm.

1123.50 - 1127.08 m.

Grey-black anhydritic shale cross-cut by red sylvinite veins. The anhydritic shale contains deep red sylvite porphyroblasts up to 1.5 cm. in width and the Borate Nodule Bed is present 0.1 m. thick near the base. Laminae within the shale are highly contorted. The sylvinite veins have a granular to gneissoze texture with crystals up to 1 cm. in maximum length. The lower contact is sharp and slightly irregular.

1127.08 - 1128.33 m.

Pale grey-pink gneissoze sylvinite. Maximum grainsize 1 cm. Rare shale inclusions up to 1 cm. in length. The lower contact is sharp.

1128.33 - 1158.33 m.

Banded, granular, coarse grained, white-brown halite

rock. Anhedral crystals up to 10 cm. occur although the majority are 2-3 cm. The uppermost 1.5 metres contains rounded inclusions of grey-green halite-clay rock.

Borehole Z

1056.00 - 1057.33 m.

Grey, gneissoze, fine grained (0.5 cm.) sylvinite with sharp slickensided base.

1057.33 - 1062.93 m.

Banded, granular, coarse grained, grey-black to white halite rock. Halite crystals are anhedral and up to 10 cm. in width. The rock contains a few disrupted shale laminae.

Borehole B

1195.33 - 1196.70 m.

Red-brown fine grained marl showing no sedimentary structures. The base is sharp and extensively slickensided.

1196.70 - 1198.27 m.

White, coarse grained (1.5 cm.), granular halite rock which becomes red towards the base. Small numbers of grey anhydritic shale inclusions up to 5 cm. in width.

The rocks are internally slickensided. Gradational lower contact.

1198.27 - 1199.33 m.

Coarse grained granular halite; grainsize up to 10 cm. Colour varies from white - grey - brown. Disrupted shale laminae (2-3 mm. thick) towards the base. Lower contact gradational.

1199.33 - 1200.17 m.

White-red granular sylvinite; grainsize up to 1 cm. The rock contains numerous grey anhydritic shale inclusions up to 4 cm. in maximum dimension. Gradational lower contact.

1200.17 - 1202.20 m.

Grey-red-brown granular halite rock; grainsize up to 3 cm. The uppermost 0.3 m. contain rounded fragments of red marl (maximum dimension 2 cm.). Sharp lower contact.

1202.20 - 1202.90 m.

White grey-pink gneissoze sylvinite of low grade; grainsize up to 1 cm. No shale inclusions. Sharp lower contact.

1202.90 - 1214.25 m.

Grey-black anhydritic shale/siltstone cross-cut by red, sometimes fibrous, sylvinite veins. The sylvinite veins are usually granular. A Borate Nodule Bed occurs 1.6 m. above its base and is composed of elongate nodules 3 cm. in length. Some of the vein walls are slickensided. The boundary with the sylvinite below is sharp.

1214.25 - 1215.00 m.

Pink-grey, granular to gneissoze sylvinite; grain-size up to 1 cm. Internal slickensides towards the base. Sharp base to the unit.

1215.00 - 1218.33 m.

Coarse grained, white to pale brown granular halite; grainsize up to 10 cm. The rock contains numerous highly distorted and disrupted shale laminae and a few milky white sylvite crystals (1 cm. in maximum dimension) with hematite enriched rims.

Borehole X1032.67 - 1033.33 m.

Fine grained, red-brown marl extensively veined by sylvinite veins. No sedimentary structures. The base is slickensided, irregular and sharp.

1033.33 - 1033.67 m.

Grey, fine-grained, anhydritic marl with a sharp base.

1033.67 - 1034.50 m.

Parallel laminated halite-anhydrite-clay rock with small red-brown halite porphyroblasts (3 mm.). Slickensided lower contact.

1034.50 - 1037.33 m.

White, gneissoze halite rock; grainsize up to 1.5 cm. The direction of elongation of the crystals is normal to the borehole walls. There are occasional patches of grey halite-anhydrite-clay rock which merge into the surrounded rock. The rock is extensively slickensided. The lowermost 10 cm. of the rock are particularly gneissoze and the unit has a sharp base.

1037.33 - 1039.33 m.

Grey-pink, banded, gneissoze-granular sylvinite; grainsize up to 0.5 cm. The basal 0.3 m. is enriched in grey-green halite-clay rock. Slickensiding is developed 20 cm. above the base of the unit. The boundary with the halite rock below is sharp.

Borehole C1143.27 - 1144.60 m.

Fine grained, parallel laminated, red-brown marl.
Sharp lower contact.

1144.60 - 1146.00 m.

Coarse, red-brown, granular halite; grainsize up to 5 cm. but in general 3 cm. or less. The rock contains a few distorted and disrupted shale laminae. In the middle of this unit is a coarse red-white granular sylvinite rock which merges slightly with the halite rocks above and below it. The halite rock has a sharp boundary with the rocks below.

1146.00 - 1148.33 m.

Black-grey anhydritic shale cross-cut by red, partially fibrous, sylvinite veins. The crystals of the sylvinite veins are up to 4 mm. in length. 0.3 metres above the base of the unit there are a few boracite-sylvite-magnesite nodules up to 2 cm. in length. The base of the unit is sharp.

1148.33 - 1149.00 m.

Red-grey gneissoze sylvinite; grainsize up to 1 cm. in length. The rock contains a few rounded shale inclusions. The base of the unit is sharp and highly

slickensided.

1149.00 - 1151.67 m.

Coarse, white-grey-brown, granular, halite rock; grainsize up to 5 cm. in width but usually around 3 cm. There are a few highly disrupted shale laminae. A pink-white halite band is present as marked on the section in Plate I.

Borehole Y

1128.67 - 1129.58 m.

Fine-grained, red-brown marl enriched in brown halite towards its base. The basal 5 cm. of this unit is composed of grey marl. The basal contact is sharp.

1129.58 - 1130.17 m.

Grey laminated halite-anhydrite-clay rock containing red-brown anhedral halite porphyroblasts up to 3 mm. in maximum dimension. The unit is internally slickensided. The lower contact is sharp and inclined at 45° to the core walls.

1130.17 - 1133.33 m.

Red-grey gneissoze sylvinite with crystals up to 1 cm. in length. The crystals are elongate perpendicular to the core walls. The rock contains a few rounded

anhydritic shale/siltstone inclusions up to 2 cm. in width. The rock has a sharp basal contact.

1133.33 - 1134.33 m.

Laminated grey-green halite-clay rock. The halite crystals range in size up to 1 cm. but the majority are 1-2 mm. in width. There are occasional patches of recrystallized white halite up to 20 cm. in width. The uppermost 1.3 m. contain deep red sylvite porphyroblasts (4 cm. in maximum dimension) which cut across the lamination. The lower contact of this unit is sharp.

1134.33 - 1140.50 m.

Coarse, granular, brown to colourless halite; grainsize up to 1.5 cm. The rock contains a few disrupted shale laminae.

Borehole D

1265.00 - 1267.45 m.

Fine grained, parallel laminated, red-brown marl containing a few rounded fragments of grey marl. There is much slickensiding in this unit. The basal contact is sharp.

1267.45 - 1267.95 m.

Coarse, red-white, granular-gneissoze sylvinite;

grainsize up to 1 cm. in maximum dimension. The rock contains a few disrupted shale laminae (1 mm. thick). Sharp lower contact.

1267.95 - 1268.33 m.

Laminated, grey, halite-anhydrite-clay rock with deep brown, anhedral, halite porphyroblasts (2 mm. in maximum dimension) cross-cut by fibrous red sylvinite veins. The basal contact is sharp.

1268.33 - 1269.02 m.

Coarse, red-white, granular-gneissoze sylvinite; grainsize up to 1 cm. in maximum dimension. Sharp basal contact.

1269.02 - 1270.13 m.

Breccia of red marl, grey marl, and grey-black anhydritic shale set in granular-fibrous red sylvinite veins (grainsize up to 4 mm.). The fragments are rounded and up to 10 cm. in maximum dimension. The base of the unit is sharp.

1270.13 - 1271.37 m.

Fibrous-granular sylvinite veins containing rounded to angular fragments of grey anhydritic shale up to 10 cm. in maximum dimension. The maximum grainsize of the crystals in the sylvinite is 1 cm. The lower contact

is sharp.

1271.37 - 1272.33 m.

Grey, medium grained, granular-gneissoze sylvinite; maximum grainsize 5 mm. Sharp lower contact.

1272.33 - 1275.00 m.

Coarse, granular, grey-brown halite rock; maximum grainsize 1 cm. There are numerous contorted and disrupted shale laminae (up to 1 mm. thick).

Borehole U

1124.00 - 1125.67 m.

Laminated, fine grained, red-brown marl which makes a sharp contact with the halite rock below.

1125.67 - 1128.23 m.

Coarse, granular, brown, halite rock; maximum grainsize 2 cm. The rock contains a few highly distorted shale laminae. Sharp lower contact.

1128.23 - 1128.67 m.

Coarse, granular-gneissoze, red-white sylvinite containing large rounded grey-black anhydritic shale fragments (maximum dimension 10 cm.). The anhydritic shale fragments contain deep red sylvite porphyroblasts

up to 1 cm. in width. Sharp lower contact.

1128.67 - 1129.45 m.

Coarse, gneissoze, red-brown to grey sylvinite; grains up to 1 cm. in maximum dimension. Sharp basal contact.

1129.45 - 1129.88 m.

Grey-black anhydritic shale containing large anhedral red sylvite porphyroblasts (maximum dimension 2 cm.). Sharp basal contact.

1129.88 - 1130.83 m.

Coarse, granular to gneissoze, red-brown sylvinite; maximum grainsize 1 cm. There is a slight enrichment in halite towards the base. Sharp basal contact.

1130.83 - 1133.53 m.

Granular to gneissoze red-grey sylvinite (grainsize up to 1.5 cm. but usually 0.3 cm.) containing rounded inclusions of black anhydritic shale up to 5 cm. in width. Sharp basal contact.

1133.53 - 1136.27 m.

The uppermost 1.5 m. is a grey gneissoze halite rock (average grainsize 2 cm.) containing a few highly distorted shale laminae (3 mm. thick). This grades down into

grey-green halite-clay rock which is enveloped in gneissoze halite (maximum grainsize 0.5 cm.). Sharp lower contact.

1136.27 - 1149.67 m.

Granular-gneissoze, red-grey sylvinite (average grainsize 0.5 cm.) containing rounded to angular fragments of grey anhydritic shale/siltstone up to 5 cm. in maximum dimension.

1149.67 - 1151.67 m.

Grey-green halite-clay rock extensively veined by fibrous halite and sylvinite veins. Some of the sylvinite has a granular texture. The boundary with the rocks below is gradational.

1151.67 - 1152.67 m.

Slickensided grey-green halite-clay rock with poorly developed parallel laminations. Anhedral halite crystals, up to 0.5 cm. in maximum dimension, cross-cut the parallel laminations. The boundary with the granular halite rock beneath is gradational.

1152.67 - 1154.67 m.

Coarse, granular, white-grey-brown halite rock. The maximum grainsize is 4 cm. but the majority of crystals are 2-3 cm. in width. There are a few disrupted

shale laminae in the rock.

Borehole F

1154.00 - 1156.08 m.

Laminated, fine-grained, red-brown marl containing small pockets of anhydrite and halite. The sample containing the contact with the rocks below is missing.

1156.08 - 1156.67 m.

The upper 45 cm. of this halite rock are composed of granular pale brown halite with crystals up to 1.5 cm. in width. This type of halite rock makes a sharp contact with the lower 15 cm. of grey-green halite-clay rock. The lower contact of this unit is sharp.

1156.67 - 1157.95 m.

Medium grained, granular to gneissoze red-white sylvinite with a maximum grainsize of 1 cm. The base grades over 5 cm. into the unit below.

1157.95 - 1158.27 m.

Red sylvinite with rounded grey-black anhydritic shale fragments up to 1 cm. in width. The crystals of the sylvinite are slightly elongate and up to 3 mm. in length. The unit has a sharp lower contact.

1158.27 - 1158.95 m.

Granular-gneissoze grey sylvinite with a maximum grainsize of 0.5 cm. The unit has a sharp, inclined, lower contact.

1158.95 - 1159.42 m.

Laminated grey-black anhydritic shale containing pseudo-hexagonal sylvite porphyroblasts up to 1.5 cm. in maximum dimension. The laminae are steeply inclined to the core wall and the unit has a sharp lower contact.

1159.42 - 1160.33 m.

Medium grained, gneissoze, grey sylvinite with a slickensided base. The maximum grainsize is 0.5 cm.

1160.33 - 1160.68 m.

Grey gneissoze halite rock with maximum grainsize 1 cm. The lower contact is gradational over 5 cm.

1160.68 - 1165.00 m.

Coarse, granular-gneissoze, pale brown halite rock. The crystals have a maximum grainsize of 2 cm.

Borehole V1158.00 - 1160.33 m.

Laminated red marl containing pockets (up to 2 cm.

in width) of halite and anhydrite. At the base of the unit there are 5 cm. of highly disrupted grey marl. The lower contact is sharp and angular with the grey marl intersecting the laminae of the rocks below.

1160.33 - 1161.17 m.

Laminated grey-black halite-anhydrite-clay rock containing anhedral red-brown porphyroblasts of halite (maximum dimension 2 mm.) cutting across the laminae. This rock type grades over 5 cm. into the rocks below.

1161.17 - 1163.38 m.

Grey-black anhydritic shale breccia which is slightly veined by sylvinite. The unit contains fragments of grey marl up to 30 cm. in width. A band of parahilgardite nodules, 20 cm. thick, occurs 1.38 m. above the base of the unit. The nodules are rounded and up to 2 cm. in diameter. The shale becomes less disturbed towards the base, which is a sharp contact.

1163.38 - 1165.33 m.

Coarse gneissoze red-white sylvinite with crystals up to 1 cm. in width. Gradational lower contact.

1165.33 - 1166.22 m.

Deep red granular sylvinite (grainsize 2 mm.) containing rounded-angular black-grey anhydritic shale

and grey marl fragments up to 5 cm. in width. The sylvinite may be recrystallized veins. These rocks grade into those below.

1166.22 - 1167.67 m.

Granular-gneissoze grey sylvinite containing a few shale fragments. The maximum length of crystals is 0.5 cm. Sharp lower contact.

1167.67 - 1170.00 m.

Coarse, granular-gneissoze, grey halite rock with crystals up to 1.5 cm. in maximum dimension.

Borehole V-D1

1161.00 - 1163.00 m.

Fine grained red marl containing a few pockets (maximum width 2 cm.) of anhydrite and halite. Sharp, slightly inclined basal contact.

1163.00 - 1165.00 m.

Laminated grey-black halite-anhydrite-clay rock containing small anhedral red-brown halite porphyroblasts up to 4 mm. in width. The top of the unit is brecciated and contains rounded red marl inclusions up to 10 cm. in diameter. The unit has a sharp basal contact.

1165.00 - 1165.67 m.

Coarse, granular-gneissoze, pale brown halite rock with a maximum grainsize of 1 cm. The unit has a sharp basal contact.

1165.67 - 1168.00 m.

Medium grained, granular to gneissoze, red-white sylvinite (grainsize 1-10 mm.) enriched in shale and marl fragments, which are rounded to angular and up to 3 cm. in maximum dimension. The fragments towards the top of the unit are black anhydritic shale and red and grey marl. The fragments at the base of the unit are of grey-green halite-clay rock. The unit has a sharp basal contact.

1168.00 - 1168.33 m.

Grey-green halite-clay rock with a slickensided base.

1168.33 - 1172.00 m.

Coarse, granular, grey halite rock with crystals up to 0.75 cm. in maximum dimension. The unit is internally slickensided near the top. A granular pink-white halite band occurs between 1170.67 and 1171.16 m.

Borehole M1148.00 - 1149.78 m.

Red-brown marl containing pockets of halite up to 4 cm. in width. Sharp lower contact.

1149.78 - 1153.08 m.

Halite rock which is composed of coarse grained (up to 1 cm.) pale brown halite in its upper parts and which grades down into grey laminated halite-anhydrite-clay rock containing anhedral red-brown halite porphyroblasts (up to 3 mm. in maximum dimension). The uppermost halite rock contains rounded fragments of black anhydritic shale and grey marl. The basal contact is sharp.

1153.08 - 1153.75 m.

Coarse, granular, red-white sylvinite with a maximum grainsize of 2 cm. The unit has a gradational lower contact.

1153.75 - 1157.73 m.

Granular-gneissoze, occasionally fibrous, red sylvinite containing many anhydritic shale inclusions. The sylvinite is almost certainly recrystallized fibrous sylvinite veins. The anhydritic shale fragments are angular and up to 5 cm. in maximum dimension. The base of the unit is gradational over 5 cm.

1157.73 - 1165.00 m.

Granular to gneissoze, red-grey sylvinite with maximum crystal length 1.5 cm. There are a few rounded inclusions of black anhydritic shale towards the base including a fragment of the white anhydrite-halite band. The unit has a sharp basal contact.

1165.00 - 1167.00 m.

Granular, grey-black halite rock containing shale inclusions. The crystals are up to 1 cm. in maximum dimension. A thin pink-white halite band also occurs in this unit as shown in Plate I.

Borehole M-D21150.00 - 1151.10 m.

Fine grained red-brown marl which grades into the rock unit below.

1151.10 - 1154.10 m.

Coarse white-brown halite rock (grainsize up to 2 cm.) containing lumps of red marl. The proportion of halite increases towards the base where it merges with the rocks below.

1154.10 - 1156.60 m.

Coarse, granular, brown-red-white halite rock with

crystals up to 2 cm. in maximum dimension. Towards the base the unit becomes rich in grey laminated halite-anhydrite-clay rock containing anhedral red-brown halite porphyroblasts up to 2 mm. in width. The unit has a sharp basal contact.

1156.60 - 1164.00 m.

Gneissoze pink-grey-black sylvinite with elongate crystals up to 1.5 cm. in length. A few rounded inclusions of grey anhydritic shale, up to 2 cm. in diameter, are disseminated throughout the rock. Occasional rounded recrystallized halite porphyroblasts (maximum diameter 3 cm.) cut across the gneissosity. The unit has a sharp basal contact.

1164.00 - 1166.00 m.

Coarse, granular, white-brown halite rock with crystals up to 3 cm. in width.

Borehole L

1206.00 - 1207.40 m.

Halite - grey marl breccia. The halite rock component consists of brown anhedral crystals up to 0.5 cm. in width. The grey marl fragments are rounded to angular and up to 5 cm. in maximum dimension. Sharp basal contact.

1207.40 - 1207.87 m.

Granular-gneissoze, pale brown halite rock (grainsize up to 1 cm.) containing a few disrupted shale laminae (1 mm. thick). Sharp basal contact.

1207.87 - 1209.40 m.

Red sylvinite containing many rounded shale fragments up to 10 cm. in diameter. The red sylvinite, which composes about 33% of the rock unit, looks very like recrystallized veins and has anhedral crystals up to 3 mm. in width. The fragments include black anhydritic shale and laminated halite-anhydrite-clay rock with anhedral red-brown halite porphyroblasts (3 mm. in maximum dimension). The disposition of the fragments suggests they have been rolled.

1209.40 - 1216.67 m.

Gneissoze grey sylvinite with elongate crystals up to 1 cm. in length. The sylvinite contains sporadically disseminated rounded inclusions of black anhydritic shale up to 5 cm. in width. The shale fragments towards the base of the rock are of grey-green halite-clay rock. The lower contact is sharp.

1216.67 - 1217.28 m.

Grey-green halite-clay rock veined by sylvinite. Sharp basal contact.

1217.28 - 1220.00 m.

Coarse, granular, white-grey-brown halite with crystals up to 2 cm. in width.

Borehole S-20

1200.00 - 1202.67 m.

Fine grained red-brown marl which makes a sharp contact with the rocks below.

1202.67 - 1203.67 m.

Pale grey marl containing subhedral crystals of halite (2 cm. in width). Red sylvinite veins up to 2 cm. in width cross-cut the rock. The basal 0.5 m. of the rock is brecciated and contains angular fragments up to 8 cm. in maximum dimension. Sharp basal contact.

1203.67 - 1205.00 m.

Grey, partially laminated halite-anhydrite-clay rock containing anhedral red-brown halite porphyroblasts up to 2 mm. in width. The dip of the laminae varies from 5 - 20°. The laminae are best developed towards the top of the unit. The unit has a sharp basal contact.

1205.00 - 1208.33 m.

Granular-gneissoze, pink-grey, sylvinite with a maximum grainsize of 5 mm. The sylvinite contains

sporadically disseminated grey anhydritic shale fragments (0.5 cm. in maximum dimension) containing deep red sylvite porphyroblasts. The shale fragments at the base of the unit are of grey-green halite-clay rock. Slickensides occur 10 cm. above the base of the sylvinite. Sharp basal contact.

1208.33 - 1208.83 m.

Laminated grey-green halite-clay rock. The anhedral halite crystals are up to 3 mm. in width. The rock is veined by coarse halite from below. The unit has a sharp lower contact.

1208.83 - 1210.00 m.

Coarse, granular, pink-orange-grey halite rock. Maximum grainsize 5 cm. There are a few highly contorted and disrupted anhydrite laminae (1 mm. thick).

Appendix 2Structural Interpretations of the BoreholesI Introduction

As the sequences of rocks in the individual boreholes are different (Plate I) it has not been possible to provide a stratigraphic correlation of these rocks between boreholes. This appendix, therefore, interprets the structural geology of the sequences of rocks in the individual boreholes in the light of our knowledge of the geological history of these rocks in the Mine. However, although many of the boreholes appear to be cross-sections through overfolds and overthrusts, it is not possible to give the orientation of these structures from the borehole data. This analysis provides important economic data on the types of geological structures likely to be met as mining proceeds in the C.P.L. concession area.

The reader is referred to the borehole cross-sections in Plate I throughout this appendix. Table 2.2 gives the idealized stratigraphy of the rocks in the C.P.L. concession area. The rocks of the S-20 borehole will not be considered here as they have already been interpreted in connection with the geology of the Mine.

II The Boreholes

In all the boreholes beds B.S.1 and 2 are absent from the sequence.

(1) Borehole A

An almost ideal sequence of rock units is found up to the top of bed B.S.4 in this borehole. However this bed is directly overlain by gneissoze Boulby Potash which is followed upwards in turn by Boulby Halite and the basal Red Rotten Marl. The Boulby Halite and Boulby Potash are mirrored about beds B.S.3 and 4.

The borehole lies to the north-east of the area of overfolding (East Spearhead and Panel No. 1; see Plate II) in the Mine. The sequence of rocks in this borehole can readily be interpreted as being a section through a tight, almost flat lying, overfold of the type shown in Figure A2.1. The writer can think of no other structure which explains the sequence of rocks in this borehole.

(2) Borehole B

In this borehole a nearly ideal sequence of rocks is found up to the top of bed B.S.4 apart from the absence of bed B.H.2. However bed B.S.4 is overlain in turn by the Boulby Potash, Boulby Halite and Red Rotten Marl rather than the normal sequence of beds of the Boulby Shale. The sylvinite of uncertain origin in the Boulby

Halite bears a remarkably close resemblance to the patches of white sylvinite found in the Boulby Halite in the South Spearhead of the Mine.

The general sequence of beds in this borehole is the same as in borehole A although the thicknesses of the individual beds in the 2 boreholes are very different. The beds of this borehole, therefore, almost certainly represent a section through a flat lying overfold (see Figure A2.1).

(3) Borehole C

In this borehole the top of the Boulby Halite beneath the Boulby Potash is markedly slickensided and bed B.H.2 is absent as a result of movement. Bed B.S.4 is directly overlain by bed B.H.1 rather than the normal sequence of beds of the Boulby Shale. The sylvinite of uncertain origin in the "upper Boulby Halite bed" closely resembles the recrystallized patches of sylvinite in the Boulby Halite in the South Spearhead of the Mine.

It seems most likely that this sequence of rocks represents Boulby Halite which has been thrust over the top of beds of Boulby Shale as shown in Figure A2.2. The Boulby Halite has been thrust over the Boulby Potash in the Mine (roadway G, East Spearhead; see Figure 2.11).

(4) Borehole D

In this borehole bed B.S.4 is extensively brecciated and overlain by a bed of sylvinite of uncertain origin enclosing unit B.S.5 which is veined by sylvinite. The sylvinite of uncertain origin is red-white in colour and has a granular to gneissoze texture. It does not resemble the Boulby Potash but is similar to recrystallized sylvinite veins in the Boulby Shale of the South Spearhead of the Mine. As bed B.S.5 is veined by sylvinite it is probable that the sylvinite of uncertain origin results from the recrystallization of sylvinite veins. The rocks of this borehole are, therefore, in the correct stratigraphic order but have been much affected by movement.

(5) Borehole E

The beds of this borehole are completely out of sequence and many of the units in the Boulby Shale are not represented. Bed B.H.2 is absent from the lower beds of the Boulby Halite but is present at the base of the upper beds beneath the Rotten Marl. Bed B.S.4 is sandwiched between an upper and lower bed of Boulby Potash and also occurs as occasional inclusions in the Boulby Potash. Repetition of the Boulby Potash and Boulby Halite about bed B.S.4 strongly suggests that this borehole is a cross-section through a flat lying overfold such as is shown in Figure A2.1.

(6) Borehole L

In this borehole the beds are in the correct stratigraphic order up to the top of the Boulby Potash which is overlain by a breccia of fragments of beds B.S.4 and 5 set in a matrix of recrystallized sylvinite veins. This breccia is overlain by bed B.H.1. This sequence of strata most probably results from the Boulby Halite being thrust over the Boulby Shale in the manner shown in Figure A2.2.

(7) Boreholes M and M-D2

In borehole M a full sequence of strata is present up to the top of the Boulby Potash. However only beds B.S.4 and 5 of the Boulby Shale are present. The sylvinite of uncertain origin overlying bed B.S.4 is a coarse grained rock composed of red-white sylvite and halite crystals which closely resemble some of the recrystallized sylvinite veins in the South Spearhead. The affinity of the halite of uncertain origin overlying bed B.S.5 is not clear. It is a brown, medium grained (1 cm.) halite rock which makes a gradational, rather than sharp or disrupted contact, with bed B.S.5. This halite rock may, therefore, be an individual bed of the Boulby Shale which has not been observed in the Mine or other boreholes. Alternatively it might be a completely reconstituted bed of coarse grey-brown halite rock (B.H.1) which lacks shale partings.

Borehole M-D2 is a vertical deflection 66.67 metres away from M. Beds B.H.2 and B.S.1-4 are absent from the borehole. The Boulby Potash encloses a few fragments of bed B.S.4 and is overlain by bed B.H.1 containing large fragments of Rotten Marl and fragments of bed B.S.5 at its base.

The absence of various beds from both the boreholes indicates that the rocks have been affected by movement. In borehole M-D2 it is most likely that the Boulby Halite has been thrust over the Boulby Shale, the beds of which have largely been eliminated by movement (see Figure A2.2). If the halite rock of uncertain origin in borehole M is a reconstituted bed of coarse grey-brown halite rock (B.H.1) then the borehole represents a cross-section through an overthrust similar to that of M-D2. If, however, it is a separate bed of the Boulby Shale, then this is a section through rocks which have been subject to movement but not overthrusting.

(8) Borehole U

The sequence of beds in this borehole is the thickest in the C.P.L. concession area. The Boulby Halite and Potash are both repeated twice. Bed B.S.4 forms a discrete unit over the depth range 1129.45 - 1129.88 metres but usually occurs as inclusions in the Boulby Potash.

The repetition of units can be accounted for in terms

of overfolding of the beds as shown in Figure A2.3. It is not possible to tell whether the abnormally large thickness of the lower Boulby Potash bed (15.40 metres) is due to overfolding or possibly subsequent gravitational uplift.

(9) Boreholes V and V-D1

Borehole V-D1 is a vertical deflection 5.33 metres away from V. Borehole V contains almost the ideal theoretical sequence of strata for the C.P.L. concession area; bed B.H.2 at the top of the Boulby Halite being the only major unit missing.

However the interpretation of borehole V-D1 is slightly more complex. Beds B.S.3 and 4 are absent from the sequence although fragments of them occur in the Boulby Potash. This suggests that these rocks have been removed by lateral flowage. The halite rock of uncertain origin overlying the Boulby Potash is colourless to pale brown, granular to gneissose in texture, and contains numerous inclusions of the overlying unit (B.S.5) which has been partially replaced by colourless halite. It seems likely, therefore, that the halite rock of uncertain origin represents bed B.S.5 which has been almost completely replaced by colourless halite and then subject to movement.

The structure in both these boreholes has, therefore, been affected by movement, although different beds have been

removed in each borehole. This demonstrates that the rapid lateral change of rock types observed in the Mine also occurs elsewhere in the C.P.L. concession area. The beds have not been overfolded.

(10) Borehole X

In this borehole all the rocks show signs of movement (i.e. brecciated beds, gneissoze textures, slickensiding). The rocks are in the correct stratigraphic order except that beds B.S.3 and 4 only occur as inclusions in a white gneissoze halite rock (crystals up to 1.5 cm. in length) of uncertain origin. This halite rock bears no resemblance to any of the rocks of the Boulby Halite. On the basis of these observations it seems likely that beds B.S.3 and 4 may have been completely replaced by colourless halite which has subsequently been deformed by movement. This is known to have occurred in borehole S-20. Alternatively it might be a primary halite bed of only limited lateral extent which has not been observed in the Mine or other boreholes. The rocks in this borehole, therefore, do not appear to have been overfolded or overthrust.

(11) Borehole Y

The Boulby Potash is directly overlain by bed B.S.5 in this borehole. The lower beds of the Boulby Shale are absent from the sequence apart from occasional

inclusions of bed B.S.4 in the Boulby Potash. Both the Boulby Potash and the rocks of bed B.S.5 have marked gneissoze textures and are slickensided. These features suggest the lower beds of the Boulby Shale have been eliminated from the sequence by lateral flowage.

(12) Borehole Z

It is not possible to put any interpretation on this borehole as most of the core is missing.

III Discussion and Conclusions

There is abundant evidence that all the rocks examined in the boreholes have been deformed by the lateral migration of beds in the C.P.L. concession area. The successions in 7 of the 15 boreholes examined indicate that the rocks have been overthrust or overfolded. However the thickness of the succession is very variable between boreholes which are interpreted as cross-sections of the same structures. For example, boreholes A and B are interpreted as cross-sections through overfolds, but the succession in B is nearly twice as thick as that in A.

The boreholes interpreted as representing overfolds (A, B, F and U) and overthrusts (C, L, M-D2 and ?M) are evenly distributed throughout the C.P.L. concession area and these structures are, therefore, likely to be continually met as the Mine is developed.

Appendix 3Analytical methods for determining the chemical composition of iron-boracite and parahilgardite

Iron-boracite and parahilgardite are insoluble in water from 25°C to 100°C. They are readily soluble in 0.2N HCl or HNO₃ on gentle heating under reflux (to prevent volatilization of boron).

The mineral for analysis was hand picked from crushed fragments of the appropriate type of nodule, then powdered, and leached in boiling distilled water (20 times) to remove small inclusions of sylvite and halite.

Both minerals were analysed using the same chemical techniques. Na, K, Fe₂O₃, Al, Mn, Sr and Mg were determined by atomic absorption spectroscopy, whilst Ca, H₂O, Br and Cl were determined gravimetrically. FeO and SiO₂ were evaluated colourimetrically. The measurement of B₂O₃ in these minerals was accomplished by a modification (Foote, 1932; Martin and Hayes, 1952) of the NaOH titrimetric technique in the presence of mannitol. Boric acid was separated from interfering cations (especially Fe) prior to titration by ion exchange (Amberlite IRA 120 resin). The analyses are given in Table 5.8.

Appendix 4

Partial chemical analyses of FeO, MnO and MgO, in apparent concentrations, in iron-boracite and ericaite crystals from nodules in bed B.S.3^x

<u>Nodule type and identification</u>	<u>Crystal identification*</u>	<u>Nature of crystal†</u>	<u>Position of the analysis in the crystal⁺</u>	<u>Apparent concentration in wt. %</u>		
				<u>MgO</u>	<u>MnO</u>	<u>FeO</u>
Iron-boracite nodule 4	B1	Er	E	12.80	1.60	14.40
	BA1	"	C	13.28	1.41	13.11
"	B2	I.B.	C	9.09	3.14	17.77
	BA2	"	E	7.69	3.40	19.03
"	B3	I.B.	C	8.79	2.39	19.13
	BA3	"	E	9.60	2.48	17.34
	BB3	"	E	8.42	2.91	18.96
"	B4	Er	E	12.09	1.61	14.69
	BA4	"	C	4.39	3.55	25.22
	BB4	"	C	12.92	1.45	13.52
"	B5	I.B.	E	11.84	1.81	14.28
	BA5	"	C	9.35	2.58	17.97
"	B6	Er	E	13.45	1.47	12.79
	BA6	"	C	13.45	1.41	12.76
"	B7	I.B.	E	7.79	2.61	18.73
	BA7	"	C	10.35	2.80	15.94

Appendix 4 (cont.)

<u>Nodule type and identification</u>	<u>Crystal identification</u>	<u>Nature of crystal</u>	<u>Position of the analysis in the crystal</u>	<u>Apparent concentration in wt. %</u>		
				<u>MgO</u>	<u>MnO</u>	<u>FeO</u>
Iron-boracite nodule 4 (cont.)	B8	Er	E	11.03	1.29	12.32
	BA8	"	C	11.76	1.81	14.97
Iron-boracite nodule 2	B9	Er	See Fig. 5.15	8.61	2.54	19.95
	BA9	"	(A)	10.43	2.62	17.60
	BB9	"	"	12.93	1.55	14.55
	BC9	I.B.	"	13.41	1.56	14.63
	BD9	"	"	4.26	4.42	26.12
	BE9	"	"	3.50	5.26	27.0
	BF9	"	"	4.03	3.96	26.7
	BG9	"	"	7.98	3.19.	21.15
"	B10	I.B.	C	8.24	3.33	20.33
	BA10	"	M	6.80	4.49	21.50
	BB10	"	E	8.49	2.89	20.30
"	B11	I.B.	C	7.54	3.80	20.5
"	B12	Er	See Fig. 5.15	11.79	1.89	16.24
	BA12	"	(B)	11.86	1.91	16.24
	BB12	"	"	11.74	2.04	16.71
	BC12	"	"	12.47	1.76	15.34
	BD12	"	"	12.55	1.87	15.55
	BE12	"	"	12.04	1.70	16.07
	BF12	"	"	12.19	1.77	15.73

Appendix 4 (cont.)

<u>Nodule type and identification</u>	<u>Crystal identification</u>	<u>Nature of crystal</u>	<u>Position of the analysis in the crystal</u>	<u>Apparent concentration in wt. %</u>		
				<u>MgO</u>	<u>MnO</u>	<u>FeO</u>
Iron-boracite nodule 2 (cont.)	B13	I.B.	C	2.72	6.13	27.8
	BA13	"	M	2.24	7.30	27.6
	BB13	"	E	3.18	5.86	27.0
"	B14	I.B.	C	2.24	7.30	27.6
	BA14	"	M	3.18	5.86	27.0
	BB14	"	E	10.50	2.91	17.3
Iron-boracite nodule 1	B15	I.B.	C	3.95	3.99	27.30
	BA15	"	M	4.00	3.74	27.40
	BB15	"	E	5.50	3.65	24.92
"	B16	Er	C	7.94	3.68	21.0
	BA16	"	M	7.20	4.33	19.89
	BB16	"	E	2.70	5.95	27.94
	BC16	"	M	9.50	2.87	19.28
	BD16	"	E	10.43	3.19	17.25
"	B17	Er	C	9.10	3.00	19.58
	BA17	"	M	11.04	2.57	16.90
	BB17	"	E	5.46	3.52	25.5
	BC17	"	M	5.09	5.16	24.38
	BD17	"	E	9.20	3.23	19.12

Appendix 4 (cont.)

<u>Nodule type and identification</u>	<u>Crystal identification</u>	<u>Nature of crystal</u>	<u>Position of the analysis in the crystal</u>	<u>Apparent concentration in wt. %</u>		
				<u>MgO</u>	<u>MnO</u>	<u>FeO</u>
Iron-boracite nodule 1 (cont.)	B18	Er	See Fig. 5.14	3.90	4.49	26.95
	BA18	"	(E) and (F)	3.48	4.87	27.75
	BB18	"	"	3.43	5.13	27.35
	BC18	"	"	6.38	3.60	23.52
	BD18	"	"	11.51	2.26	16.8
	BE18	"	"	8.49	3.18	20.6
	BF18	"	"	10.81	2.45	17.44
	BG18	"	"	4.97	3.32	25.6
	BH18	"	"	10.79	2.20	17.91
	BI18	"	"	11.71	2.03	16.98
	BJ18	"	"	4.16	4.74	26.3
	BK18	"	"	3.98	4.80	26.53
	BL18	"	"	2.01	0.50	5.57
	BM18	"	"	9.42	2.34	16.63
	BN18	"	"	10.01	2.48	19.2
	B19	Er	C	13.94	1.54	13.66
	BA19	"	M	12.63	1.70	15.18
	BB19	"	E	11.13	2.09	17.30
Individual crystals from the S-20 borehole	B22	I.B.	C	1.51	8.11	25.94
	BA22	"	M	1.18	6.33	20.08
	BB22	"	E	0.96	11.16	24.7
"	B23	I.B.	C	1.13	8.70	26.48
	BA23	"	M	0.91	9.09	26.4
	BB23	"	E	1.64	7.84	24.6

Appendix 4 (cont.)

<u>Nodule type and identification</u>	<u>Crystal identification</u>	<u>Nature of crystal</u>	<u>Position of the analysis in the crystal</u>	<u>Apparent concentration in wt. %</u>		
				<u>MgO</u>	<u>MnO</u>	<u>FeO</u>
Individual crystals from the S-20 borehole	B25	I.B.	C	1.43	7.88	26.22
	BA25	"	M	1.44	8.01	26.50
	BB25	"	E	1.34	9.14	25.06
"	B26	I.B.	C	1.46	7.54	26.51
	BA26	"	M	1.54	8.03	26.14
	BB26	"	E	1.34	8.91	24.2
Parahilgardite nodule 1	B27	Er	C	9.98	1.20	17.9
	BA27	"	M	10.06	0.75	18.74
	BB27	"	E	12.10	0.41	16.21
"	B28	I.B.	C	9.42	0.93	18.90
	BA28	"	M	11.34	0.52	17.14
	BB28	"	E	12.29	0.36	15.67
	BC28	"	C	7.93	2.04	20.0
	BD28	"	M	8.22	1.06	21.00
	BE28	"	E	10.26	0.62	18.67
"	B29	Er	C	8.62	0.89	19.98
	BA29	"	M	9.80	1.06	18.38
	BB29	"	E	10.31	0.62	17.79
"	B31	Er	E	9.20	1.21	18.81
	BA31	"	M	11.11	1.03	16.63
	BB31	"	C	11.79	0.35	16.47

Appendix 4 (cont.)

<u>Nodule type and identification</u>	<u>Crystal identification</u>	<u>Nature of crystal</u>	<u>Position of the analysis in the crystal</u>	<u>Apparent concentration in wt. %</u>		
				<u>MgO</u>	<u>MnO</u>	<u>FeO</u>
Parahilgardite nodule 1 (cont.)	B32	Er	C	10.61	0.49	17.75
	BA32	"	E	11.36	0.34	16.51
"	B33	Er	C	9.24	0.88	19.04
	BA33	"	M	9.53	1.07	18.77
	BB33	"	E	11.84	0.34	16.21

* B1, BA1, BB1 indicate individual analysis points within the crystal.

† Er = ericaite; I.B. = iron-boracite; some of the crystals contain ericaite and iron-boracite within the same crystal outline.

+ C = analysis point in the centre of the crystal; M = analysis point between the centre and the edge of the crystal; E = analysis point at the edge of the crystal. Where an individual crystal has been analysed many times the positions of the analyses in the crystal are shown in insets in Figures.

x The analyses were performed using the electron microscope.

Appendix 5Aspects of the hilgardite group of minerals
and their nomenclatureI Introduction

Hurlbut and Taylor (1937) first discovered hilgardite (of general formula $(\text{Ca}_2 [\text{B}_5\text{O}_8(\text{OH})_2] \text{Cl})$ in water insoluble residues of rock salt from a brine well in Choctaw salt dome, Louisiana. Hurlbut (1938) then described parahilgardite, whose general formula is that of hilgardite, from the same locality. Yarzhemsky (1945) reported the occurrence of hilgardite in the Inder borate deposit of Russia, but no chemical or physical data was included. Braitsch (1959) documented a mineral which he called 1 Tc-strontiohilgardite, of formula $(\text{Ca}_{1.08}\text{Sr}_{0.92}) [\text{B}_5\text{O}_8(\text{OH})_2] \text{Cl}$, from insoluble residues in a sylvite-halite-anhydrite rock from Königshall-Hindenberg Mine, near Reyerhausen, north Germany. For convenience of reference in this appendix the mineral found by Braitsch will be called strontiohilgardite. The lattice parameters and chemical composition of the hilgardite minerals described by Hurlbut and Taylor (1937) and Hurlbut (1938) were re-determined by Braitsch (1959) who also compared and revised many of the properties of the hilgardite minerals (Tables A5.1, A5.2, A5.3).

Table A5.1Chemical Analyses of Hilgardite Minerals (Wt%)

	1	2	3	4	5
B ₂ O ₃	51.83	40-45	50.22	50.26	52.49
CaO	33.15	15.-20	35.14	35.13	33.82
SrO	0.82	20-25	1.3	1.6	-
Cl	10.66	8.2	10.59	10.82	10.68
H ₂ O	5.50	5.3	6.44	6.23	5.43
Al ₂ O ₃	0.03	0.2	0.5	0.2	-
MgO	0.10	0.1	0.25	0.1	-
MnO	0.01	-	-	-	-
Fe ₂ O ₃	0.02	-	-	-	-
Na ₂ O	0.03	-	-	-	-
K ₂ O	0.02	-	-	-	-
SiO ₂	0.03	-	-	-	-
Total	102.20	90-105	102.39	102.44	102.42
O = Cl	2.41		2.39	2.44	2.42
	99.79		100.00	100.00	100.00

1. Parahilgardite from Boulby (this thesis)
2. Strontiohilgardite from Reyerhausen (Braitsch (1959))
3. Hilgardite from Choctaw salt dome (Hurlbut and Taylor (1937))
4. Parahilgardite from Choctaw salt dome (Hurlbut (1938))
5. Theoretical analysis for $\text{Ca}_2 [\text{B}_5\text{O}_8(\text{OH})_2] \text{Cl}$

Table A5.2 Lattice Parameters of the Hilgardite Minerals

	1	2	3	4	5	6	7	8
<u>Unit Cell Parameters</u>								
a	6.38Å	6.273Å	6.297Å	6.297Å	6.31Å	6.20Å	6.31Å	6.41Å
b	6.480Å	6.491Å	6.464Å	11.335Å	11.33Å	22.28Å	6.484Å	6.44Å
c	6.608Å	6.570Å	6.565Å	11.541Å	11.44Å	11.24Å	17.50Å	6.45Å
α	74.4°	73.50°	74.14°	93.33°	90.00°	91.20°	84.00°	73.50°
β	61.2°	64.67°	61.58°	89.78°	90.00°	90.00°	79.60°	61.76°
γ	60.5°	60.66°	61.26°	90.43°	90.00°	90.00°	60.90°	60.25°
<u>Principal d spacings</u>								
d100	5.01Å	5.012Å	5.035Å	-*	6.31Å	-*	5.45Å	-*
d010	5.64Å	5.672Å	5.652Å	-*	11.33Å	-*	5.66Å	-*
d001	5.78Å	5.756Å	5.756Å	-*	11.44Å	-*	17.21Å	-*
<u>Miscellaneous</u>								
Space Group	PI	PI	PI	⋈	Cc	PI	PI	PI
Unit Cell Vol.	208Å ³	203.58Å ³	205.73Å ³	822.34Å ³	817Å ³	1568.10Å ³	615Å ³	202.32Å ³
No. of molecules in the unit cell	1	1	1	4	4	8	3	1

1. Strontiohilgardite, Braitsch (1959)
 2. Boulby parahilgardite (this thesis)
 3. Boulby parahilgardite, Von Hodenberg and Kühn (1977)
 4. The second hilgardite mineral of Von Hodenberg and Kühn (1977)
 5. Hilgardite from Choctaw Salt Dome, Braitsch (1959)
 6. Parahilgardite from Choctaw Salt Dome, Hurlbut (1938)
 7. Parahilgardite from Choctaw Salt Dome, Braitsch (1959)
 8. Tyretskite, Kondrat'eva (1964)
- * Not given ⋈ Not given, but either PI or PT

Table A5.3

Comparison of the Optical Orientations and Optical Properties of the Hilgardite Group of

Minerals

Strontio-1
hilgardite Hilgardite² Parahilgardite³
from Choctaw Parahilgardite⁴
from Boulby

Optical
Orientations

n_α	ϕ	ϵ	ϕ	ϵ	ϕ	ϵ
	-146°	14°	90°	90°	156°	84°
n_β	-6°	79°	0°	90°	66°	89°
n_γ	86°	81°	0°	0°	0°	5°

Optical
Properties

n_α	1.638	1.630	1.630	1.630
n_β	1.639	1.636	1.636	1.636
n_γ	1.670	1.664	1.664	1.664
$2V_\gamma$	19°	35°	35°	34.8° & 37.2°

Inclination
of the axial
plane to (010)

12°	0°	20°	61°
-----	----	-----	-----

1. Braitsch (1959)
2. Hurlbut and Taylor (1937)
3. Hurlbut (1938)
4. This thesis

The purpose of this appendix is to compare the Boulby parahilgardite with the other hilgardite minerals and reassess certain of Braitsch's hypotheses and conclusions in the light of the data presented in this thesis. A new nomenclature for the hilgardite group of minerals is also proposed.

II Polymorphic relations in the hilgardite group of minerals

The structures of the hilgardite group of minerals have not yet been determined. There is, however, a dimensional relationship between the $d_{100,010,001}$ spacings (Table A5.2) from which Braitsch (1959) concluded that there was a simple geometric interpretation relating the polymorphs. The hilgardite polymorphs could be derived by stacking left and right handed elementary cells, which are mirror images of one another, in different sequences; see Figure A5.1.

The 'a' lattice parameters for parahilgardite in v. Hodenberg and Kühn (1977) and this thesis are in agreement with the other hilgardite minerals (Table A5.2) and on the basis of this similarity they are compatible with the Braitsch model for polymorphism. Further, the lattice parameters of one of the Boulby parahilgardites (Table A5.2; columns 2 and 3) are similar to those of strontiohilgardite (column 1) and thus the parahilgardite

might be expected to form left and right handed crystals as is the case of strontiohilgardite (Figure A5.1). Column 4 of Table A5.2 shows the second set of lattice parameters for the Boulby parahilgardite (v. Hodenberg and Kühn, 1977) and these are similar to those of hilgardite (Table A5.2, column 5). As may be seen in Figure A5.1, this polymorph would not be expected to show polymorphism.

III The Choctaw parahilgardite

Hurlbut (1938) and Braitsch (1959) obtained different sets of lattice parameters for the parahilgardite from the Choctaw salt dome (Table A5.2; columns 6 and 7). Braitsch, however, was unable to reproduce the cell dimensions of Hurlbut and concluded they were incorrect. The work of v. Hodenberg and Kühn (1977) has shown that two different polymorphs of the hilgardite group of minerals exist together in the same nodule from the Boulby Mine. There is, therefore, a strong possibility that both the sets of lattice parameters for the Choctaw parahilgardite are correct and that the differences arose because two different polymorphs were analysed.

IV The SrO content and lattice parameters in the hilgardite group of minerals

Braitsch (1959) observed that the cell dimensions and SrO content of hilgardite (1.3% SrO) and parahilgardite (1.6% SrO) from Choctaw were markedly different from those of strontiohilgardite (20 - 25% SrO) from Reyerhausen. On the basis of this evidence Braitsch concluded that the lattice parameters of the hilgardite minerals depended upon the SrO content.

The chemical composition of the Boulby parahilgardite is presented in column 1 of Table A5.1. The mineral has a low SrO content but has lattice parameters similar to hilgardite and strontiohilgardite (see Table A5.2). In addition, if the lattice parameters of Choctaw parahilgardite determined by Hurlbut (1938) are correct, then this mineral also has two different sets of cell dimensions for the same chemical composition. These observations indicate, therefore, that it is unlikely that there is a relationship between the strontium content and lattice parameters in the hilgardite group of minerals as concluded by Braitsch (1959).

V The relationship between tyretskite and the hilgardite group of minerals

This particular relationship is considered because v. Hodenberg and Kühn (1977) called the Boulby parahilgardite chlorine-tyretskite because of its approximate similarity in unit cell dimensions and chemistry to strontiohilgardite and tyretskite which Davies and Machin (1968) regard as isotype minerals. There is, however, doubt as to whether strontiohilgardite and tyretskite are in fact isotype minerals. Ivanov and Yarzhemskii (1954) described tyretskite from the Leno-Angar basin (U.S.S.R.) but, according to Davies and Machin (1968) presented the incorrect formula of, $(\text{Ca}, \text{Sr})_2 \text{B}_8 \text{O}_{13} (\text{OH}, \text{Cl})_4$. OH, for this mineral. From a chemical analysis, on the other hand, Kondrat'eva (1964) calculated the formula of tyretskite as $\text{Ca}_3 \text{B}_8 \text{O}_{13} (\text{OH})$. Furthermore, Davies and Machin (1968) gave the chemical formula of tyretskite as $\text{Ca}_2 \left[\text{B}_5 \text{O}_8 (\text{OH})_2 \right] \text{OH}$, and because of the close similarity in unit cell parameters (Table A5.2) and chemical formulae suggested it was an isotype mineral of strontiohilgardite $((\text{Ca}, \text{Sr})_2 \left[\text{B}_5 \text{O}_8 (\text{OH})_2 \right] \text{Cl})$.

For several reasons it is doubtful if these minerals should be regarded as isotypes. The chemical analysis of tyretskite presented by Davies and Machin (1968) was modified after that of Ivanov and Yarzhemskii (1954). In the modification Davies and Machin subtracted the

impurities halite, anhydrite, calcite and dolomite from the bulk chemical analysis of a composite rock sample to derive the mineral analysis. Anhydrite, calcite and dolomite were all impurities which might have contained SrO, but none was deducted for these minerals. The deduction of impurities in this way may well increase the overall SrO content of the mineral analysis.

The calculated specific gravity of tyretskite (2.571 g/cm^3), given by Davies and Machin, differed markedly from their experimental density determination (2.189 g/cm^3) and their explanation of this discrepancy was that they might have made an error in the measurement of the experimental density. If the experimental density of Davies and Machin is correct then the cell volume and molecular weight are the same as that required for the mineral kurgantaite, of chemical formula, $(\text{Ca},\text{Sr})_2\text{B}_4\text{O}_7(\text{OH})_2$, and not tyretskite. The calculated density would give a tyretskite mineral of composition $(\text{Ca},\text{Sr})_2[\text{B}_5\text{O}_8(\text{OH})_2]\text{OH}$. The X ray spectra for tyretskite based on Kondrat'eva (1964), however, show a greater similarity to strontiohilgardite than to kurgantaite.

On the basis of the gross uncertainties of Davies and Machin's data there seems little conclusive evidence that tyretskite and strontiohilgardite are isotype minerals. It seems unreasonable, therefore, to make comparisons between the Boulby parahilgardite and tyretskite.

VI A modified nomenclature for the hilgardite group
of minerals

Hurlbut and Taylor (1937), Hurlbut (1938), and Braitsch (1959) have all proposed classifications for naming the hilgardite minerals. Braitsch (1959) has devised the most detailed classification for naming the hilgardite polymorphs based on a statement of the number of component cells piled one upon another in the [001] stacking direction, the symmetry of the lattice, and the principal cations present. These various relationships are shown in Table A5.4 together with the modified nomenclature proposed in this thesis and discussed below.

The nomenclature of Braitsch (1959) did not differentiate between either the varieties of triclinic lattice known at that time or the variable optical properties of these minerals (Table A5.3). Until such time as the structures of these minerals have been determined, a preferable nomenclature would be one which differentiates only between the symmetry and principal cations of the hilgardite minerals.

The new nomenclature, shown in Table A5.4, has been modified from that proposed by Hurlbut and Taylor (1937) and Hurlbut (1938). Hilgardite would refer to calcium rich monoclinic members and parahilgardite to calcium rich triclinic members of the hilgardite group. If the minerals are enriched in additional divalent cations,

Table A5.4

A Comparison of the Braitsch Nomenclature and the New Modified Nomenclature for Naming the
Hilgardite Minerals

Braitsch Nomenclature						Modified Nomenclature
No. of left & right handed component cells parallel to Co	No. of units	No. of formula	Principal			Name following new, modified nomenclature
			Symmetry	Space Group	Cation	
						Name
1	1	1	Triclinic	Pl	Ca	1Tc-calciumhilgardite
1	1	1	Triclinic	Pl	Ca,Sr	1Tc-strontiohilgardite
2	4	4	Monoclinic	Cc	Ca	2M(Cc)-calciumhilgardite
2	4	4	Triclinic	nd*	Ca	2Tc-calciumhilgardite
3	3	3	Triclinic	Pl	Ca	3Tc-calciumhilgardite
						Parahilgardite
						Sr-parahilgardite
						Hilgardite
						Parahilgardite
						Parahilgardite

* nd = no data

such that $y \geq 0.5$ in the general formula $(\text{Ca}_x \text{M}_y) \text{B}_5 \text{O}_8 (\text{OH})_2 \text{Cl}$ where M is any cation other than calcium, and $x + y = 2$, then these cations should be prefixed at the beginning of the mineral name. For example 1Tc-strontiohilgardite (Braitsch, 1959) becomes Sr-parahilgardite and 1Tc-calcium hilgardite becomes parahilgardite.

Appendix 6Permutations of stratigraphic data to estimate the depth
of burial of the beds of the sequence examinedRelevant bed thicknesses

The thickness of the beds from the base of the Rotten Marl to the Rhaetic in the S-20 borehole (Woods, 1973) = 793 metres.

The thickness of the Lower and Middle Liassic beds in the S-20 borehole (Woods, 1973) = 365 metres.

The thickness of beds from the Upper Liassic to the Kimmeridge clays in the Fordon borehole (Falcon and Kent, 1960) = 602 metres.

The thickness of the Jurassic rocks in the Jurassic type wells in the North Sea (Rhys, 1974) = 768 metres.

The thickness of the Lower Cretaceous beds in the Fordon borehole (Falcon and Kent, 1960) = 179 metres.

The thickness of Lower Cretaceous beds in the Cretaceous type wells (Rhys, 1974) = 253 metres.

The thickness of the Upper Cretaceous in the Cretaceous type wells (Rhys, 1974) = 730 metres.

Average thickness of the Upper Cretaceous in the North Sea (Hancock and Scholle, 1974) = 500 metres.

Permutations

1.	Rotten Marl to Rhaetic (S-20 borehole)	=	793 metres
	Jurassic (S-20 + Fordon boreholes)	=	967 "
	Cretaceous (type section)	=	983 "
			<hr/>
	TOTAL THICKNESS	=	2743 metres
2.	Rotten Marl to Rhaetic (S-20 borehole)	=	793 metres
	Jurassic (type section)	=	768 "
	Cretaceous (type section)	=	983 "
			<hr/>
	TOTAL THICKNESS	=	2544 metres
3.	Rotten Marl to Rhaetic (S-20 borehole)	=	793 metres
	Jurassic (S-20 + Fordon boreholes)	=	967 "
	Lower Cretaceous (type section)	=	253 "
	Average thickness of Upper Cretaceous	=	500 "
			<hr/>
	TOTAL THICKNESS	=	2513 metres
4.	Rotten Marl to Rhaetic (S-20 borehole)	=	793 metres
	Jurassic (type section)	=	768 "
	Lower Cretaceous (type section)	=	253 "
	Average thickness of Upper Cretaceous	=	500 "
			<hr/>
	TOTAL THICKNESS	=	2314 metres

5.	Rotten Marl to Rhaetic (S-20 borehole)	=	793 metres
	Jurassic (S-20 + Fordon boreholes)	=	967 "
	Lower Cretaceous (Fordon borehole)	=	179 "
	Average thickness of Upper Cretaceous	=	<u>500 "</u>
	TOTAL THICKNESS	=	2439 metres
6.	Rotten Marl to Rhaetic (S-20 borehole)	=	793 metres
	Jurassic (type section)	=	768 "
	Lower Cretaceous (Fordon borehole)	=	179 "
	Average thickness of Upper Cretaceous	=	<u>500 "</u>
	TOTAL THICKNESS	=	2240 metres
7.	Rotten Marl to Rhaetic (S-20 borehole)	=	793 metres
	Jurassic (S-20 + Fordon boreholes)	=	967 "
	Lower Cretaceous (Fordon borehole)	=	179 "
	Upper Cretaceous (type section)	=	<u>730 "</u>
	TOTAL THICKNESS	=	2669 metres
8.	Rotten Marl to Rhaetic (S-20 borehole)	=	793 metres
	Jurassic (type section)	=	768 "
	Lower Cretaceous (Fordon borehole)	=	179 "
	Upper Cretaceous (type section)	=	<u>730 "</u>
	TOTAL THICKNESS	=	2470 metres

Range in maximum depth of burial of the sequence examined
= 2240 - 2743 metres.

Average maximum depth of burial of the sequence examined
= 2492 metres.

Appendix 7Design of pressure vessel used to study the system NaCl-H₂O

The requirements of the vessel to study saturated salt solutions at high pressures were:-

(i) It should easily cover the pressure and temperature range of interest; in this case set at limits of 2.5 kilobars and 200°C.

(ii) It should be possible to separate crystals and liquid without changing the composition of either and in sufficient quantities to obtain precise chemical analyses of both.

(iii) It should be possible to stir or agitate the material to promote rapid achievement of equilibrium.

(iv) It should be reliable, economical and safe.

These requirements are largely met by the apparatus shown in Figures 12.5 and 12.6.

The basic equation (from the High Pressure Safety Code, 1975) used in the design of a pressure vessel is:-

$$P = \frac{\sigma_y}{2} \frac{(K^2 - 1)}{K^2}$$

where P = maximum working pressure; K = radius ratio (3); and σ_y = tensile yield strength (5.486 kilobars for stainless steel).

Therefore the maximum working pressure of the vessel used in these experiments was 2.438 kilobars.

The load on the end nuts at maximum working pressure was 2.59 k.bars/cm² but the end brackets could withstand loads of up to 27.47 k.bars/cm²; giving a safety factor of 10.5 for the vessel.

The pressure vessel showed no signs (i.e. development of cracks etc.) of fatigue or stress whilst in use. Corrosion occurred on a very small scale when the vessel was first used (see Appendix 8) but was not a problem after the initial experiments.

The end nuts proved effective in sealing the solution chamber of the pressure vessel. Chemical analyses showed that when pressure was applied oil from behind the teflon plunger did not leak into the salt solution and vice versa.

The solutions inside the pressure vessel were agitated by placing the pressure vessel on an oscillating rack (Figure 12.6) for the duration of each experiment.

Appendix 8Calibration and Assessment of the Performance of the
Pressure Vessel

After the pressure vessel was built it was necessary to conduct a number of experiments to calibrate and assess its performance. These were as follows:-

- (a) Determination of how constant the temperature is within the pressure vessel over long periods of time.
- (b) Comparison of the thermocouple temperature within the pressure vessel with that of a thermometer in the waterbath.
- (c) Measurement of the rate of extraction of a liquid from the pressure vessel.
- (d) Determination of the iron, nickel, manganese, and chromium content of the extracted solutions.
- (e) Determination of the time required for a solution to come to equilibrium.

These will be considered in turn.

- (a) In any pressure vessel it is necessary to check that the temperature is constant over a given period of time. To do this a thermocouple unit was inserted in place of the usual filter at one end of the pressure vessel. The thermocouple was attached to a continuous chart recorder which monitored the temperature. Table A8.1 gives typical observed temperatures and shows that the

Table A8.1

Typical temperature-time readings in the pressure vessel

<u>Time</u>	<u>Conditions</u>	<u>Thermocouple temp. in °C</u>
0950	Atmospheric pressure	39.7
1025	" "	39.8
1040	" "	39.7
1100	" "	39.7
1107	0.5 kilobars pressure	39.9
1125	" " "	39.7
1135	" " "	39.7
1140	1.0 kilobars pressure	40.0
1150	" " "	39.7
1200	" " "	39.7
1230	" " " & rocking	39.7
1236	" " " "	39.7

Table A8.2Comparison of pressure vessel and waterbath temperatures

<u>Time</u>	<u>Conditions</u>	<u>Pressure vessel temp. (°C) measured by thermocouple</u>	<u>Waterbath temp. (°C) measured by thermometer</u>
1135	Atmospheric Pressure	29.0	29.0
1145	" "	28.9	28.9
1204	" "	28.9	29.0
1330	" "	28.9	29.0
1705	" "	47.8	47.5
1715	" "	47.9	47.7
1805	" "	47.9	47.7
1830	" "	48.0	47.7
2015	" "	47.9	47.9
1355	" "	84.2	84.0
1650	" "	83.6	84.0
1700	" "	83.7	83.9

Table A8.3Rate of extraction values for the pressure vessel

<u>Vol. of liquid extracted</u>	<u>Length of time for extraction</u>	<u>Pressure vessel temp. (°C)</u>	<u>Pressure vessel pressure (in psi)</u>	<u>Rate of extraction (ml/s)</u>	<u>Time required to extract 10 mls.</u>
8 mls	80s	47.6°C	atmos. pres.	0.1 mls/s	10s
10.5 mls	39s	47.8°C	12,000 psi	0.26 ml/s	38.4s
10.5 mls	36s	53.5°C	25,500 psi	0.29 ml/s	34.4s

Table A8.4

The Fe, Mn, Ni and Cr content of solutions extracted from
the pressure vessel

<u>Experiment No.</u>	<u>Fe content</u>	<u>Ni content</u>	<u>Mn content</u>	<u>Cr content</u>
2	0.1 ppm	0.0	0.0	0.0
4	0.0	0.0	0.0	0.0
5	0.0	0.0	0.0	0.0

Table A8.5Fe values for 6 aliquots taken in Experiment 12

Aliquot	12,1	12,2	12,3	12,4	12,5	12,6	Standard 4 ppm Fe
AA Reading	2	4	3	2	0	10	272
ppm Fe	0.029	0.059	0.044	0.029	0.000	0.147	4.000

Average Fe content of the aliquots = 0.06 ppm

temperature remained constant over long periods of time and under different conditions. The continuous chart recorder showed no variation in temperature over days.

(b) Under normal running conditions the temperature of the solution within the pressure vessel was determined by an accurate thermometer in the waterbath. However it was only possible to do this having first checked that the temperature of the solution in the pressure vessel was the same as the waterbath. This was done by recording the thermocouple and thermometer temperatures simultaneously over a given period of time. Table A8.2 shows that up to 50°C the temperature agreed to within 0.2°C and those above 50°C agreed to within 0.4°C . Hence it was valid to say the waterbath temperature was almost exactly that of the pressure vessel.

(c) The rate of extraction of a solution from the pressure vessel was determined by noting the time it took to extract a known volume of liquid. Table A8.3 shows that the time required to extract 10 mls. of solution is less than seconds and the higher the pressure in the pressure vessel the more rapid the rate of extraction.

(d) Salt solutions in the initial experiments were found to be brown on extraction because of iron contamination. This coloration disappeared after the first five experiments. However the solutions were occasionally checked for iron, manganese, chromium and nickel contamination and the results are shown in Table A8.4.

In one of the experiments six aliquots of the same solution were analysed for iron (Table A8.5). From these tables it can be seen that the iron, manganese, chromium and nickel content of the solutions was below the limit of detection. It was concluded that in the initial experiments all the available surface iron migrated from the inner walls of the pressure vessel into solutions because of oxidation of the metal or structural defects. The pressure vessel became usable after five runs.

(e) In any experiment it is important to determine the time the solution takes to come to equilibrium.

Therefore it was decided to study the system $\text{NaCl-H}_2\text{O}$ at atmospheric pressure to establish the time it took for crystals to come to equilibrium with a solution of constant composition. Solutions of water containing different weight percents NaCl were placed in the pressure vessel at 25°C and left to see if they precipitated halite. It was found that halite formed in solutions containing more than 26.42 weight percent NaCl. It was then necessary to determine how long it took the solution to stabilize at this weight percent NaCl, i.e. the equilibration time. Figure 12.7 shows it took 10 to 15 hours for the solution to attain constant composition. All subsequent experiments were run for 24 hours to ensure equilibrium.

Appendix 9Determination of the Relative Standard Deviation of
an Analysis

Precision is a measure of the reproducibility of an analysis (Kolthoff, Sandell, Meehan and Bruckenstein, 1969). To place confidence in one's analyses they must be of high precision. The standard deviation (S.D.) and the relative standard deviation (R.S.D. or coefficient of variation) are measures of precision. The smaller the S.D. or R.S.D. the greater the precision of the analysis.

$$\text{S.D.} = \left(\frac{(X - \bar{X})^2}{N-1} \right)^{\frac{1}{2}}$$

where X = average analysis value

\bar{X} = the specific analysis value

N = number of aliquots analysed

$$\text{R.S.D.} = \frac{\text{S.D.} \times 100}{(X)}$$

The following worked example indicates how to calculate the S.D. and R.S.D.

Four aliquots of a sample were analysed and found to contain 26.31, 26.45, 26.36, and 26.48 weight percent NaCl giving a mean of 26.42 weight percent NaCl.

<u>Aliquot Number</u>	<u>$(X - \bar{X})$</u>	<u>$(X - \bar{X})^2$</u>
1	0.11	0.0121
2	0.03	0.0009
3	0.06	0.0036
4	0.06	0.0036
		<hr/>
		0.0202

$$S.D. = \left(\frac{(X - \bar{X})^2}{N-1} \right)^{\frac{1}{2}} = \left(\frac{0.0202}{3} \right)^{\frac{1}{2}} = 0.08$$

$$R.S.D. = \frac{S.D. \times 100}{(X)} = \frac{8}{26.42} = 0.30$$

Appendix 10

Publication

Kühn (R.) and Schaacke (I.), 1955. *Kali u. Steinsalz*, 11, 1-10.

Stewart (F. H.), 1951. *Mineral. Mag.* 27, 445-75.

[Manuscript received 13 August 1976; revised 8 December 1976]

© Copyright the Mineralogical Society.

MINERALOGICAL MAGAZINE, SEPTEMBER 1977, VOL. 41, PP. 406-8

An occurrence of brucite at Merehead Quarry, Cranmore, Somerset

THIS note offers the first record of an occurrence of brucite in the Mendip Hills. The locality is in Merehead Quarry (grid ref. O.S. 1" map ST 698443), which is situated on the south flank of the Beacon Hill Pericline. The rocks quarried are well-bedded limestones that are referred to the Lower Carboniferous Clifton Down Limestone. A notable feature of this locality is the occurrence of a varied assemblage of rare lead and copper minerals. These have recently been described by Alabaster (1975: see references there to the no. 2 vein, at which brucite has now been discovered). The rare minerals are found within the pods of manganese oxide that occur, together with iron oxides, as replacement deposits set in faults and Trias-filled fissures developed in the Carboniferous Limestone. Doultong Stone (mid Jurassic: Upper Inferior Oolite) rests unconformably on the Carboniferous Limestone at Merehead and can be seen to truncate the mineralized fissures. The fissures occasionally contain inserted sedimentary materials ranging in age from Rhaetic to Upper Inferior Oolite.

The pods of manganese oxide contain numerous small cavities, the ore from no. 2 vein being especially cavernous. The secondary minerals occur either as simple cavity fillings or else are contained in calcite nodules, which have themselves grown in, and may in some instances have enlarged, the original cavities. The brucite has been found occupying a small central cavity in two of these calcite nodules.

Brucite occurs in each of these two cases as a compact mass of transparent, prismatic-acicular crystals, arranged in radiating groups that are intergrown with one another. The crystals are elongate || [0001] and grow out from the cavity walls. In both specimens there is some degree of alteration to white hydromagnesite and pseudomorphs after brucite are seen. A thin (up to 0.5 mm) discontinuous light-brown rim occurs at the brucite/calcite interface. This light-brown material is translucent, has a vitreous-resinous lustre, and is appreciably harder than the brucite, which it invariably pseudomorphs. XRD analysis shows it to consist of a mixture of brucite and crystalline hydromagnesite. Both the brucite and the white hydromagnesite are seen to grade into this material.

In one specimen (now in two parts deposited in the Geology Museum, University of Bristol, numbered B3624 and B3625: see the former in fig. 1) brucite is associated with massive orange blixite, which shows partial alteration to hydrocerussite. Contacts between brucite and blixite are sharp. The gently undulating contact is uninfluenced by both cleavages and crystallographic orientation of the brucite crystal groups. There is no evidence to suggest that brucite is intergrown with the blixite/hydrocerussite. It seems to be the case that brucite formed before blixite in this nodule.

The two brucites are of different colours, brownish green in the nodule that has blixite and pale green in the other. Refractive indices (determined using white light) too are different in

Iron-boracite from the English Zechstein

IRON-BORACITE, $(\text{Fe, Mg, Mn})_3\text{B}_7\text{O}_{13}\text{Cl}$, has been found in nodules in an anhydritic shale that overlies the sylvinite (sylvine-halite rock) of the third Zechstein Evaporite Cycle at the Boulby Mine, Loftus, Saltburn, Cleveland. This is the first record of the mineral in this country. The succession in the type roadway is:

Anhydritic shale with the iron-boracite nodule bed near its base; the Shale and Nodule Beds are cross-cut by red sylvine-halite veins from the sylvinite below: 2 m.

Pink-grey sylvinite with red and pink sub-horizontal colour bands; 2 m.

Coarse-grained red and white halite with streaked-out fragments of anhydrite at its top; 3 m.

Iron-boracite is an orthorhombic variety of boracite ($\text{Mg}_3\text{B}_7\text{O}_{13}\text{Cl}$) in which divalent iron is the predominant cation (Dr. R. Kühn, personal communication). The iron-boracites from Boulby contain minor Mn in the cation sites. Boracite has been recorded in the U.K. in insoluble residues from the E2 boring, near Aislaby, Yorkshire, by Guppy (1944) and Stewart (1951).

Above 265 °C, boracite is cubic but below this temperature it is orthorhombic due to differences in the positions of the magnesium and chlorine atoms. This inversion results in the crystals becoming twinned by a rotation of 120° about [111]. The inversion temperatures of ferroan boracites are higher than 265 °C and rise with increasing iron and manganese content (Heide, Walker, and Urlau, 1961). Heide, however, in a personal communication to Braitsch (1962, p. 167), said that he had synthesized pseudocubic boracite crystals well below 265 °C. The rocks of the English Zechstein almost certainly were never heated to 265 °C.

The iron-boracite nodules are ellipsoidal in shape with major axes varying in length from 1 to 15 cm and minor axes being approximately half the major ones. The nodules are frequently tightly packed within the Nodule bed.

Individual grains and clusters of iron-boracite are found in the nodules together with sylvine, halite, magnesite, talc, and hematite. Some nodules are composed entirely of iron-boracite whilst in others sylvine and magnesite predominate.

Iron-boracite crystals in the nodules are either large euhedral blue-green pseudocubic crystals (up to 3 mm edges) with well-developed faces of the form {100} and subsidiary faces of the form {111}, or anhedral brown-purple grains up to 0.5 mm in width.

Both types of iron-boracite crystals are turbid although occasional pseudocubic crystals show remnant sector twinning characteristic of the boracite group of minerals. Large pseudocubic crystals are seen to have broken down and recrystallized to form the small anhedral grains. When the iron-boracite occurs in clusters the large euhedral crystals tend to be found around the rim whilst the anhedral grains occur in the centre. It has been difficult to determine the exact optical properties of the crystals owing to their turbid nature. The maximum refractive index is 1.727 and $2 V_y = 80-90^\circ$.

The substitution of iron and manganese into the magnesium site of boracite results in an expansion of the unit-cell parameters (Kühn and Schaacke, 1955). Many crystals from different nodules were X-rayed and shown to have unit cell parameters in the range of iron-boracite (Table I). The small anhedral grains have larger unit-cell parameters and greater MnO and

FeO contents compared with the pseudocubic crystals. In each case the unit-cell parameters were determined from a group of crystals and probably represent averages. The lines on the X-ray films were frequently sharp.

The inversion temperatures for the iron-boracites were determined using a Du Pont differential thermal analyser (Table I). The large pseudocubic crystals (lower FeO and MnO) have an inversion temperature of 297 °C whilst the small grains (with higher FeO and MnO) show a range from 287 °C upwards.

TABLE I. *Comparison of the properties of English and German boracites and iron-boracites*

Type and locality	Wt. %			Cations, %			a	b	c	T†
	MgO*	FeO	MnO	Mg ²⁺	Fe ²⁺	Mn ²⁺				
Small anhedral grains from Boulby†	12.44	28.38	4.34	40.34	51.65	8.00	8.63	8.63	12.19 Å	287°C
Large crystals from Boulby†	16.82	22.11	2.85	54.53	40.21	5.25	8.59	8.59	12.15	297
Riedel, Hainigsen	8.55	38.69	0.46	28.71	70.44	0.85	8.58	8.69	12.17	310-315
Niedersachsen, Wathlingen	29.90	1.68	—	96.94	3.06	—	8.53	8.60	12.15	—
Segeberg	30.84	—	—	100	—	—	8.53	8.53	12.12	265
Stassfurt**	30.84	—	—	100	—	—	8.54	8.54	12.07	265
E2 borehole, Yorkshire††	31.00	—	—	100	—	—	8.56	8.56	12.10	272

* Calculated by difference, knowing FeO and MnO%

† Orthorhombic to cubic inversion temperature

‡ Cell dimensions determined using a Haag-Guinier camera of 200 mm equivalent diameter and Cu-K α radiation.

|| Kühn and Schaacke, 1955 ** Ito, Morimoto and Sadanaga, 1951 †† Guppy, 1944

Errata: * applies to anals. 1 and 2 only; last col., line 1, for 287 °C read ≥ 287 °C

Iron-boracite from a nodule in which the crystals only occurred as anhedral grains gave a chemical analysis of 3.82 MnO, 24.05 FeO, 11.75 MgO, 0.27 CaO, 0.55 SiO₂, 53.80 B₂O₃, 0.10 Na₂O, 0.01 K₂O, 0.01 % Br, and 7.38 % Cl. Total (less O \equiv Cl) = 100.07 %. It contains 49.09 mole % FeO, 42.86 mole % MgO, and 8.05 mole % MnO. The analysis gives a formula of (Mn_{0.24}Fe_{1.50}Mg_{1.30})B_{6.9}Si_{0.04}O_{13.07}Cl_{0.93} based on fourteen anions (oxygen and chlorine).

The turbidity of the crystals suggests breakdown of the structure and in some cases this has resulted in recrystallization. The variation of iron and manganese contents of these crystals suggests that the breakdown may have been caused by the influx of a solution rich in iron and manganese into nodules containing pre-existing boracite or low-Mn iron boracite.

Acknowledgements. The authors would like to thank the Management of Cleveland Potash Ltd. for permission to publish this article and the members of the Geology Department who first found the nodules. Thanks are also due to Dr. F. Glasser for allowing the use of X-ray facilities in the Chemistry Department of Aberdeen University, Professor Sir Frederick Stewart for continuous interest and encouragement in this study and the Natural Environment Research Council for financial support.

Grant Institute of Geology,
West Mains Road, Edinburgh

JOHN K. MILNE
and
MICHAEL J. SAUNDERS

Cleveland Potash Ltd.,
Boulby Mine, Loftus, Saltburn, Cleveland

PETER J. E. WOODS

REFERENCES

- Braitsch (O.), 1962. *Entstehung der Salzlagerstätten* (Springer).
Guppy (E. M.), 1944. *Mineral. Mag.* 27, 51-3.
Heide (F.), Walker (G.), and Urlau (R.), 1961. *Naturwiss.* 4, 97-8.
Ito (T.), Morimoto (N.), and Sadanaga (R.), 1951. *Acta Cryst.* 4, 310-16.

References

- Adams, J.E. and Rhodes, M.L., 1960. Dolomitization by seepage refluxion. Bull. Am. Ass. Petrol. Geol., V 44, pp 1912-1920.
- Adams, L.H., 1931. Equilibrium in binary systems under pressure. I. An experimental and thermodynamic investigation of the system NaCl-H₂O at 25°C. J. Am. Chem. Soc., V 53, pp 3769-3813.
- Armstrong, G., Dunham, K.C., Harvey, C.O., Sabine, P.A. and Waters, W.F., 1951. The paragenesis of sylvine, carnallite, polyhalite and kieserite in Eskdale borings nos. 3, 4 and 6, N.E. Yorkshire. Min. Mag., V 29, pp 667-689.
- Assarsson, G., 1957. Kristallisationserscheinungen und Paragenese in dem System der Alkalichloride-Erdalkalichloride-Wasser. Sveriges Geol. Undersökn, Ser. C, V 556, pp 1-17.
- Bathurst, R.G.C., 1976. Carbonate sediments and their diagenesis. In Developments in sedimentology 12: Elsevier Scientific Publishing Co.
- Beevers, C.A. and Stewart, F.H., 1960. p-Veachite from Yorkshire. Min. Mag., V 32, pp 500-501.
- Belmonte, Y., Hirtz, P. and Wenger, R., 1965. The salt basins of the Gabon and Congo (brazzaville), pp 55-78. In Salt basins around Africa: London, Institute of Petroleum, 235 p.
- Benedict, M., 1939. Properties of saturated aqueous solutions of KCl at temperatures above 250°C. J. Geol., V 47, pp 252-276.
- Biltz, W. and Marius, E., 1911. Über die Verbreitung von borsäuren Salzen in den Kalisalzlagernstätten. Zeitschr. Anorg. Allg. Chem., V 72, pp 302-312.
- Borchert, H. and Muir, R., 1964. Salt deposits - their origin, metamorphism and deformation of evaporites: Van Nostrand, 338 p.
- Braitsch, O., 1959. 1Tc-Strontiohilgardit (Ca,Sr)₂[B₅O₈(OH)₂Cl] und seine Stellung in der Hilgarditgruppe X₂[B₅O₈(OH)₂Cl]. Beit. zur Min. & Pet., V 6, pp 233-247.

- Braitsch, O., 1960. Die Borate und Phosphate im Zechsteinsalz Südhannovers. Fortschr. Mineralog., V 38, pp 190-191.
- Braitsch, O., 1972. Salt Deposits Their Origin and Composition: Springer-Verlag, 297 p.
- Brunstrom, R.G.W. and Walmsley, P.J., 1969. Permian evaporites in North Sea basin. Bull. Am. Ass. Petrol. Geol., V 53, pp 870-883.
- Bush, P.R., 1970. Chloride-rich brines from sabkha sediments and their possible role in ore formation. Trans. Instn. Min. Metall. (B), V 79, pp B137-144.
- Carter, N.L., 1965. Basal quartz deformation lamellae - a criterion for recognition of impactites. Am. J. Sci., V 263, pp 786-806.
- Carter, N.L. and Friedman, M., 1965. Dynamic analysis of deformed quartz and calcite from the Dry Creek Ridge Anticline, Montana. Am. J. Sci., V 263, pp 747-785.
- Clarke, F.W., 1924. The data of geochemistry. U.S. Geol. Surv. Bull. 770, pp 1-841.
- Correns, C.W., 1960. H. Borchert, Ozeane Salzlagerstätten (Buchbesprechung). Neues Jahrbuch Mineralog. Monatsch., pp 190-192.
- D'Ans, J., 1961. Über die Bildungsmöglichkeiten des Tachyhydrits in Kalisalzlagerstätten. Kali u. Steinsalz, V 3, pp 119-125.
- D'Ans, J. and Behrendt, K.H., 1957. Über die Existenzbedingungen einiger Magnesiumborate. Kali u. Steinsalz, V 2, pp 121-137.
- Davies, W.O. and Machin, M.P., 1968. Strontiohilgardite-1Tc and tyretskite, a structural pair. Am. Min., V 53, pp 2084-2087.
- Deffeyes, K.S., Lucia, F.J. and Weyl, P.K., 1965. Dolomitization of Recent and Plio-Pleistocene sediments by marine evaporite waters on Bonaire, Netherlands Antilles. In Dolomitization and Limestone Diagenesis, Soc. Econ. Palaeon. Mineralog. Spec. Publ. 13, pp 71-88.

- Dickson, F.W., Blount, C.W. and Tunnell, G., 1963. Use of hydrothermal solution equipment to determine the solubility of anhydrite in water from 100°C to 275°C and from 1 to 1000 bars pressure. *Am. J. Sci.*, V 261, pp 61-78.
- Dunham, K.C., 1948. A contribution to the petrology of the Permian evaporite deposits of north-eastern England. *Proc. Yorks. Geol. Soc.*, V 27, pp 217-227.
- Dunham, K.C., 1966. Role of juvenile solutions, connate waters and evaporite brines, in the genesis of Pb-Zn-Ba-F deposits. *Trans. Instn. Min. Metall. (B)*, V 75, pp 226-229.
- Durney, D.W. and Ramsay, J.G., 1973. Incremental strains measured by syntectonic crystal growth. In De Jong, K.A. and Schuster, R. (Editors), *Gravity and Tectonics*: Wiley, pp 67-96.
- Falcon, N.L. and Kent, P.E., 1960. Geological results of petroleum exploration in Britain 1945-57. *Geol. Soc. Lond. Mem.* 2.
- Fleck, A., 1950. Deposits of potassium salts in north-east Yorkshire. *Chem. Ind. (Suppl. Oct. 17)*, 15 p.
- Foote, F.J., 1932. Determination of boron in water. *Ind. & Eng. Chem.*, V 4, p 39.
- Glennie, K.W., 1972. Permian Rotliegendes of northwest Europe interpreted in the light of modern desert sedimentation studies. *Bull. Am. Ass. Petrol. Geol.*, V 56, pp 1048-71.
- Godlevsky, M.N., 1937. Mineralogical investigations of the Inder borate deposits. *Mémoires de la Société Russe de Minéralogie*, V 66, pp 345-368.
- Graf, D.L., 1974. X-ray cells for diffraction analysis of flat powder mounts in contact with liquid at elevated temperature and pressure. *Am. Min.*, V 59, pp 851-862.
- Guppy, E.M., 1944. Boracite from a boring at Aislaby, Yorkshire. *Min. Mag.*, V 27, pp 51-53.
- Ham, W.E., Mankin, C.J. and Schleicher, J.A., 1961. Borate minerals in Permian gypsum of west central Oklahoma. *Oklahoma Geol. Sur. Bull.* 92.

- Hancock, J.M. and Scholle, P.A., 1974. Chalk of the North Sea. In Petroleum and the Continental Shelf of N.W. Europe. V 1, pp 413-425. Edit. A.W. Woodland.
- Harder, H., 1959. Beiträge zur Geochemie des Bors. Akad. Wiss. Göttingen, Nachr. II. Math-Physik No.5, pp 67-122.
- Heide, F., Walker, G. and Urlau, R., 1961. Zur Kristallchemie des Borozits. Naturwiss., V 4, pp 97-98.
- Hentschel, J., 1961. Die Faciesunterschiede im Flöz Stassfurt des Kalisalzbergwerks Königshall-Hindenberg. Kali u. Steinsalz, V 3, pp 137-145.
- Hermann, A.G., 1977. Modelle zur Bestimmung der Bildungstemperaturen primärer Sylvinit und Carnallit im MgSO_4 -freien Meerwasser-System mittels der Bromid Thermométrie. Kali u. Steinsalz, V 7, pp 134-146.
- Hermann, A.G. and Hoffmann, R.O., 1961. Zur Genese einiger Borate in den Salzablagerungen der Stassfurt-Serie des Südharzbezirkes einschliesslich der Grube Königshall-Hindenberg. Neues Jahrbuch Mineralog. Monatsh., pp 52-60.
- High Pressure Technology Association, 1975. High Pressure Safety Code. E.J. Milner & Sons.
- v. Hodenberg, R. and Kühn, R., 1974. The modifications of Mg-Fe boracites. Abstracts IMA 9th General Meeting in W. Berlin and Regensburg, p 92.
- v. Hodenberg, R. and Kühn, R., 1977. Ein neues Mineral der Hilgarditgruppe: der Cl-Tyretskite von Boulby. Kali u. Steinsalz, V 7, pp 165-170.
- Holliday, D.W., 1967. Discussion of Shearman, D.J., 1966, on the "Origin of marine evaporites". Trans. Inst. Min. Metall. (B), V 76, pp B179-180.
- Holser, W.T., 1966. Diagenetic polyhalite in recent salt from Baja California. Am. Min., V 51, pp 99-109.
- Honea, R.M. and Beck, F.R., 1962. Chambersite, a new mineral. Am. Min., V 47, pp 665-671.
- Hurlbut, C.S., 1938. Parahilgardite, a new triclinic pedial mineral. Am. Min., V 23, pp 765-771.

- Hurlbut, C.S. and Taylor, R.E., 1937. Hilgardite, a new mineral species from Choctaw Salt Dome, Louisiana. *Am. Min.*, V 22, pp 1052-1057.
- Hurlbut, C.S. and Taylor, R.E., 1938. Notes on minerals associated with hilgardite. *Am. Min.*, V 23, pp 898-902.
- Ito, T., Morimoto, N. and Sandanaga, R., 1951. The crystal structure of boracite. *Acta Cryst.*, V 4, pp 310-316.
- Ivanov, A.A. and Yarzhemskii, Y.Y., 1954. Boron manifestations in the saline strata of the Leno-Angar Basin. *Trudy Vses. Nauchn. Issled. Inst. Galurg.*, V 29, pp 210-214. (In Russian)
- Jänecke, E., 1915. Die Enstelung der Deutschen Kalisalz-lager: Brunswick.
- Keevil, N.B., 1942. High temperature vapour pressures of saturated salt solutions. *J. Am. Chem. Soc.*, V 64, p 841.
- Kelly, J.W. and Gifkins, R.C., 1953. Metallographic observations on cell formation and development in aluminium. *J. Inst. of Metals*, V 82, pp 475-480.
- Kent, P.E., 1967. Outline geology of the southern North Sea Basin. *Proc. York. Geol. Soc.*, V 36, pp 1-22.
- Kent, P.E., 1974. The tectonic development of Great Britain and the surrounding seas. In *Petroleum and the Continental Shelf of North-west Europe*, V 1, pp 3-28. Edit. A.W. Woodland.
- King, R.H., 1947. Sedimentation in the Permian Castile Sea. *Bull. Am. Ass. Petrol. Geol.*, V 31, pp 470-477.
- Kinsman, D.J.J., 1969. Modes of formation, sedimentary associations, and diagnostic features of shallow water and supratidal evaporites. *Bull. Am. Ass. Petrol. Geol.*, V 53, pp 830-840.
- Kokorsch, R., 1960. Zur Kenntnis von Genesis, Metamorphose und Faziesverhältnissen des Stassfurtlagers im Grubenfeld Hildesia-Mathildenhall, Diekholzen bei Hildesheim. *Geol. Jahrbuch Beihefte* 41.
- Kolthoff, I.M., Sandell, E.B., Meehan, E.J. and Bruckenstein, S., 1969. *Quantitative Chemical Analysis*. 4th Edition. The MacMillan Company.

- Kondrat'eva, V.V., 1964. X-ray diffraction studies of some minerals of the Hilgardite Group. Rentgenogr. Mineral'm. Syr'ya. Vses. Nauchn. Issled. Inst., Akad. Nauk SSSR, V 4, pp 10-18. (In Russian)
- Kühn, R., 1955. Mineralogische Fragen der in den Kalisalzlagern vorkommenden Salze. Kalium Symposium 1955. (International Kali-Inst., Bern) pp 51-105.
- Kühn, R., 1962. Geochemistry of German potash deposits. In Saline Deposits. Geol. Soc. Am. Special paper No. 88, pp 427-504.
- Kühn, R., 1969. Zum Tachyhydritvorkommen im Flöz Stassfurt. Kali u. Steinsalz, V 5, pp 166-170.
- Kühn, R., 1972. Salzminerale aus niedersächsischen Lagerstätten. Ber. Naturhist. Ges., V 116, pp 115-142.
- Kühn, R and Schaacke, I., 1955. Vorkommen und Analyse der Boracit und Ericaitkristalle aus dem Salzhorst von Wathlingen-Hänigsen. Kali u. Steinsalz, V 11, pp 1-10.
- Kühn, R., Roese, K.-L. and Gaertner, H., 1962. Fabianit $\text{CaB}_3\text{O}_5(\text{OH})$ - ein neues Mineral. Kali u. Steinsalz, V 3, pp 285-290.
- Loewengart, S., 1962. The geochemical evolution of the Dead Sea basin. Bull. Research Council Israel, V 11G, pp 85-96.
- MacDonald, G.J.F., 1953. Anhydrite-gypsum equilibrium relations. Am. J. Sci., V 251, pp 884-898.
- Marie, J.P.P., 1974. Rotliegendes stratigraphy and diagenesis. In Petroleum and the Continental Shelf of N.W. Europe, V 1, pp 205-210. Edit. A.W. Woodland.
- Martin, R.J. and Hayes, J.R., 1952. Application of ion exchange to the determination of boron. Anal. Chem., V 24, pp 182-185.
- Milliman, J.D., 1974. Marine Carbonates. Springer-Verlag, 375 p.
- Milne, J.K., Saunders, M.J. and Woods, P.J.E., 1977. Iron-boracite from the English Zechstein. Min. Mag., V 41, pp 404-406.

- Morse, H.W., Warren, C.H. and Donnay, J.D.H., 1932. Artificial spherulites and related aggregates. *Am. J. Sci.*, V 23, pp 421-439.
- Neev, D. and Emery, K.O., 1967. The Dead Sea - depositional processes and environments of evaporites. *Geol. Sur. Israel Bull. No. 41.* 147 p.
- Nikolaev, A.V. and Chelishcheva, A.G., 1940a. On the primary deposition of borates from seawater. *Comptes Rendus (Doklady) de l'Academie des Sciences de l'URSS*, V 28, pp 502-504.
- Nikolaev, A.V. and Chelishcheva, A.G., 1940b. Influence of boric acid on the evaporation of natural brines. *Comptes Rendus (Doklady) de l'Academie des Sciences de l'URSS*, V 28, pp 505-506.
- Ölander, A. and Liander, H., 1950. *Acta Chemica Scandinavica*, V 42, pp 1437-1445.
- Palache, C., Berman, H. and Frondel, C., 1951. *The System of Mineralogy*, Vols. I-III. Seventh Edition. Wiley.
- Phleger, F.B., 1969. A modern evaporite deposit in Mexico. *Bull. Am. Ass. Petrol. Geol.*, V 53, pp 824-829.
- Porrenga, D.H., 1967. Clay mineralogy and geochemistry of Recent marine sediments in tropical areas. *Publicaties van het Fysisch-Geografisch Laboratorium van de Universiteit van Amsterdam.* No. 9.
- Potter, R.W., Babcock, R.S. and Brown, D.L., 1975. Solubility relationships in the NaCl-KCl-H₂O system. *Trans. Am. Geophys. Union*, V 56. No. 12.
- Ramberg, H., 1972. Experimental and theoretical study of salt dome evolution. In *Proc. of the Hanover Symposium on saline deposits*, pp 247-251. Unesco Publications.
- Raup, O.B., 1972. Origin of rare-earths in a marine evaporite mineral. In *Geology of Saline Deposits. Proc. Hannover Symp.*, 1968. pp 103-109.
- Raup, O.B., Gude, A.J. 3d and Groves, H.L., 1967. Rare-earth mineral occurrence in marine evaporites, Paradox Basin, Utah. *U.S. Geol. Surv. Prof. paper* 575-C, pp C38-C41.

- Raup, O.B., Gude, A.J. 3d, Dwornik, E.J., Cuttitta, F. and Rose, H. Jr., 1968. Braitschite, a new hydrous calcium rare-earth borate mineral from the Paradox Basin, Grand County, Utah. *Am. Min.*, V 53, pp 1081-1095.
- Rawitsch, M.I., 1958. Die heterogenen Gleichgewichte in Wasser-Salz-Systemen bei hohen Temperaturen. *Freiberger Forschungsch.* V 123, pp 269-286.
- Raymond, L.R., 1953. Some geological results from the exploration for potash in North East Yorkshire. *Q. J. Geol. Soc. Lond.*, V 108, pp 283-310.
- Raymond, L.R., 1960. The pre-Permian floor beneath Billingham, Co. Durham, and structures in overlying Permian sediments. *Q. J. Geol. Soc. Lond.*, V 116, pp 297-315.
- Rhys, G.H., 1974. A proposed standard lithostratigraphic nomenclature for the southern North Sea and an outline structural nomenclature for the whole of the (U.K.) North Sea. *Institute of Geological Sciences Report No. 74/8.* H.M.S.O. 14 p.
- Richter-Bernburg, G., 1955. Über salinare Sedimentation. *Deutsche Geol. Gesell. Zeitschr.*, V 105, pp 593-645.
- Richter-Bernburg, G., 1957. Zur Paläogeographie des Zechsteins. *Atti del Convegno di Milano*, V 1 pp 87-99.
- Roth, H., 1972. Deformations in subhorizontal salt deposits of German Zechstein I. *In Geology of Saline Deposits, Proc. Hannover Symp.*, 1968. pp 225-233.
- Sabine, P.A., 1953. *Petrog. Dept. Report Summ. Prog. Geol. Surv. for 1951*, p 60.
- Schaller, W.T., 1937. Borax and borates in industrial minerals and rocks, 1st Ed: New York, Amer. Inst. Min. Metall. Engineers, pp 149-162.
- Schaller, W.T. and Henderson, E.P., 1932. Mineralogy of drill cores from the potash field of New Mexico and Texas. *U.S. Geol. Sur. Bull.* 833. 124 p.
- Schmalz, R.F., 1969. Deep water evaporite deposition A genetic model. *Bull. Am. Ass. Petrol. Geol.*, V 53, pp 798-823.
- Scruton, P.C., 1953. Deposition of evaporites. *Bull. Am. Ass. Petrol. Geol.*, V 37, pp 2498-2512.

- Shearman, D.J., 1966. Origin of marine evaporites by diagenesis. Trans. Instn. Min. Metall. (B), V 75, pp B208-215.
- Shearman, D.J., 1970. Recent halite rock, Baja California, Mexico. Trans. Instn. Min. Metall. (B), V 79, pp B155-162.
- Smith, D.B., 1970. The palaeogeography of the British Zechstein. In Third Symposium on Salt, VI, pp 20-23. Northern Ohio Geol. Soc. Edit. J.L. Rose and L.F. Delling.
- Smith, D.B., 1971. Discussion of paper by D.J. Shearman, 1970. Trans. Instn. Min. Metall. (B), V 80, pp B66-67.
- Smith, D.B., 1973. The origin of Middle and Upper Permian potash deposits of Yorkshire - an alternative hypothesis. Proc. York. Geol. Soc., V 39, pp 327-346.
- Smith, D.B., 1974. The Permian. In Geology and Mineral Resources of Yorkshire. Edit. D.H. Rayner and J.E. Hemingway. Publ. Yorkshire Geol. Soc.
- Smith, S., 1971. Discussion on paper by D.J. Shearman. Trans. Instn. Min. Metall. (B), V 80, pp 68-69.
- Sourirajan, S. and Kennedy, G.C., 1962. The system $H_2O-NaCl$ at elevated temperatures and pressures. Am. J. Sci., V 260, pp 115-141.
- Spry, A., 1969. Metamorphic Textures. Pergamon Press. 350 p.
- Stewart, F.H., 1949. The petrology of the evaporites of the Eskdale no. 2 boring, E. Yorkshire. Part I. The lower evaporite bed. Min. Mag., V 28, pp 621-675.
- Stewart, F.H., 1951(a). The petrology of the evaporites of the Eskdale no. 2 boring, E. Yorkshire. Part II. The middle evaporite bed. Min. Mag., V 29, pp 445-475.
- Stewart, F.H., 1951(b). The petrology of the evaporites of the Eskdale no. 2 boring, E. Yorkshire. Part III. The upper evaporite bed. Min. Mag., V 29, pp 557-572.

- Stewart, F.H., 1954. Permian evaporites and associated rocks in Texas and New Mexico compared with those of northern England. *Proc. York. Geol. Soc.*, V 29, pp 185-235.
- Stewart, F.H., 1956. Replacements involving early carnallite in potassium-bearing evaporites of Yorkshire. *Min. Mag.*, V 31, pp 127-135.
- Stewart, F.H., 1963(a). The Permian lower evaporites of Fordon in Yorkshire. *Proc. York. Geol. Soc.*, V 34, pp 1-44.
- Stewart, F.H., 1963(b). Marine evaporites, data of geochemistry, Chapter Y. *Geol. Survey Prof. Paper* 440-Y, 52 p.
- Stewart, F.H., 1965. The mineralogy of the British Permian evaporites. *Min. Mag.*, V 34, pp 460-470.
- Stewart, F.H., Chalmers, R.A. and Phillips, R., 1954. Veachite from the Permian evaporites of Yorkshire. *Min. Mag.*, V 30, pp 389-392.
- Strunz, H., 1949. *Mineralogische Tabellen*, 2nd. Edition. Leipzig: Akademische Verlagsgesellschaft Geet und Portig.
- Talbot, C., 1975. Near seam geological structures at Cleveland Potash Ltd. Consultants Report.
- Talbot, C., 1977. Second report on structures at Cleveland Potash Ltd. Consultants Report.
- Taylor, J.C.M. and Colter, V.S., 1974. Zechstein of the English sector of the southern North Sea basin. In *Petroleum and the Continental Shelf of North West Europe*, V 1, pp 249-264. Edit. A.W. Woodland.
- Trusheim, F., 1960. Mechanism of salt migration in northern Germany. *Bull. Am. Ass. Petrol. Geol.*, V 44, pp 1519-1540.
- *
- Valyashko, M.G., 1956. Geochemistry of deposits of potassium salts. *Izd. Akad. Nauk SSSR Otdel. Geologo-Geograficheskikh Nauk*, pp 182-207.
- Valyashko, M.G., 1958. Die wichtigsten geochemischen Parameter für die Bildung der Kalisalzagerstätten. *Freiberger Forsch. Series A.*, V 123, pp 197-233.

- Valyashko, M.G., 1972(a). Playa lakes - a necessary stage in the development of a salt bearing basin. In UNESCO publication: Hannover Symposium on the Geology of Saline Deposits, 1968, pp 41-51.
- Valyashko, M.G., 1972(b). Scientific works in the field of geochemistry and the genesis of salt deposits in the USSR. In UNESCO publication: Hannover Symposium on the Geology of Saline Deposits, 1968, pp 289-311.
- Van't Hoff, J.H., 1909. Zur Bildung der ozeanischen Salzablagerungen. 85 u. 90S. Braunschweig: Fr. Vieweg 1905, 1909.
- Walstrom, E.E., 1969. Optical Crystallography. 4th Edition. Wiley. 489 p.
- Wardlaw, N.C., 1972. Unusual marine evaporites with salts of calcium and magnesium chloride in Cretaceous basins of Sergipe, Brazil. Econ. Geol., V 67, pp 156-168.
- Wendling, E., v. Hodenberg, R. and Kühn, R., 1972. Congolit, der trigonale Eisenboracit. Kali u. Steinsalz, V 1, pp 1-3.
- Woods, P.J.E., 1973. Potash exploration in Yorkshire: Boulby Mine pilot borehole. Trans. Instn. Min. Metall. (B), V 82, pp B99-105.
- Wooster, W.A., 1938. A Text Book of Crystal Physics. Cambridge.
- Yarzhemsky, J.J., 1945. On questions related to the origins of the Inder Borates. Doklady, V 47, pp 642-645.
- Zen, E.-An., 1965. Solubility measurements in the system $\text{CaSO}_4\text{-NaCl-H}_2\text{O}$ at 35° , 50° , and 70°C and one atmosphere pressure. J. Pet., V 6, pp 104-164.
- Ziegler, W.H., 1974. Outline of the geological history of the North Sea. In Petroleum and the Continental Shelf of N.W. Europe. V 1, pp 165-187. Edit. A.W. Woodland.
- * Usiglio, J., 1849. Analyse de l'eau de la Méditerranée sur les côtes de France. Ann. Chem. Phys., V 27, pp 92-107 and pp 172-191.